

UNCLASSIFIED

AD NUMBER

ADB003220

LIMITATION CHANGES

TO:

Approved for public release; distribution is unlimited.

FROM:

Distribution authorized to U.S. Gov't. agencies only; Test and Evaluation; APR 1975. Other requests shall be referred to Air Force Weapons Laboratory, ATTN: DEX, Kirtland AFB, NM 87117.

AUTHORITY

AFWL ltr dtd 29 Apr 1985

THIS PAGE IS UNCLASSIFIED

AD

B003220

AUTHORITY:

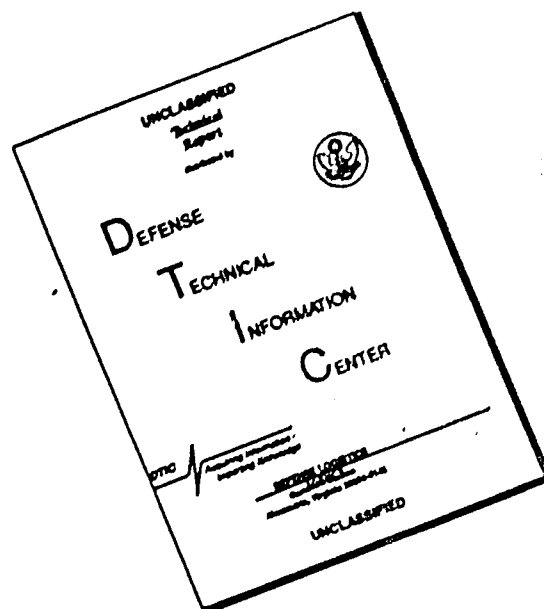
AFWL 17, 29 Apr 85

THIS REPORT HAS BEEN DELIMITED
AND CLEARED FOR PUBLIC RELEASE
UNDER DOD DIRECTIVE 5200.20 AND
NO RESTRICTIONS ARE IMPOSED UPON
ITS USE AND DISCLOSURE.

DISTRIBUTION STATEMENT A

APPROVED FOR PUBLIC RELEASE;
DISTRIBUTION UNLIMITED.

DISCLAIMER NOTICE



THIS DOCUMENT IS BEST QUALITY AVAILABLE. THE COPY FURNISHED TO DTIC CONTAINED A SIGNIFICANT NUMBER OF PAGES WHICH DO NOT REPRODUCE LEGIBLY.

ADB003220



PERFORMANCE EVALUATION OF VELOCITY MEASUREMENT SYSTEMS

Stephen F. Pickett
Adalbert J. Smiel

CERF, University of New Mexico
Albuquerque, NM 87131

April 1975

Final Report for Period July 1971 - March 1973

Distribution limited to US Government agencies only because of test and evaluation of commercial products (April 1975). Other requests for this document must be referred to AFWL (DEX), Kirtland AFB, NM 87117.

Prepared for
SPACE AND MISSILE SYSTEMS ORGANIZATION
Norton AFB, CA 92409

AIR FORCE WEAPONS LABORATORY
Air Force Systems Command
Kirtland Air Force Base, NM 87117



This final report was prepared by the Eric H. Wang Civil Engineering Research Facility, University of New Mexico, Albuquerque, New Mexico, under Contract F29601-72-C-0024, Job Order 133B1414 with the Air Force Weapons Laboratory, Kirtland Air Force Base, New Mexico. Mr. Josef F. Schneider (DEX) was the Laboratory Project Officer-in-Charge.

When US Government drawings, specifications, or other data are used for any purpose other than a definitely related Government procurement operation, the Government thereby incurs no responsibility nor any obligation whatsoever, and the fact that the Government may have formulated, furnished, or in any way supplied the said drawings, specifications, or other data, is not to be regarded by implication or otherwise, as in any manner licensing the holder or any other person or corporation, or conveying any rights or permission to manufacture, use, or sell any patented invention that may in any way be related thereto.

This technical report has been reviewed and is approved for publication.

Josef F. Schneider

JOSEF F. SCHNEIDER
Project Officer

Patrick O'Toole

PATRICK O'TOOLE
Lt Colonel, USAF
Chief, Experimental Branch

William B. Liddicoet

WILLIAM B. LIDDICOET
Colonel, USAF
Chief, Civil Engineering Research
Division

UNCLASSIFIED

SECURITY CLASSIFICATION OF THIS PAGE (When Data Entered)

REPORT DOCUMENTATION PAGE		READ INSTRUCTIONS BEFORE COMPLETING FORM
1. REPORT NUMBER AFWL-TR-74-219	2. GOVT ACCESSION NO.	3. RECIPIENT'S CATALOG NUMBER
4. TITLE (and Subtitle) PERFORMANCE EVALUATION OF VELOCITY MEASUREMENT SYSTEMS		5. TYPE OF REPORT & PERIOD COVERED Final Report July 1971 - March 1973
		6. PERFORMING ORG. REPORT NUMBER
7. AUTHOR(s) Stephen F. Pickett Adalbert J. Smiel		8. CONTRACT OR GRANT NUMBER(s) F29601-72-C-0024
9. PERFORMING ORGANIZATION NAME AND ADDRESS Eric H. Wang Civil Engineering Research Facility University of New Mexico, Box 188, University Sta. Albuquerque, New Mexico 87131		10. PROGRAM ELEMENT, PROJECT, TASK AREA & WORK UNIT NUMBERS 11213F 1338 1414
11. CONTROLLING OFFICE NAME AND ADDRESS Space and Missile Systems Organization Norton Air Force Base, California 92409		12. REPORT DATE April 1975
		13. NUMBER OF PAGES 176
14. MONITORING AGENCY NAME & ADDRESS (if different from Controlling Office) Air Force Weapons Laboratory (DEX) Kirtland Air Force Base, New Mexico 87117		15. SECURITY CLASS. (of this report) Unclassified
		15a. DECLASSIFICATION/DOWNGRADING SCHEDULE
16. DISTRIBUTION STATEMENT (of this Report) Distribution limited to US Government agencies only because of test and evaluation of commercial products (April 1975). Other requests for this document must be referred to AFWL (DEX), Kirtland AFB, NM 87117.		
17. DISTRIBUTION STATEMENT (of the abstract entered in Block 20, if different from Report)		
18. SUPPLEMENTARY NOTES		
19. KEY WORDS (Continue on reverse side if necessary and identify by block number) Seismic motion transducers Velocity measurement systems Field test instrumentation Fast Fourier transform system analysis		
20. ABSTRACT (Continue on reverse side if necessary and identify by block number) Since velocity measurements are an important aspect of many dynamic field tests, performance evaluations of velocity measurement systems from six manu- facturers were made at the Eric H. Wang Civil Engineering Research Facility (CEPF). These systems, which consisted of both linear and pendulous trans- ducers and associated signal conditioners were tested on the CERF drop tower for dynamic inputs to the vertical systems and on the CERF sled track for dynamic inputs to the horizontal systems. Dynamic transducer inputs were (over)		

UNCLASSIFIED

SECURITY CLASSIFICATION OF THIS PAGE (When Data Entered)

UNCLASSIFIED

SECURITY CLASSIFICATION OF THIS PAGE(When Data Entered)

ABSTRACT (cont'd)

used to obtain data for evaluating upper frequency limits, accuracy, rise-time capabilities, long-line effects, and on-axis and cross-axis shock survivability. Eight dynamic tests were performed on each measurement system and a selected horizontal pendulous transducer was evaluated dynamically to determine the dynamic performance effects due to various internal damping fluids. Static and near-static test techniques were developed, verified, and used to evaluate system droop characteristics and low-frequency capabilities. External carrier-demodulator signal conditioners which were compatible with the DX-type pendulous transducers were also tested and evaluated for rise-time capability, high-frequency capability, overshoot, ringing, noise, and long-line performance effects. Computer programs were used in plotting and analyzing the data. After individual evaluations were made on each system, an overall evaluation was made. From this it was concluded that CEC transducers with Natel 6-kHz signal conditioners are the best suited for most AFWL field measurements.

UNCLASSIFIED

SECURITY CLASSIFICATION OF THIS PAGE(When Data Entered)

CONTENTS

<u>Section</u>		<u>Page</u>
I	INTRODUCTION	1
II	SYSTEMS TESTED	3
	1. Signal Conditioner	3
	2. Pendulous Transducer	7
	3. Linear Transducer	9
III	TESTING APPARATUS	11
	1. Horizontal Sled Track	11
	2. Vertical Drop Tower	17
IV	TEST PLAN	19
	1. Transducer Tests	19
	2. Damping Fluid Tests	21
	3. System Fast Rise Time Tests	22
V	TEST PROCEDURES	23
	1. Fallthrough Tests	23
	a. 1- and 2-g Fallthrough	23
	b. Exponential Fallthrough	26
	2. System Fast Rise Time Tests	29
VI	EVALUATION TECHNIQUES	31
	1. Droop	31
	2. Low- and High-Frequency Cutoff	31
	a. Exponential Fallthrough Determination of f_{CH} and f_{CL}	31
	b. Fast Fourier Transform Determination of f_{CH} and f_{CL}	33
	3. 1- and 2-g Fallthrough	38
VII	TEST RESULTS	43
	1. Signal Conditioner Fast Rise Time Data	43
	2. Pendulous Transducer Data	60
	a. Cibola	60
	b. CEC	68
	c. Sparton Brass	75
	d. Sparton Aluminum	84
	e. Sparton 604	89

CONTENTS (Concl'd.)

<u>Section</u>	<u>Page</u>
f. Sparton 602 (FM)	90
3. Linear Transducer Data	94
a. EG&G	94
b. Endevco	100
c. Setra	104
4. Damping Fluid Test Data	109
VIII ANALYSIS OF LOW- AND HIGH-FREQUENCY CUTOFF	124
IX CONCLUSIONS AND RECOMMENDATIONS	126
 Appendixes:	
I Operating Principles of Transducer Systems	133
II Sled Track Problems	150
III Justification for 1- and 2-g Fallthrough Procedure	153
IV Justification for Exponential Fallthrough Procedure	157
V Damping Ratio Determination from Exponential Fallthrough Data	160
VI Justification for Haversine Termination	163
 Distribution	 168

ILLUSTRATIONS

<u>Figure</u>		<u>Page</u>
1	Natel Model 2088M Carrier Amplifier System	4
2	Downhole Completion Circuit for Natel System	6
3	Horizontal Sled Track System	12
4	Pneumatic Impact Ram	12
5	Sled Track	13
6	Canister Sled and Inserts	15
7	Data Acquisition System	16
8	Vertical Drop Tower	18
9	System Instrumentation for Fallthrough Tests	24
10	Resistor Calibrate Box	24
11	Fallthrough Fixture with Transducer	25
12	Sample Fallthrough Oscillograph Record	26
13	Transducer Response	27
14	System Instrumentation for Fast Rise Time Tests	29
15	Droop Determination from Exponential Fallthrough Data	32
16	Typical Velocity Transducer Input and Output	35
17	Velocity Transducer Input and Output with Artificial Haversine Termination	35
18	Signal Conditioner Input and Output	37
19	Pendulous Transducer 1-g Fallthrough Output	39
20	Pretest and Posttest 1-g Fallthrough (Example 1)	39
21	Pretest and Posttest 1-g Fallthrough (Example 2)	41
22	Pretest and Posttest 1-g Fallthrough (Example 3)	42
23	Natel Fast Rise Time Test Data	45
24	WES Fast Rise Time Test Data	47
25	Crescent (3 kHz) Fast Rise Time Test Data	49
26	Crescent (10 kHz) Fast Rise Time Test Data	51
27	CEC 1-118 Fast Rise Time Test Data	53
28	CEC 1-113B Fast Rise Time Test Data	55
29	EG&G Fast Rise Time Test Data	57
30	Sparton 602 (FM) Fast Rise Time Test Data (Short Lines)	59
31	Typical Input for Dynamic Tests	63
32	Cibola Test Series 2 High-Level, Normal Data	65

ILLUSTRATIONS (Cont'd.)

<u>Figure</u>		<u>Page</u>
33	Cibola Test Series 3 Low-Level, Short-Line Data	65
34	Cibola Test Series 3 Low-Level, Long-Line Data	66
35	Cibola Transducer 1-g Fallthrough Output	67
36	CEC Horizontal Test Series 1 Low-Level, Post-High-g Data	72
37	CEC Horizontal Test Series 2 High-Level, Normal Data	72
38	CEC Vertical Test Series 2 High-Level, Normal Data	73
39	CEC Vertical Test Series 3 Low-Level, Short-Line Data	73
40	CEC Vertical Test Series 3 Low-Level, Long-Line Data	74
41	Sparton Brass Horizontal Test Series 1 Low-Level, Pre-High-g Data	79
42	Sparton Brass Horizontal Test Series 1 High-Level, Normal Data	79
43	Sparton Brass Horizontal Test Series 1 Post-High-g Data	80
44	Sparton Brass Horizontal Test Series 2 High-Level, Normal Data	80
45	Sparton Brass Vertical Test Series 1 Low-Level, Post-High-g Data	81
46	Sparton Brass Vertical Test Series 2 High-Level, Normal Data	81
47	Sparton Brass Vertical Test Series 3 Low-Level, Short-Line Data	82
48	30° Test Fallthroughs for Sparton Brass Transducer	83
49	Sparton Aluminum Test Series 1 High-Level, Normal Data	87
50	Sparton Aluminum Test Series 1 Low-Level, Post-High-g Data	87
51	Sparton Aluminum Test Series 2 High-Level, Normal Data	88
52	Sparton Aluminum Test Series 3 Low-Level, Long-Line Data	88
53	Sparton 604 Test Series 3 Low-Level, Short-Line Data	92
54	Sparton 604 Test Series 3 Low-Level, Long-Line Data	92
55	Sparton 602 (FM) Test Series 1 Low-Level, Normal Data	93
56	Sparton 602 (FM) Transducer 1-g Fallthrough Output	93
57	EG&G Horizontal Test Series 1 High-Level, Normal Data	97
58	EG&G Horizontal Test Series 1 Low-Level, Post-High-g Data	97
59	EG&G Horizontal Test Series 3 Low-Level, Long-Line Data	98
60	EG&G Vertical Test Series 1 High-Level, Normal Data	98

ILLUSTRATIONS (Concl'd.)

<u>Figure</u>		<u>Page</u>
61	Endevco 150-g, Normal Data	101
62	Setra Horizontal Test Series 1 Low-Level, Pre-High-g Data	106
63	Setra Horizontal Test Series 1 High-Level, Normal Data	106
64	Setra Horizontal Test Series 1 Low-Level, Post-High-g Data	107
65	Setra Vertical Test Series 1 Low-Level, Pre-High-g Data	107
66	Setra Vertical Test Series 2 High-Level, Normal Data	108
67	Typical Setra Transducer Calibration Output	110
68	CEC Transducer Response with 500-Centistoke Damping Oil	111
69	CEC Transducer Response with 1000-Centistoke Damping Oil	113
70	CEC Transducer Response with 2000-Centistoke Damping Oil	115
71	CEC Transducer Response with 5000-Centistoke Damping Oil	117
72	CEC Transducer Response with 7500-Centistoke Damping Oil	119
73	Damping Ratio versus Oil Centistoke Rating for CEC Horizontal Transducer	121
74	Velocity/Voltage Ratio versus Oil Centistoke Rating for CEC Horizontal Transducer	122
75	Horizontal Pendulous Transducer Mechanics	133
76	Vertical Pendulous Transducer Mechanics	135
77	Pendulous Transducer E-Core and Armature Assembly	137
78	Pendulous Transducer Electrical Bridge Circuit	137
79	FM Velocity Transducer Signal Conditioning System	139
80	FM Velocity Transducer Outputs	140
81	Horizontal Linear Transducer Mechanics	141
82	Setra Transducer Mechanics	143
83	Setra Transducer Voltage Levels During Two Modulation Cycles	145
84	Gain versus Frequency for Setra Velocity System	146
85	L-Shaped Sled and Canister	151
86	Normal Operating Mode of Horizontal Pendulous Transducer	154
87	1-g Fallthrough Mode of Horizontal Pendulous Transducer	156
88	Typical Seismic Transducer Input/Output Record	164
89	Seismic Transducer Input and Output with Haversine Termination	164

TABLES

<u>Table</u>	<u>Page</u>
I Signal Conditioners Tested	3
II Pendulous Transducers Tested	8
III Linear Transducers Tested	10
IV Transducer Test Series	20
V Summary of Signal Conditioner Test Results	44
VI Comparative Ranking of DX-Compatible Signal Conditioners	61
VII Summary of Pendulous Transducer Test Results	62
VIII Static Calibration Fallthrough Data for Cibola Transducer	63
IX Data Summary for Cibola Transducer Testing	64
X Static Calibration Fallthrough Data for CEC Transducers	69
XI Data Summary for CEC Transducer Testing	70
XII Static Calibration Fallthrough Data for Sparton Brass Transducers	76
XIII Data Summary for Sparton Brass Transducer Testing	77
XIV Static Calibration Fallthrough Data for Sparton Aluminum Transducer	85
XV Data Summary for Sparton Aluminum Transducer Testing	86
XVI Static Calibration Fallthrough Data for Sparton 604 Transducer	90
XVII Data Summary for Sparton 604 Transducer Testing	91
XVIII Summary of Linear Transducer Test Results	95
XIX Dynamic Data Summary for EG&G Transducer Testing	96
XX Dynamic Data Summary for Setra Transducer Testing	105
XXI Summary of Damping Fluid Test Results	121

ABBREVIATIONS AND SYMBOLS

A	arbitrary constant
C	system damping constant
$C(j\omega)$	output function described in complex frequency domain
$G(j\omega)$	input function described in complex frequency domain
$H(j\omega)$	transfer function
$ H(j\omega) $	modulus ratio
$H(\phi)$	phase differential
Im	imaginary component
Re	real component
S	Laplace operator
T	gravity-induced pendulum tension force
T_1, T_2	time required during pretest and posttest fallthrough for transducer output to go from calibration level to zero, respectively
V_I	input velocity
V_m	maximum velocity
V_O	output velocity
X	horizontal case displacement
$X(s)$	Laplace transform of X
Y	vertical case displacement
$c(t)$	output function described in time domain
f_{CH}	high-frequency cutoff
f_{CL}	low-frequency cutoff
f_n	natural frequency
f_1, f_2	arbitrary time functions
g	acceleration of gravity (32.2 fps)
\bar{g}	gravity vector
$g(t)$	input function described in time domain
h	system damping ratio
k	spring constant
ℓ	radius of gyration
m	mass of pendulum
n	arbitrary constant
ngT_1, ngT_2	calibration level equivalent for pretest and posttest data, respectively

ABBREVIATIONS AND SYMBOLS (Concl'd)

(s)	Laplace function notation
t	time
t_0	time at which case step velocity occurs
t_f	folding start point
t_p	time at which peak output occurs
x	horizontal pendulum displacement
$x(s)$	Laplace transform of x
\ddot{x}	input absolute acceleration
y	vertical pendulum displacement
α	$\omega_n (h + \sqrt{h^2 - 1})$
β	$\omega_n (h - \sqrt{h^2 - 1})$
δ	transfer function
δt	droop (elapsed time between peak output and one-half peak output)
ζ	scale factor
θ	pendulum angle
$\dot{\theta}$	angular velocity of pendulum
$\dot{\theta}_m$	maximum angular velocity of pendulum
$\theta(s)$	Laplace transform of θ
ω	2π times frequency
ω_n	2π times natural frequency

SECTION I INTRODUCTION

1. BACKGROUND

Velocity measurements are an important part of many underground dynamic field tests. However, no capability limits based on actual performance testing have been clearly established, although users of velocity measurement systems are aware of a number of transducer and system limitations. In many instances, mathematical model limits were the only basis for estimating system performance.

2. OBJECTIVE

The objective of this effort was to evaluate velocity measurement system performance through dynamic, static, and near-static testing. Transducer rise-time capabilities, steady state falloff (droop) characteristics, upper- and lower-frequency limits, accuracy, shock survivability, and long (4000 ft) transmission line effects were evaluated in order to determine a *system of choice* for most AFWL field requirements.

3. SCOPE

Various linear and pendulous transducers, both horizontal and vertical, were statically and dynamically tested.

The vertical velocity transducers were dynamically tested on the CERF vertical drop tower and the horizontal velocity transducers were dynamically tested on the CERF horizontal sled track. The associated tests were designed for both mild and severe environmental inputs. All pendulous velocity transducer tests were performed with a Natel signal conditioner; the linear transducers utilized their own self-contained or external signal conditioners. The dynamic outputs were compared to integrated data from two reference accelerometers.

The transducers were subjected to (1) high- and low-g-level, normal inputs; (2) high-g-level inputs in the 30°, 90°, and normal axis orientation; and (3) low-g-level inputs with short and long lines. Prior to and after each test, all transducers were statically calibrated in order to observe changes, anomalies, or damage after the dynamic inputs.

Step input tests of new and existing signal conditioner systems were also performed. These data yielded rise time, overshoot, and noise characteristics.

Other testing involving low-g-level inputs to pendulous transducers containing various damping fluids enabled an evaluation of the effect of fluid viscosity on the transducer performance characteristics mentioned above.

SECTION II SYSTEMS TESTED

1. SIGNAL CONDITIONER

The external signal conditioner needed for all the pendulous velocity transducers tested, except Sparton Model 602 (FM), is a major subsystem of the entire velocity data acquisition system. Many available systems are compatible with these transducers. In addition to the DX-compatible signal conditioners, the Sparton 602 (FM) and the EG&G signal conditioners were tested (table I).

a. Natel Model 2088M

The Natel Model 2088M is a solid-state carrier amplifier type signal conditioner system (fig. 1) which provides the required ac voltage for variable inductance type velocity transducers. It also transforms the ac phase and amplitude signal into a linear analog output signal.

Basically, the system functions as follows: a master oscillator generates an ac carrier signal which can be amplitude controlled by the excitation amplifier. The transducer frequency of this carrier for the Natel is 6 kHz (with an

Table I
SIGNAL CONDITIONERS TESTED

Manufacturer	Model	Carrier Frequency, kHz	Manufacturer's Nominal Cutoff Specification, Hz
Natel	2088M	6	2200
Crescent	8303	3	300
Crescent	8303 (Modified)	10	1500
CEC	1-113B	3	500
CEC	1-118	3	500
WES	---	3	1000
Sparton	602 (FM)	40-kHz Differential*	Not specified.
EG&G	---	10	Not specified.

*This is not a carrier system. One oscillator runs at 320 kHz nominal, the other at 280 kHz nominal.

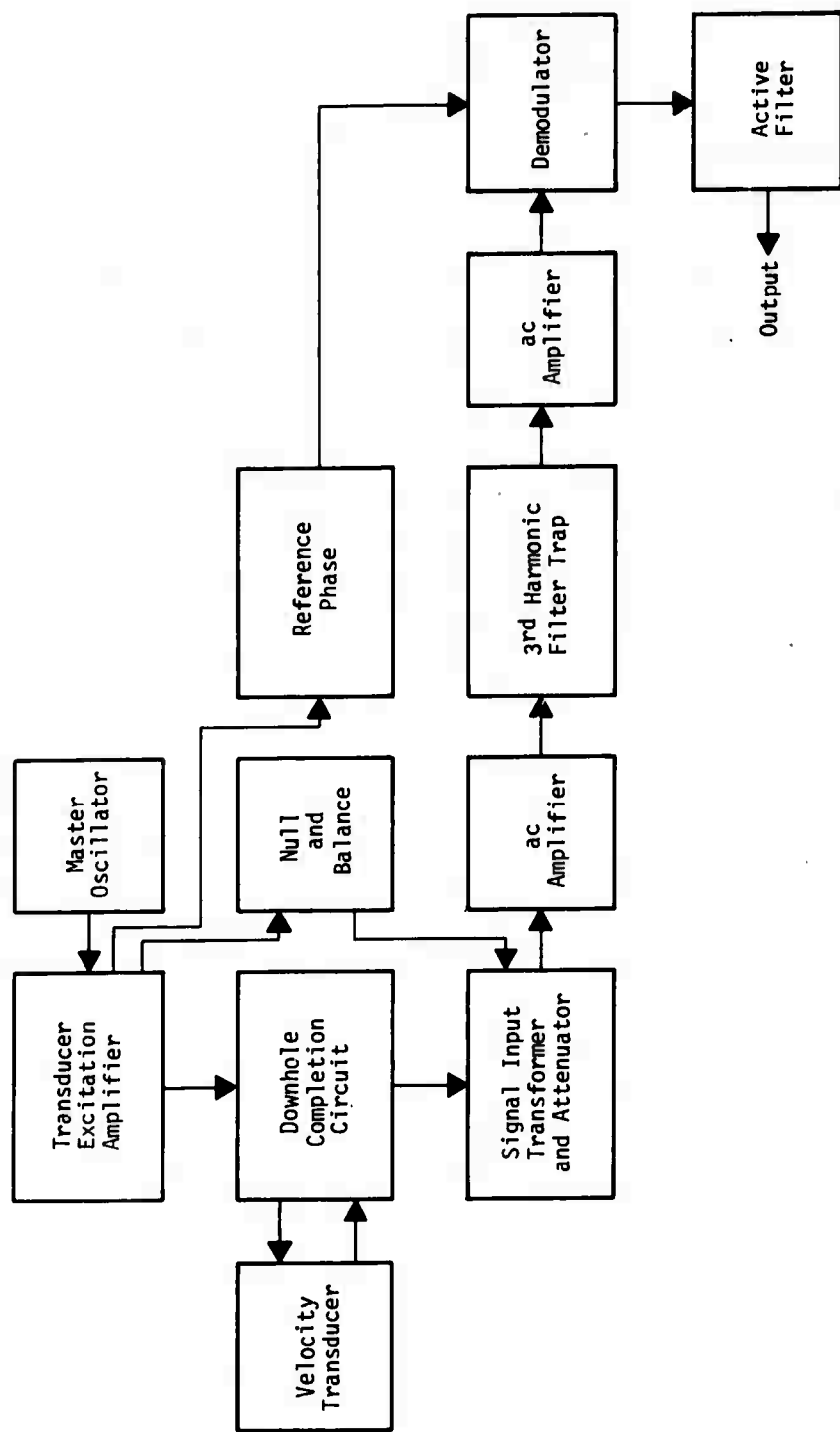


Figure 1. Natel Model 2088M Carrier Amplifier System

optional 20-kHz carrier). This carrier supplies the necessary voltage to the variable inductance type velocity transducer. The inductance coils of the velocity transducer form half of a full-bridge circuit, and bridge-completion resistors form the other half. The relative potential difference between the center-tapped coils and the center-tapped resistors of the bridge provides the input signal to the carrier amplifier system. When the pendulum of the velocity transducer moves, an imbalance between the two coils occurs; this in turn unbalances the bridge circuit and sends a phase- and amplitude-sensitive signal to the carrier amplifier system. The signal then passes through a downhole type bridge completion and calibrate circuit. The signal is passed through an attenuator and a phase- and amplitude-balance nulling circuit for the compensation of a quiescent voltage of the velocity transducer in its neutral position. The input signal is then directed to an ac amplifier, a 3rd harmonic filter trap to attenuate the 18-kHz component, another ac amplifier, and then into the demodulator circuit. The demodulator also has another input, referred to as the *reference phase signal*. This signal is adjustable from -90° to $+90^\circ$ relative to the master oscillator signal. The reference phase voltage is compared to the velocity transducer signal and can be phase-adjusted to compensate for any shifts due to long cables to the transducer. The full-wave demodulator compares the reference phase signal and the incoming transducer signal; the output is a full-wave rectified signal. If the two signals are in phase, the demodulated dc output is positive; if they are out of phase (i.e., 180° difference), the demodulated dc output is negative. The amplitude of the output voltage is directly proportional to the amplitude of the transducer input signal. The demodulated signal then passes through an active filter network to minimize any ac ripple components which are not part of the incoming data signal. This active filter, which is designed for the highest, practical frequency response permissible*, also limits the frequency response of the signal conditioner.

Two very important features about the downhole completion circuit (fig. 2) are the bridge completion resistors (R_1 and R_2) and the provision for calibration and insertion of the calibrate resistor. These circuit components are

* Pickett, Stephen F., *Development and Evaluation of Measurement Systems for Blast-Induced Motions in Buried Structures*, AFWL-TR-73-230, Air Force Weapons Laboratory, Kirtland Air Force Base, New Mexico, 1974.

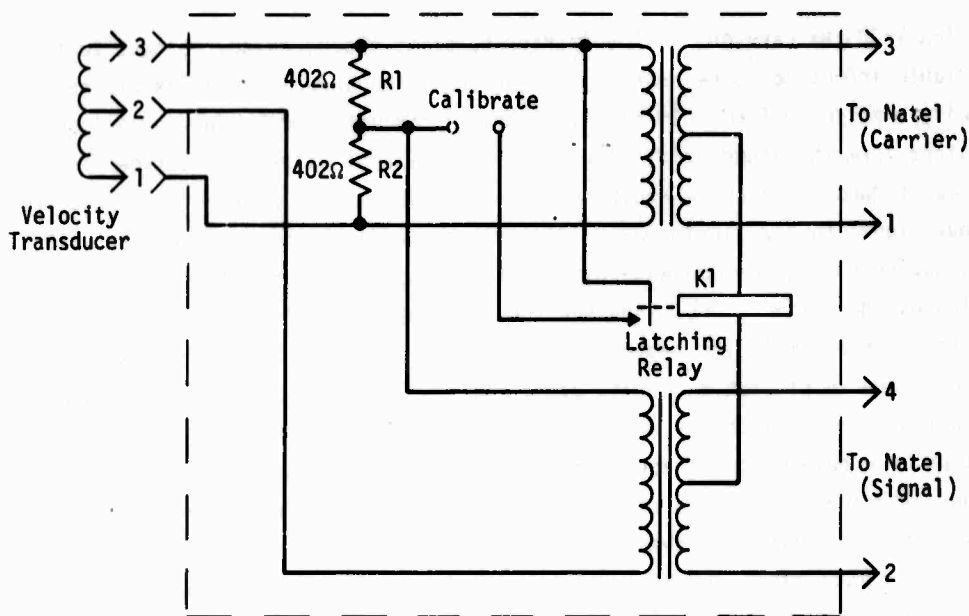


Figure 2. Downhole Completion Circuit for Natel System

normally an essential part of most signal conditioners. However, there are certain advantages in having these components in close proximity to the velocity transducer, and since the downhole completion circuit is placed near the transducer, these advantages can be realized. Long cables used in a field test add undesirable resistance and capacitance to the bridge and calibrate circuit if the calibrate resistor and bridge completion resistors are physically located in the signal conditioner. However, if these components are located close to the velocity transducer, as they are in the downhole completion circuit, the long-cable effects are minimized. This results in more accurate data acquisition and less variable balance adjustments of the signal conditioner.

b. Crescent Model 8303

The Crescent Model 8303 is another carrier amplifier type signal conditioner, basically similar to the Natel Model 2088M. However, there are some major differences between the two carrier amplifier systems.

Two Model 8303s were used in this test series--a 3-kHz carrier system and a 3-kHz carrier system modified to perform as a 10-kHz system. Other than this difference, they performed basically the same.

The Crescent Model 8303 does not have an individual reference phase control. Instead, it has a balance control which is capable of nulling out an incoming residual signal to provide a zero output voltage. The passband of the 3-kHz carrier system was set for 300 Hz and that of the 10-kHz carrier system was set for 1.5 kHz.

c. CEC Model 1-113B

The CEC Model 1-113B carrier amplifier is also basically similar to the Natel Model 2088M. It is a vacuum tube operated system with a reference phase control that can be adjusted from nearly zero to approximately 120° in reference to the carrier. The carrier frequency is 3 kHz. It also has long-line capability and a modified ring-type demodulator. The passband of the system is 0 to 600 Hz.

d. CEC Model 1-118

The CEC Model 1-118 3-kHz carrier amplifier signal conditioner is also basically similar to the Natel Model 2088M. However, it is a vacuum tube operated system with no reference phase control. It does have a reactance balance control which shifts the phase by 90° . It develops a balancing voltage in quadrature with the carrier and balances out reactive imbalance voltage from the velocity transducer. The passband of the system is 0 to 600 Hz.

e. WES Model

The WES carrier amplifier system is again basically similar to the Natel Model 2088M. It has a 3-kHz carrier signal, is completely solid state, and has no reference phase control. The system rise time is 0.5 msec, or approximately 700 Hz.

2. PENDULOUS TRANSDUCER

Table II lists the pendulous velocity transducers tested in this program. (Operating principles for the pendulous transducer are described in appendix I.) These transducers were filled with Dow-Corning 3000-centistoke damping oil which is frequently used in AFWL testing; this represents a nominal value between 500 and 7500 centistokes. (Transducers filled with oils of centistoke ratings less than 500 or more than 7500 are rarely used.) The use of the same centistoke value eliminates the possibility of differences between tested transducers due to different damping oil characteristics.

Damping ratio of the mechanical transduction system greatly affects both midband gain and transducer frequency passband. This ratio is determined by

Table II
PENDULOUS TRANSDUCERS TESTED

Manufacturer	Model	Serial No.	Signal Conditioner	Sensitive Axis
Cibola Scientific, Inc.	CSV-V-25	001	Carrier	Horizontal
		002	Demodulator	
		003	(External)	
Consolidated Electroynamics Corp.	364137	2003	Carrier	Horizontal
		2004	Demodulator	
		2005	(External)	
	364142	2119		Vertical
		2120		
		2121		
Sparton Southwest, Inc.	601-M (Aluminum)	2881	Carrier Demodulator (External)	Horizontal
		2882		
	601-M (Brass)	3594		
		3595		Vertical
		3596		
		3597		
		3598		Vertical
		3599		
	604	3603		Vertical
		3607		
	602	3592	Frequency Modulator (External)	Horizontal
		3593		

pendulum/case clearances and the viscosity of the damping oil, which users are free to select. Generally speaking, high viscosity damping oils provide a higher mechanical frequency passband, and lower sensitivity; lower viscosity damping oils yield higher sensitivities and lower frequency passbands.

Since the pendulous velocity transducer must be used in conjunction with a signal conditioner, it is important that the signal conditioner chosen have as few limitations as possible. This requirement must be met in order to adequately evaluate transducer performance. For example, it is desirable to have a signal conditioner with a high-frequency capability greater than the high-frequency cutoff, f_{CH} , of the transducers to be evaluated. If this condition does not exist, the f_{CH} observed in the data will not represent the upper frequency capability of the velocity transducer but instead will represent the upper frequency capability of the data subsystem which is composed of both the transducer and the signal conditioner.

The Natel signal conditioner was chosen. The 6-kHz carrier frequency and the 2.2-kHz frequency response of the Natel system were the determining factors in this choice. The use of this system allowed observations of the abnormalities of some velocity transducers that would not have been observed with a lower frequency response type signal conditioner.

A standard downhole completion and calibration circuit (fig. 2) was used in conjunction with the signal conditioner. Since downhole completion and calibration are available for field tests and since the Natel signal conditioner was designed to function with this circuit, it was used in all tests involving the Natel signal conditioner. The use of long lines also enabled close duplication of the field conditions during the test program.

3. LINEAR TRANSDUCER

Table III lists the linear systems tested. Since there are numerous variations in operating principles among these transducers and systems, the reader is referred to appendix I for specific information.

Table III
LINEAR TRANSDUCERS TESTED

Manufacturer	Model	Serial No.	Signal Conditioner	Sensitive Axis
EG&G	100	024	Self-Contained Carrier Demodulator System	Vertical or Horizontal
		025		
		026		
Endevco	2269-150	05	Endevco Model 4830 Integrator System	Triaxial
Setra Systems, Inc.	151	903	Self-Contained Pulse-Width Modulation System	Horizontal
		904		Horizontal
		905		Vertical
		906		Vertical

SECTION III

TESTING APPARATUS

1. HORIZONTAL SLED TRACK

The CERF horizontal velocity sled is a laboratory device for dynamic testing and calibration of accelerometers and horizontal velocity transducers. The acceleration waveforms generated in this test program approximated haversines with amplitudes of 150 to 5000 g and pulse widths from 0.25 to 0.50 msec. Thus, nominal dynamic peak velocities of 5 to 40 ft/sec were achieved. Two reference accelerometers were mounted directly on the sled and the average accelerometer data were integrated for comparison with the velocity transducer data.

The horizontal sled track (fig. 3) consists of a pneumatic impact ram, a sled track, a canister sled and inserts, a set of 1-in.-diameter solid steel rails approximately 16 ft long mounted on 6-1/8-in. centers, and instrumentation.

Various minor problems were encountered in testing with the sled track. These difficulties and the solutions are discussed in detail in appendix II.

a. Pneumatic Impact Ram

The impact ram (fig. 4) is a simple pneumatic cylinder consisting of an internal front and rear chamber. These chambers are separated by an orifice plate and a sliding piston which moves within the front cylinder only. When the front chamber is opened to an external gas pressure, the piston (located behind the gas entrance port) is forced against the orifice plate. A rubber seal prevents the front chamber pressure from escaping to the rear chamber. The area of the piston on which the front chamber pressure acts to force the piston toward the rear chamber orifice plate is four times larger than the orifice area where the rear chamber pressure acts on the piston to force it forward. Since the area differential is approximately four to one, a pressure differential of four to one can be held without forcing the piston outward. The force to drive the impact ram is obtained from a regulated pressure output from a 2000-psi nitrogen bottle.

The impact ram housing is firmly bolted to a 3-1/4-in. solid metal baseplate. Three leveling screws are mounted to the baseplate and are used to align the piston so that it strikes the center of gravity on the canister sled.

To fire the impact ram, the quick-opening solenoid valve in the front chamber is opened to atmospheric pressure. The pressure in the front chamber

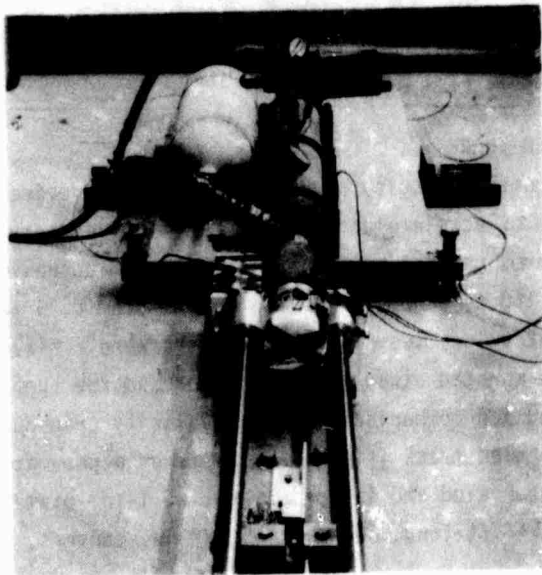


Figure 3. Horizontal Sled Track

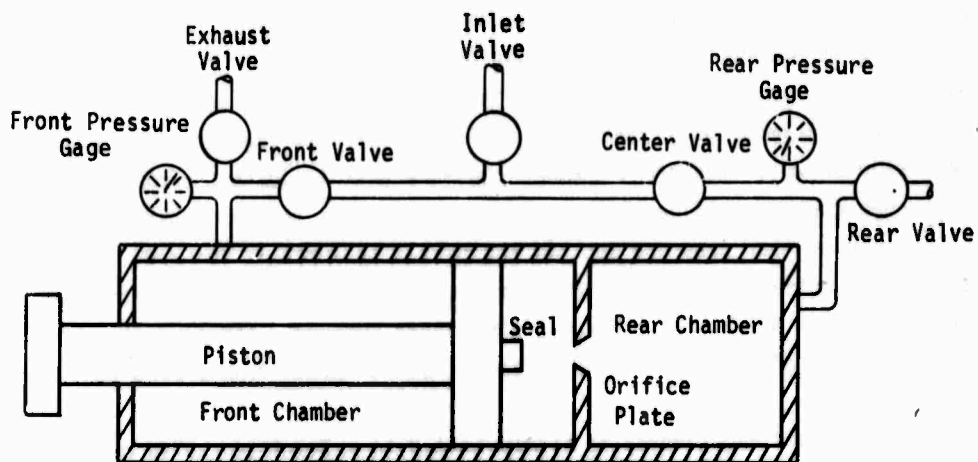


Figure 4. Pneumatic Impact Ram

drops to atmospheric pressure in approximately 0.5 sec, allowing the orifice area pressure to move the piston forward. When the orifice is opened, rear chamber pressure acts on the entire piston area. Once the piston passes the exhaust valve it works against the gas in the confined volume ahead of it and thus the piston decelerates. A reservoir is used to increase the pressure ahead of the piston; this provides an *air spring* which stops the piston and prevents it from being damaged. The cylinder is isolated from the air tank by a one-way valve which allows flow only into the tank.

The velocity and energy of the moving piston depends on the rear chamber pressure. Maximum piston velocity occurs at about 8 in. of travel. Throughout this testing program, a maximum rear chamber pressure of 80 psi and a minimum rear chamber pressure of 35 psi were used.

b. Sled Track

The sled track (fig. 5) consists of a single 16-ft channel base, two round solid 1-in.-diameter steel rails, four adjustable mounting blocks, and eight threaded adjusting studs. The channel base is bolted to a solid concrete floor. The mounting blocks and threaded studs are mounted to the base. The two

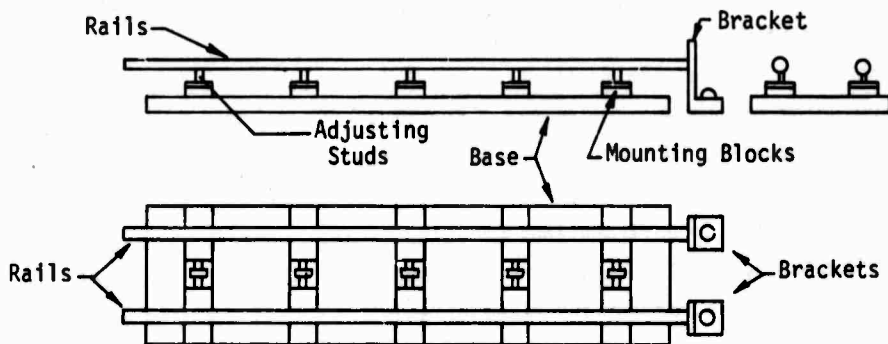


Figure 5. Sled Track

rails are attached to the threaded studs. Horizontal adjustment of the mounting blocks and vertical adjustment of the threaded studs provide leveling and correct displacement of the rails. Two brackets are bolted between the rails and the concrete floor at the end nearest the impact ram to minimize low-frequency vibration.

c. Canister Sled and Inserts

The canister sled (fig. 6) is composed of three major components: the canister, two detachable bushing housings, and a unique velocity transducer insert. The canister sled is designed for versatility, minimization of high-frequency noise generation, and ease of operation. The canister, which is compatible with a variety of velocity transducers, can be used on both the horizontal sled track and the vertical drop tower.

The bushing housings, when used as the sled on the horizontal rails, are bolted to the outside of the canister. A Teflon bushing is enclosed in each of the housings. Each bushing has indentations at the locations of the bushing adjustment bolts to keep it from sliding relative to the housings. The adjustment bolts are threaded into the housings and adjusted when the canister sled is in its starting position on the track. These bolts apply mechanical pressure to the Teflon; this provides a snug fit against the rails and tends to minimize any horizontal or vertical wobble of the canister sled. The Teflon bushings also eliminate the need for dust-collecting grease or oil on the rails. The friction force is increased by tightening these bushings. For this test program the friction force was adjusted so that the canister sled stopped approximately 3-1/2 ft from its starting position.

The canister has a large opening parallel to its vertical axis and two clearance holes on one end for mounting the reference accelerometers to the insert being used for testing. The large insert opening allows various inserts to be used in the same canister. Various inserts are needed because of the variations in the mechanical configurations of velocity transducers. The canister has three threaded holes for securing the transducer and insert to the canister. There are also four holes for the insertion of sticks of lead when the canister is used on the drop tower.

The velocity transducer is placed in the insert in its proper orientation, and then this assembly is inserted in the canister sled. Five pieces of blotter pad material (2 x 3 x 3/32 in.) are placed between the outer wall of the insert and the inner wall of the canister on the side nearest the impact

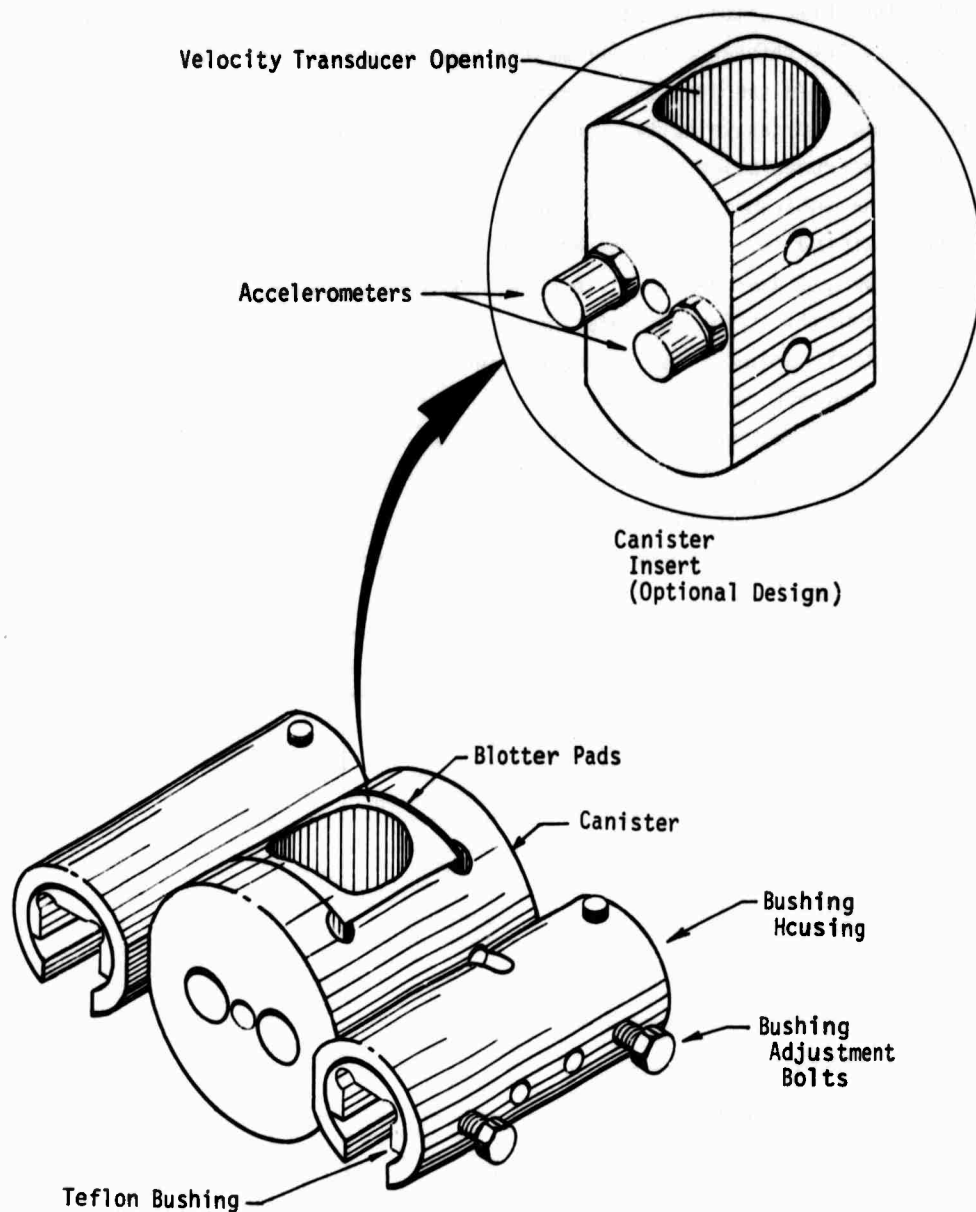


Figure 6. Canister Sled and Inserts

surface. Five additional pieces of blotter material (the same size) are placed between the outer insert wall and the inner wall of the canister on the side opposite the three velocity transducer clamp-down bolts which are tightened securely. The two reference accelerometers are mounted to the outer wall of the insert through the openings in the canister. Finally, all electrical connections are made to the velocity transducer and the reference accelerometers.

d. Instrumentation

The instrumentation used for data acquisition throughout this testing program consisted of a 14-channel FM tape recorder, an IRIG A time code generator and reader, a dual-beam oscilloscope, a Polaroid camera, an oscillograph, two charge amplifiers for the reference accelerometers, two Endevco Model 2225 reference accelerometers, and a control panel (fig. 7). The control panel consisted of an on/off switch to energize the front chamber exhaust solenoid on the impact ram, the tape recorder outputs, and a push-button calibrate switch for remote calibration of the velocity transducer signal conditioner. Other instrumentation used for the data acquisition included a digital voltmeter, a digital frequency counter, and a regulated 60-vdc supply.

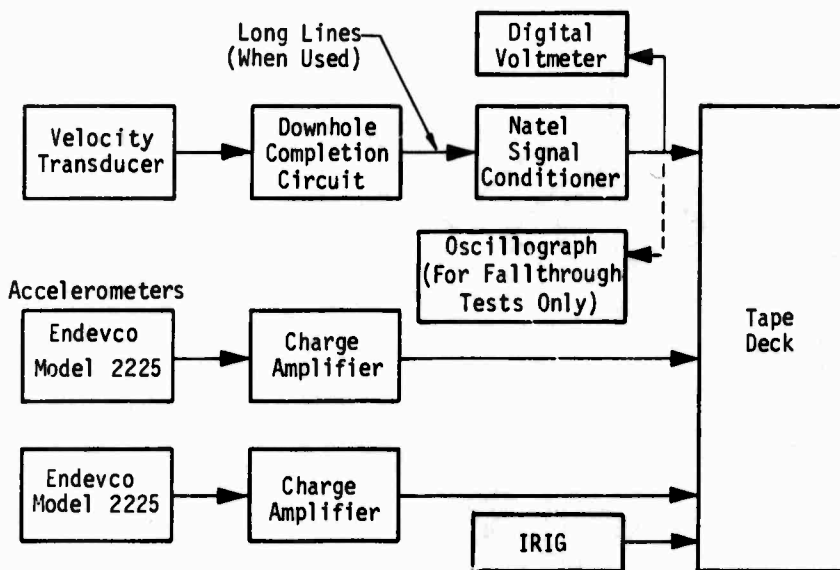


Figure 7. Data Acquisition System

Two Endevco Model 2225 accelerometers were chosen as the reference accelerometers for canister acceleration measurements. These accelerometers have an acceleration limit of $\pm 20,000$ g, a mounted resonant frequency of 80 kHz, and a frequency response ($\pm 10\%$) of 2 Hz to 15 kHz. A CERF-made, pendulum-type, drop calibrator was used to calibrate the accelerometers. A known standard laboratory accelerometer was used to compare and check the two reference accelerometers. The standard accelerometer and one reference accelerometer were dynamically tested at the same time on the same fixture, and the data were compared. The reference accelerometers were within the manufacturer's specifications and were considered to be reliable reference accelerometers for the testing program.

Except for those tests in which long cables were deliberately used, all testing of velocity transducers was performed with approximately 25 ft of Belden 8434, 4-wire shielded cable. All long-line testing was performed with 4,000 ft of Belden 8434, 4-wire shielded cable or Belden 8777, 6-wire shielded cable. The reference accelerometer cables were 10 ft long for all sled-track tests and 30 ft long for all drop-tower tests.

2. VERTICAL DROP TOWER

The CERF vertical drop tower (fig. 8), used for the vertical velocity transducer testing, consists of a drop-tower mass which is guided by wheels in two parallel tracks. The mass is raised and lowered by an electric wench and steel cables. The mass is attached to the wench/cable assembly by a solenoid-operated holding mechanism. Activation of the solenoid releases the holding mechanism, allowing the drop-tower mass to fall and strike the test object. The test object, in this case, the same canister assembly (without bushing housings) used for sled track testing, is positioned on the center of a metal ring and temporarily suspended with drafting pencil leads. The metal ring is supported 3-1/2 ft above the floor by four legs. After initial impact, the drop-tower mass velocity is arrested by foam padding material on the ring. The test object is caught in a sand box after falling about 1 ft. Although the ring support assembly is capable of sustaining drops of 6 ft or more, drop heights used in this test were, generally speaking, 30 in. or less.

Since the drop tower is located only 12 ft from the sled track, the sled-track instrumentation was used for the vertical drop-tower testing as well. This was considered absolutely necessary to maintain data consistency throughout the

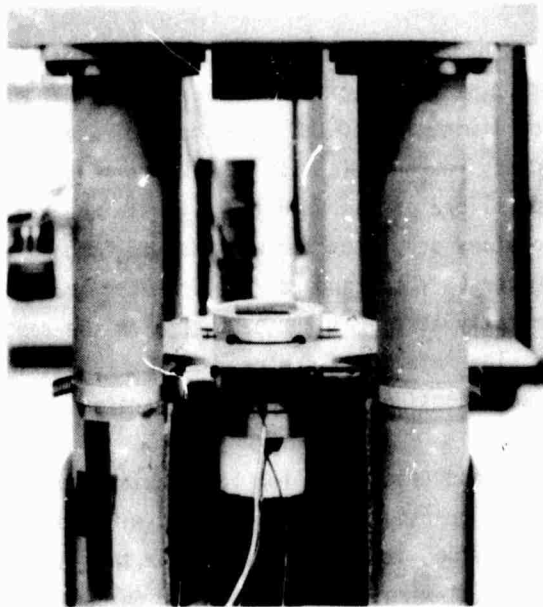


Figure 8. Vertical Drop Tower

testing program. The only electrical difference between the sled-track and the drop-tower setup was an additional 30 ft of RG/58 coaxial cable for each of the reference accelerometers. Since the signal conditioners were charge amplifiers, the reasonably short (30 ft) cables had no noticeable effect on the data.

SECTION IV TEST PLAN

1. TRANSDUCER TESTS

Various types of velocity transducers were tested in sets of three. Each of the identical samples in a set was subjected to one of three specific series of tests (table IV). Samples 1, 2, and 3 were used for low- and high-g-level acceleration (test series 1), high-g-level cross-axis acceleration (test series 2), and low-g-level acceleration, short and long line (test series 3), respectively. Generally this was the test plan. However, in several cases, only two sample velocity transducers of a particular type were available. Therefore, one test series could not be performed unless one sample was subjected to two of the test series. Testing in this case was performed in the following manner: Sample transducer 1 was subjected to test series 1 and sample 2 was subjected to test series 3. If sample 1 showed no damage or degradation of its signal output, then it was reused for test series 2; if the transducer was not usable, test series 2 was run on sample 3 if that transducer had not been damaged. If both transducers were damaged, test series 2 was not run*. The 1- and 2-g fall-through tests (table IV) were applicable to the pendulous velocity transducers only. These tests were performed in order to determine the scale factor relating the parameter of interest (velocity) to the output velocity analog (volts) to determine the value of a shunting calibration resistor to yield a signal output equivalent to a desired case velocity input.

a. Low- and High-g-Level Acceleration (Test Series 1)

All sample 1 velocity transducers had the following tests performed on them in the following sequence: (1) a static fallthrough (calibration) test to record linearity and to determine an electrical calibrate resistor value for the dynamic tests, (2) a low-g-level dynamic test using an input of 1,000 g at a nominal pulse width of 0.4 msec, (3) a high-g-level dynamic test using an input of 4,000 g at a nominal pulse width of 0.4 msec. (This test provided data relating to velocity transducer rise-time characteristics, overshoot, output (in ft/sec), anomalies due to high-g-level inputs, and possible transducer damage.), (4) another low-g-level dynamic test using an input of 1000 g at a

*Test series 2 was chosen as the last series of tests because of the severity of the inputs.

Table IV
TRANSDUCER TEST SERIES

Test No.	Test Series 1	Test Series 2	Test Series 3
1	Fallthrough (Calibration)	Fallthrough (Calibration)	Fallthrough (Calibration)
2	1000 g (Low Level)	4000 g - 30° (High Level)	Exponential Fallthrough
3	4000 g (High Level)	Fallthrough (Calibration)	1000 g (Short Lines)
4	1000 g (Low Level)	4000 g - 90° (High Level)	Fallthrough (Short Lines)
5	Fallthrough (Calibration)	Fallthrough (Calibration)	Fallthrough (Long Lines)
6		4000 g - Normal (High Level)	1000 g (Long Lines)
7		Fallthrough (Calibration)	Fallthrough (Long Lines)

nominal pulse width of 0.4 msec. (This test provided a comparison with test 2 so as to determine any dynamic change in the velocity transducer after it was subjected to the high-g-level input.), and (5) another static fallthrough for comparison with test 1 to verify that the transducer had not changed or been damaged.

b. High-g-Level, Cross-Axis Acceleration (Test Series 2)

All sample 2 velocity transducers had the following tests performed on them in the following sequence: (1) a static fallthrough (calibration) test to record linearity and to determine an electrical calibrate resistor value for the dynamic tests, (2) a high-g-level dynamic test using an input of 4,000 g at a nominal pulse width of 0.4 msec on a transducer which was positioned 30° off the normal axis. (This test provided information relating to electrical and mechanical damage.), (3) another static fallthrough test for comparison with test 1 to verify that the transducer had not been damaged during the previous dynamic test, (4) a high-g-level dynamic test using an input of 4,000 g at a

nominal pulse width of 0.4 msec on a transducer which was positioned 90° off the normal axis. (This test also provided data relating to possible physical damage to the transducer under severe conditions.), (5) another static fall-through test for comparison with tests 1 and 3 to verify that the transducer was not damaged by the previous dynamic test, (6) a high-g-level dynamic test using an input of 4,000 g at a nominal pulse width of 0.4 msec on a transducer which was positioned normally. (This test provided data relating to transducer performance during a high-g-level, normal-axis test after the transducer was subjected to high-g-level, cross-axis tests.), (7) a static fallthrough test to determine possible transducer damage or change by comparing these data with that from tests 1, 3, and 5.

c. Low-g-Level Acceleration, Short and Long Line (Test Series 3)

All sample 3 velocity transducers had the following tests performed on them in the following sequence: (1) a static fallthrough (calibration) test to record linearity and to determine an electrical calibrate resistor value for the dynamic test, (2) a static exponential fallthrough test* to determine droop and low-frequency response, (3) a low-g-level dynamic test using an input of 1,000 g at a nominal pulse width of 0.4 msec. (This test was run with 25-ft lines and the data were used as a reference for the long-line test.), (4) another static fallthrough test with short lines for comparison with test 1 to check for possible transducer damage from the previous dynamic test, (5) a static fallthrough test with long lines (4,000 ft of Belden cable) attached to the transducer, (6) a low-g-level dynamic test using long lines and an input of 1,000 g at a nominal pulse width of 0.4 msec. (This test was compared to test 3 to determine the effects of long lines on the velocity transducer data.), (7) a static fallthrough test using long lines to compare against test 5 to check for possible transducer damage from the previous dynamic test.

2. DAMPING FLUID TESTS

In addition to the velocity transducer testing previously mentioned (test series 1 through 3), a brief test series was run on five CEC horizontal transducers to determine droop and passband using five different oil fills--500, 1000, 2000, 5000, and 7500 centistokes.

*The static exponential fallthrough test was performed only on the overdamped transducers.

3. SYSTEM FAST RISE TIME TESTS

System fast rise time tests were performed to determine rise times and upper frequency limits of the various signal conditioner systems available for compatible pendulous velocity transducers.

SECTION V

TEST PROCEDURES

1. FALLTHROUGH TESTS

a. 1- and 2-g Fallthrough

The procedure for obtaining static fallthrough data for the pendulum-type horizontal velocity transducers was as follows. The system instrumentation was connected as shown in figure 9. The velocity transducer was placed in a vertical position on the base of the fallthrough fixture and allowed to stabilize for 5 to 10 min. The phase and amplitude controls of the signal conditioner were then adjusted for a minimum output reading with the signal gain control at maximum. The gain sensitivity was reduced to a minimum and the calibrate switch on the calibrate box (fig. 10) was initiated. (A 10- or 20-k Ω calibrate resistor was used.) The gain sensitivity was increased until the output panel meter indicated approximately one-quarter of full scale. The reference phase was then adjusted for a maximum output reading on the digital voltmeter. (As an option the transducer may be tilted approximately 6° and the reference phase adjusted for maximum output. After this the transducer must be allowed to stabilize in the vertical position.) With the oscillograph running at 0.25 in./sec and the resistor calibrate box switch in position 1, the signal conditioner calibrate switch was initiated and held for several seconds. The resistor calibrate box switch was moved to position 2 and again the signal conditioner calibrate switch was initiated. This procedure was repeated for the remaining eight calibrate switch positions. The oscillograph was stopped and the velocity transducer was placed in the fallthrough fixture using a strong magnet to hold the pendulum in the extreme uppermost position (fig. 11). With the oscillograph running at 4 in./sec, the magnet was rapidly pulled away from the transducer and when the pendulum hit the bottom of the outer case, the oscillograph was stopped. The following information was added to the oscillograph recording paper: (1) value of calibrate resistors, (2) maximum positive and negative outputs, (3) ambient room temperature, (4) paper speed, and (5) velocity transducer and signal-conditioning information.

The vertical velocity transducer static fallthrough procedure was almost identical to that for the horizontal transducers except that the mechanics of the test were different because of the 1-g compensating spring in the velocity transducer. The transducer was placed in the fallthrough fixture as shown in

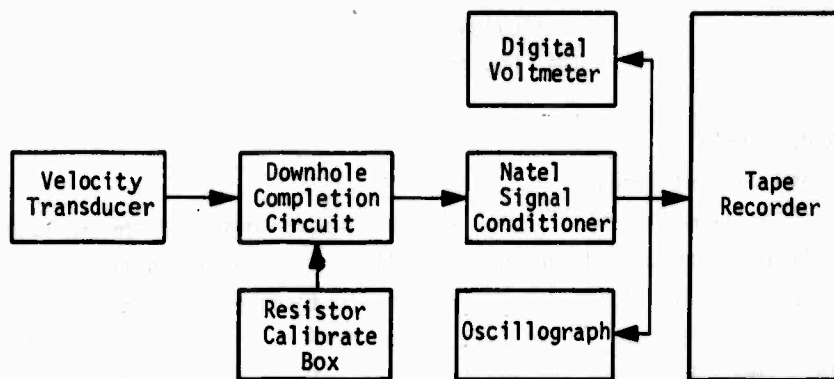


Figure 9. System Instrumentation for Fallthrough Tests

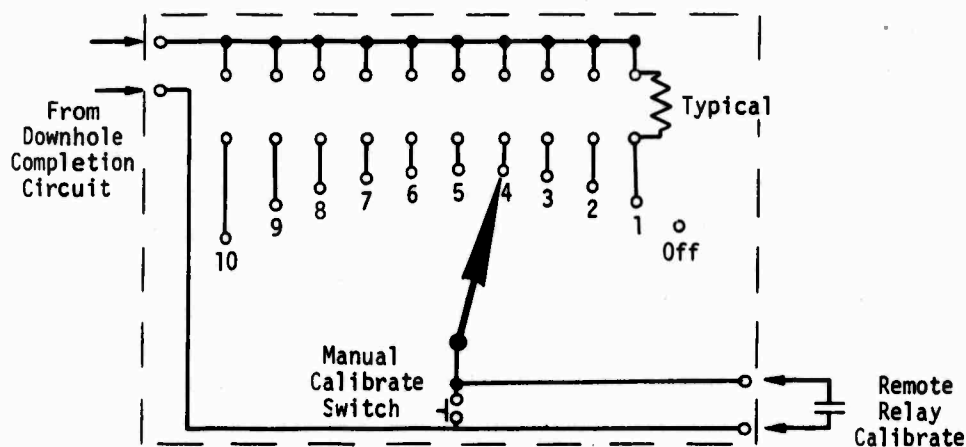


Figure 10. Resistor Calibrate Box

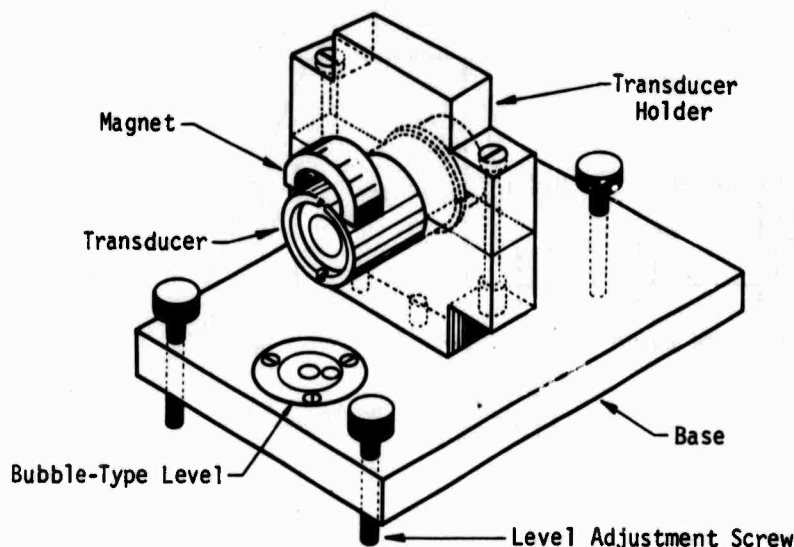


Figure 11. Fallthrough Fixture with Transducer

figure 11 for stabilization and adjustment of the signal conditioner. After the electrical calibration, a magnet was placed against the bottom side of the velocity transducer outer case, and then the upper stand of the fixture was reversed 180°. The magnet was held firmly against the transducer outer case so that the pendulum would not fall to the opposite side of the transducer case.

A sample fallthrough oscillograph record is shown in figure 12. What value calibrate resistor to use for a specific ft/sec output of a pendulum velocity transducer was determined as follows. Line 1 (fig. 12) was drawn from the zero output baseline through the fallthrough curve. Exactly 4 in. (chart paper speed = 4 in./sec) from the fallthrough curve and baseline intersection, the vertical line 2 was drawn. The horizontal line 3 was then drawn at the intersection of line 2 and the fallthrough curve. The vertical distance between lines 1 and 3 was then measured. Dividing this dimension (1.61 in. in this case) into 32.2 ft/sec (for vertical transducers, 64.4 ft/sec was used), one obtains 20 ft/sec/in. For a calibrate value of 10 ft/sec, a calibrate level of 0.5 in. (15 k Ω) was chosen. This value was obtained by multiplying 0.5 in. by 20 ft/sec/in. In the sample plot (fig. 12), a 15-k Ω resistor equals 0.5 in. of

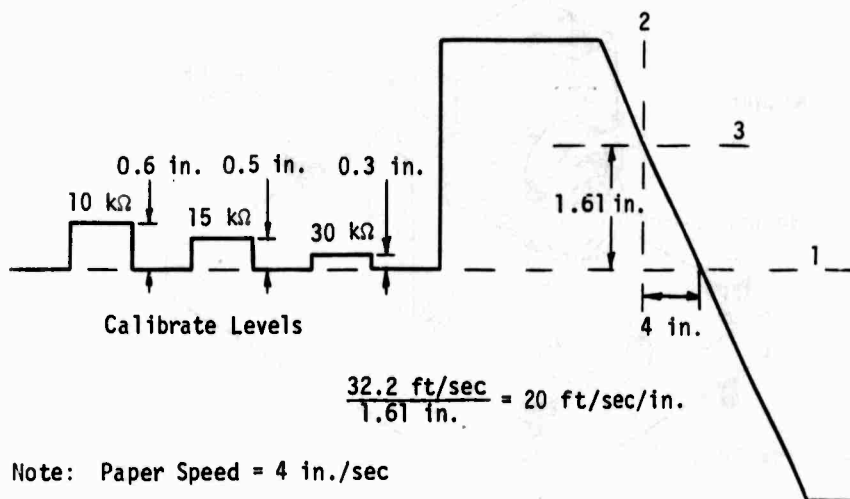
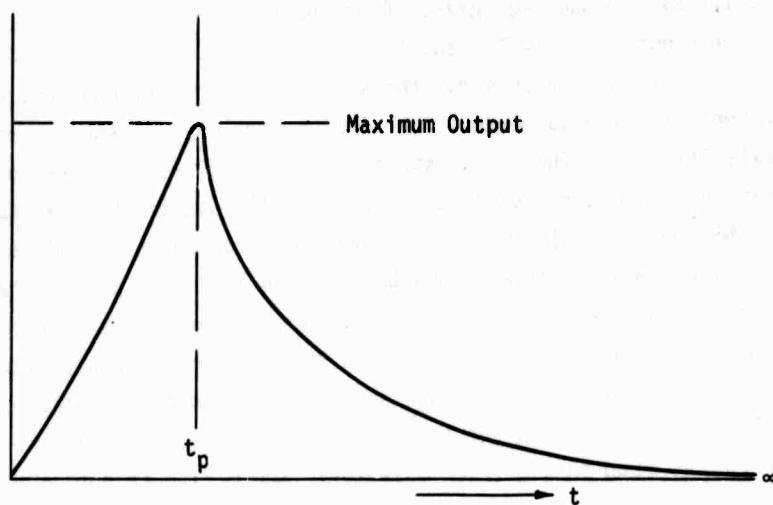


Figure 12. Sample Fallthrough Oscillograph Record

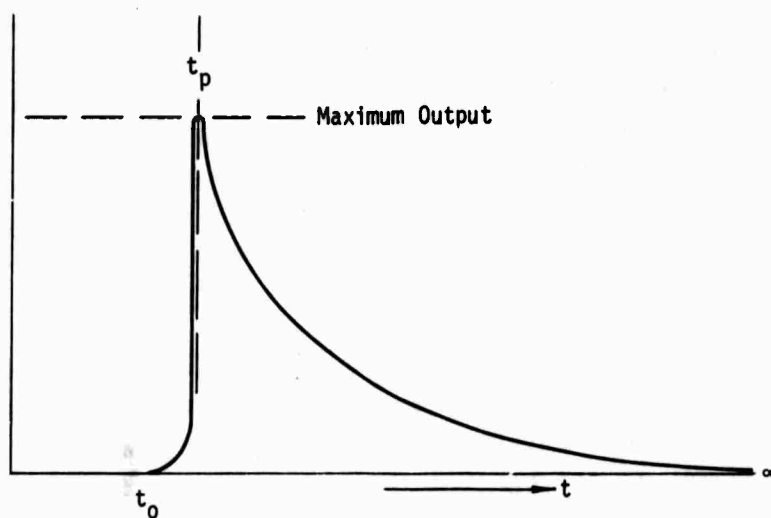
displacement on the oscillograph record; this is equivalent to a velocity transducer output of 10 ft/sec for this particular transducer. A 0.6-in. (10-k Ω) displacement on the oscillograph record would represent 12 ft/sec (0.6 x 20). If the signal conditioner gain is linear and is either increased or decreased, this calibrate resistor would still represent the same ft/sec output for this transducer. For a theoretical justification refer to appendix III.

b. Exponential Fallthrough

The exponential fallthrough tests were used to determine the droop and the frequency cutoff points for both the linear and pendulous velocity transducers. The output of an unexcited (nonmoving case) velocity transducer after its seismic mass (pendulum) is offset and released at t_p is exactly the same as that from the same transducer when the case experiences a step velocity from t_p to ∞ . t_p is the time at which the transducer registers a peak velocity and it occurs after t_0 , the time at which case step velocity occurs (fig. 13). Therefore, the data generated by the exponential fallthrough test are exactly the same as the data (after the peak) that the same transducer generate when a sustained step input velocity is experienced. For a theoretical justification



(a) Exponential Fallthrough



(b) Step Velocity Input

Figure 13. Transducer Response

refer to appendix IV.

In addition, data from the exponential fallthrough test may be used to determine h , the system damping ratio. (See appendix V.)

(1) Pendulous Velocity Transducers

The test fixture used for the exponential fallthrough test of the horizontal pendulous transducer was the same as that used in the 1- and 2-g fallthrough tests (fig. 11). The instrumentation was connected as shown in figure 9. The velocity transducer was placed in a vertical position on the base of the fallthrough fixture and allowed to stabilize, both mechanically and electrically. The signal conditioner was then balanced as in the 1- and 2-g fallthrough procedure. A calibrate resistor representing approximately 75 percent of full-scale output was used for the electrical calibration. The signal conditioner gain was set for a 1.0-v output when the calibrate button was depressed. The tape recorder and oscillograph (at a paper speed of 0.25 in./sec) were started, and at 15 sec (as read on the IRIG generator), the calibrate button was depressed for 1 sec. At 27 sec, a magnet was placed against the outer case of the velocity transducer so that the pendulum was attracted to the magnet. The signal conditioner output was checked to ensure that it was of the same polarity as the calibrate output. The magnet was held stationary against the case until the velocity transducer output reached 1.0 v (approximately 1 sec), then the magnet was rapidly moved away from the velocity transducer. Data were continuously recorded until the IRIG generator read 50 sec, the tape recorder and oscillograph were stopped, and all necessary data were recorded.

The procedure for the vertical pendulous transducers was exactly the same as that for the horizontal transducers, except that the vertical transducer was stabilized and tested on the fallthrough fixture in a horizontal position.

(2) Linear Velocity Transducers

Since the internal moving masses of the several different types of linear velocity transducers were not of the pendulum type and were not attracted by a permanent magnet, a slightly different procedure for accomplishing exponential fallthrough was required. Even though the method was different, the same type of test results were obtained.

The only difference between the pendulum-type method and the nonpendulum-type method was in the mechanical procedures. Instead of using a magnet to move the internal mass, the mass was moved by physically rotating the

transducer until the output reached approximately 75 percent of maximum and then rapidly placing the transducer on the flat, level surface of the fall-through fixture base. In this way, the internal mass falls back to its neutral position at an exponential rate.

2. SYSTEM FAST RISE TIME TESTS

System instrumentation for the fast rise-time tests of the various signal conditioners is shown in figure 14. The same pendulum-type velocity transducer was connected to the particular signal conditioner under test. This velocity transducer was stabilized in its mechanically neutral state and was then electrically balanced. The output step function of the signal conditioner was recorded on magnetic tape.

The step function was generated by a mercury relay and a calibrate resistor. The mercury relay used to switch a calibrate resistor in the signal conditioner circuit has a rise-time capability of 9 nsec or less. Because the signal conditioner rise time is much slower than the mercury relay rise time, the input function is considered, for all practical purposes, a step. The

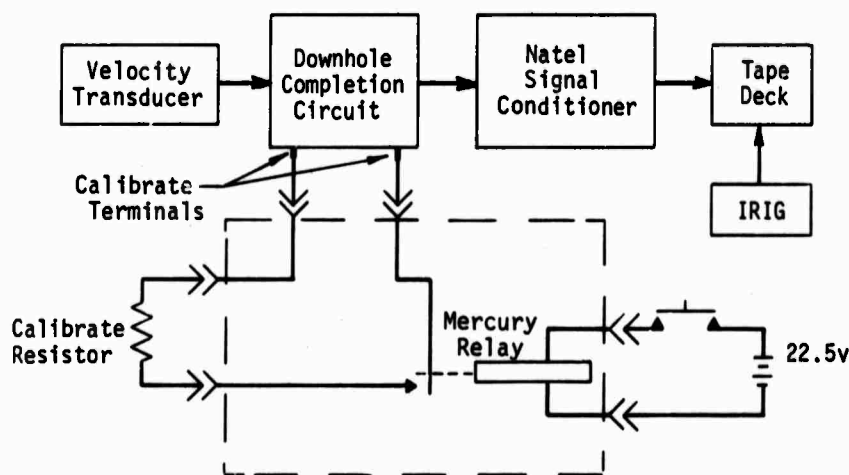


Figure 14. System Instrumentation for Fast Rise-Time Tests

calibrate resistor used during these tests was of the carbon type rather than the wirewound type. The carbon resistor was used to prevent the rise-time degradation caused by the inductance of a wirewound resistor.

SECTION VI EVALUATION TECHNIQUES

1. DROOP

Droop, δt , in this report is defined as the elapsed time, during transducer response to a step input, between peak output (occurring at t_p) and the first point at which the transducer output equals one-half the peak output (occurring at $t_p + \delta t$) where t_p is the time at which peak output occurs.

Exponential fallthrough data were used to determine droop for all compatible velocity transducers, since the output from exponential fallthrough provides the necessary step-response data required (appendix IV). Figure 15 shows how δt was determined for these transducers.

In terms of application, δt is the length of time that a transducer's velocity output is within 50 percent of the actual constant-velocity input applied to the transducer with initial transducer output (at t_p) equal to the constant-velocity input.

2. LOW- AND HIGH-FREQUENCY CUTOFF

a. Exponential Fallthrough Determination of f_{CH} and f_{CL}

The low-frequency cutoff, f_{CL} , was also determined for the transducers from exponential fallthrough data (appendix V). Determining h from exponential fallthrough and knowing $\omega_n/2\pi$, one may calculate f_{CL} .

$$f_{CL} = \frac{\omega_n}{2\pi} (\sqrt{h^2 + 1} - h)$$

Also, f_{CH} may be calculated.

$$f_{CH} = \frac{\omega_n}{2\pi} (\sqrt{h^2 + 1} + h)$$

These calculations are good only if the transducer responds as predicted by the mathematical model and, in particular, if h and ω_n are both constant. There is evidence based on recent AFWL velocity transducer testing to indicate that h , for at least the pendulous-type transducer, is not constant and is a nonlinear function of the angular velocity of the pendulum, $\dot{\theta}$. For $0 \leq |\dot{\theta}| \leq 0.5$ rad/sec, however, h is relatively constant.

Since $\dot{\theta}$ relative to the case during exponential fallthrough was

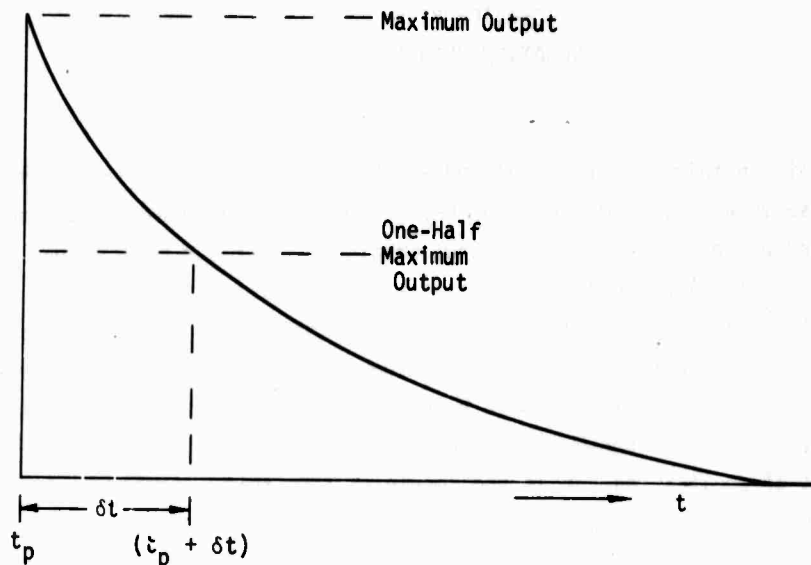


Figure 15. Droop Determination from Exponential Fallthrough Data

extremely low and well below the critical maximum angular velocity, $\dot{\theta}_m$, h was considered to be constant during the exponential fallthrough tests. Since ω_n in seismic systems is governed by ratios and/or multiples of constants, it was reasonable to assume that ω_n was a constant.

If the transducer is excited with a case velocity input at a constant frequency of f_{CL} , it would be impossible to exceed the $|\dot{\theta}_m|$ limit even if the pendulum were to swing from case stop to case stop. However, if the transducer is excited with a case velocity input at a constant frequency of f_{CH} (calculated from exponential fallthrough data), the maximum $|\dot{\theta}|$ in the transducer response could exceed $|\dot{\theta}_m|$.

If the transducer were excited with an input such that

$$\theta = \frac{A}{\omega} \sin \omega t$$

and $\dot{\theta} = A \cos \omega t$ (making the peak-to-peak value of $\dot{\theta}$ a constant regardless of frequency, $\omega/2\pi$), and if it is also stipulated that $|A| \leq |\dot{\theta}_m|$, we have established that h is a constant regardless of ω and that f_{CH} (calculated from

exponential fallthrough data) is indeed the upper cutoff frequency of the velocity transducer under these conditions. From this it should be obvious that if h is a nonlinear function of $\dot{\theta}$, f_{CH} will be heavily dependent on any $\dot{\theta}$ encountered in any test used to determine f_{CH} . Tests such as the exponential fallthrough encounter only one h value throughout the test, while tests such as step velocity inputs may encounter a broad range of h values which includes the one unique to exponential fallthrough. Therefore, it is reasonable to expect different f_{CH} depending on the different $|\dot{\theta}|$ values encountered in different tests.

b. Fast Fourier Transform Determination of f_{CH}

Since both transducer and signal conditioner outputs and inputs were recorded simultaneously, both functions were available for time history comparisons. Of particular interest were input/output history comparisons where the input function consisted in part of long durations where the input was constant with respect to time (i.e., the step-response output from exponential fallthrough tests) and where the input function changed rapidly with respect to time (i.e., fast rise time sled track, drop tower, and signal conditioner system step inputs). From these tests, droop and rise-time capabilities may be determined to provide useful evaluation parameters for time domain transducer or signal conditioner system performance.

In the frequency domain, both high- and low-frequency cutoffs were calculated from data and both had acceptable passband limits if certain conditions were met. However, the f_{CH} determined from exponential fallthrough data for seismic transducers may not be unique. To determine f_{CH} for a transducer operating under conditions where h may not be constant, another method must be employed--fast Fourier transform modulus ratio method.

The input and output functions of a system may be transformed into complex frequency functions by the Fourier integral transforms

$$G(j\omega) = \int_{-\infty}^{\infty} g(t) e^{-j\omega t} dt$$

$$C(j\omega) = \int_{-\infty}^{\infty} c(t) e^{-j\omega t} dt$$

where $g(t)$ is the input function described in the time domain, $G(j\omega)$ is the input function described in the complex frequency domain, $c(t)$ is the output or response function described in the time domain, and $C(j\omega)$ is the output function described in the complex frequency domain. The transfer function, $H(j\omega)$, can be defined as the ratio of the output transform to the input transform.

$$H(j\omega) = \frac{C(j\omega)}{G(j\omega)}$$

To compute the functions $C(j\omega)$ and $G(j\omega)$, the Cooley-Tukey fast Fourier transform algorithm was used*.

The magnitude (modulus ratio) may be calculated and plotted.

$$|H(j\omega)| = \frac{|C(j\omega)|}{|G(j\omega)|}$$

The phase differential, $H(\phi)$, may also be plotted.

$$H(\phi) = \arctan \frac{\text{Im}C(j\omega)}{\text{Re}C(j\omega)} - \arctan \frac{\text{Im}G(j\omega)}{\text{Re}G(j\omega)}$$

The modulus ratio, $|H(j\omega)|$, may then be used to determine f_{CL} and f_{CH} .

$$|H(j\omega_c)| = \frac{|C(j\omega_c)|}{|G(j\omega_c)|} = 0.707$$

when $\omega = 2\pi f_{CL}$, or $\omega = 2\pi f_{CH}$.

(1) Transducer Fast Rise Time Data

The data generated from velocity transducer testing on the sled track and drop tower were used to determine f_{CH} for the transducers tested. Typical data from these tests are shown in figure 16. For compatibility with the Cooley-Tukey fast Fourier transform process, it is essential that the input and output time-domain data start and end at the same velocity. The data, therefore, were modified with artificial inputs and outputs originating at t_f . This yielded the input and output patterns shown in figure 17. The two artificial

*Schulz, G., *Method of Transfer Function Calculation and Distorted Data Correction*, AFWL Technical Report, Air Force Weapons Laboratory, Kirtland Air Force Base, New Mexico, to be published.

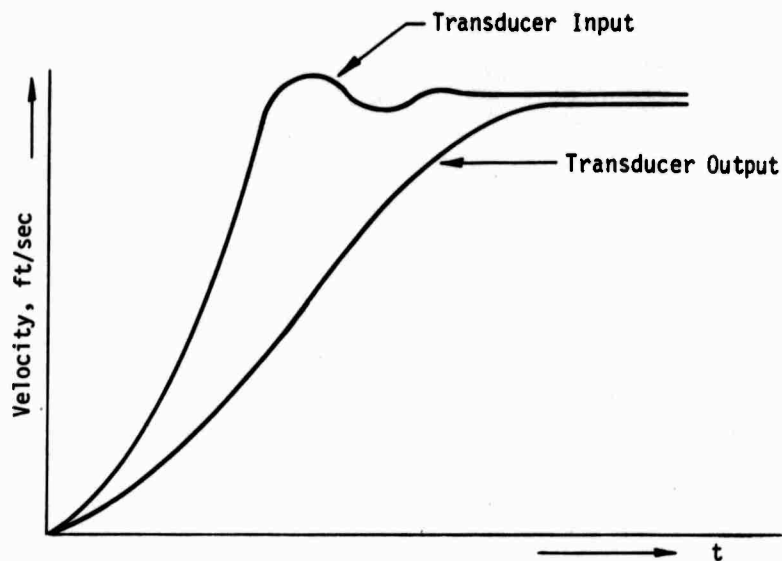


Figure 16. Typical Velocity Transducer Input and Output

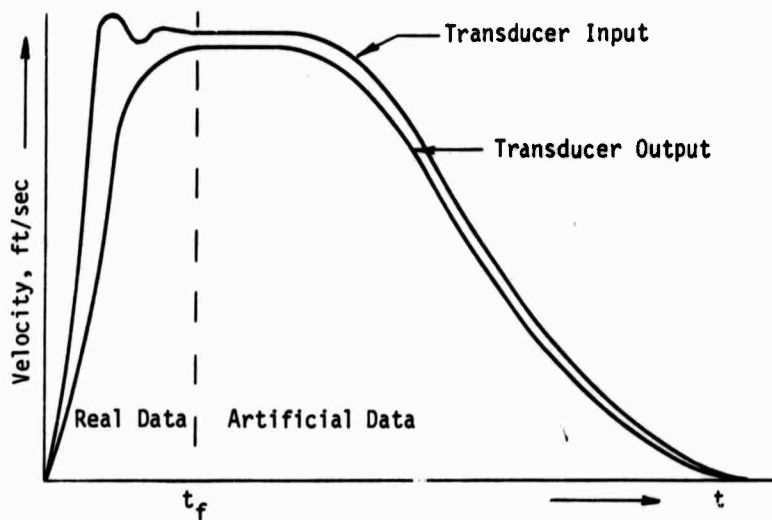


Figure 17. Velocity Transducer Input and Output with Artificial Haversine Terminations

inputs began at t_f such that

$$\left. \frac{dV_I}{dt} \right|_{t=t_f} = \left. \frac{dV_O}{dt} \right|_{t=t_f} = 0$$

where

V_I = input velocity

V_O = output velocity

A 7-Hz haversine function was used for both artificial functions.

$$V_I(\text{artificial}) = \frac{V_I|_{t=t_f}}{2} [1 - \cos 14\pi(t - t_f + 1/14)]$$

$$0 \leq t - t_f \leq 1/14$$

$$= 0 \text{ otherwise}$$

$$V_O(\text{artificial}) = \frac{V_O|_{t=t_f}}{2} [1 - \cos 14\pi(t - t_f + 1/14)]$$

$$0 \leq t - t_f \leq 1/14$$

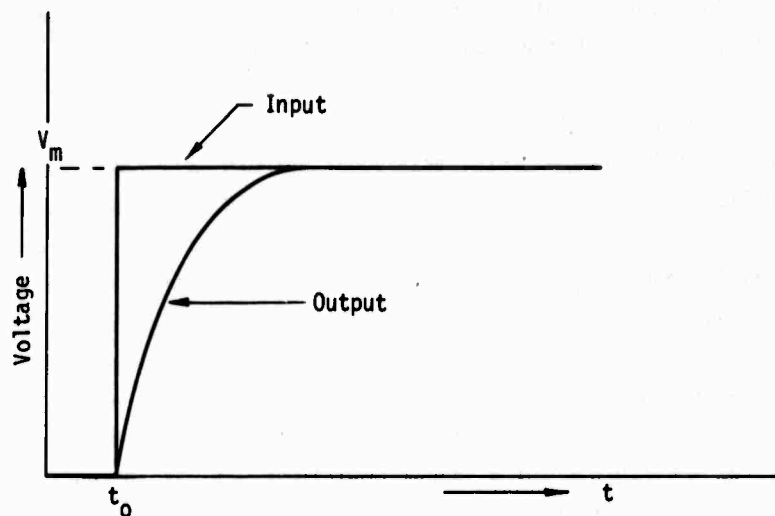
$$= 0 \text{ otherwise}$$

The 7-Hz haversine extension was chosen because it is near enough to the natural frequency of all overdamped velocity transducers to be considered well within the transducer passband, because the time from peak artificial input to zero artificial input is not extremely long compared to transducer use times, and to reduce the total number of FFT points calculated while still providing an adequate sampling rate. (Justification for using this artificial extension is given in appendix VI.)

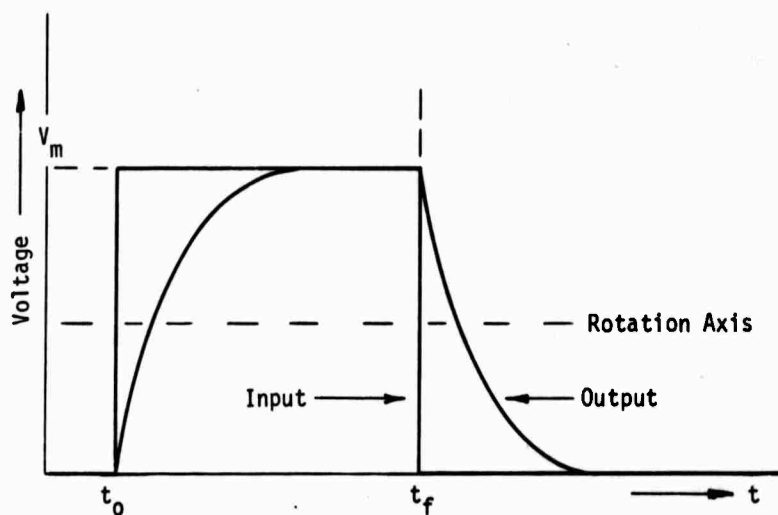
(2) Signal Conditioner Step-Input Response

Typical signal conditioner input and output data are shown in figure 18a. Again at t_f , such that

$$\left. \frac{dV_I}{dt} \right|_{t=t_f} \approx 0 \approx \left. \frac{dV_O}{dt} \right|_{t=t_f}$$



(a) Real Data



(b) Folded Real Data Termination

Figure 18. Typical Signal Conditioner Input and Output

both input and output functions were rotated an axis at level $V_m/2$ and advanced $t_f - t_0$ time units (fig. 18b). This process is commonly called *folding*, data in this form are compatible with the fast Fourier transform process*.

3. 1- AND 2-g FALLTHROUGH

During 1- and 2-g fallthrough tests, transducer outputs were observed as the pendulum traveled between its mechanical limits (fig. 19). It is easy to determine both the time at which pendulum travel starts, t_0 , and the time at which pendulum travel ceases, $t_0 + \Delta t$. Δt is the stop-to-stop travel time of the transducer. In addition to using the fallthrough data to establish calibration levels, two aspects of fallthrough repeatability may be observed to determine changes in transducer properties. By comparing Δt before and after a dynamic test, certain important observations may be made. If trace 1 in figure 20 is a pretest fallthrough of a sample transducer, Δt_1 is the corresponding pretest stop-to-stop travel time; if trace 2 is the posttest fallthrough, Δt_2 is the corresponding posttest stop-to-stop travel time. Note that when $\Delta t_1 \neq \Delta t_2$ (as is the case here), the indication is that the transducer has undergone a mechanical change during the test. The changes which increase Δt could be any of the following or any combination thereof:

- (1) an increase in the total stop-to-stop distance,
- (2) an increase in damping oil viscosity,
- (3) a decrease in the natural frequency of the pendulum,
- (4) a change in pendulum/housing clearance,
- (5) an increase in suspension friction throughout part of the stop-to-stop travel.

If there is no change in the ambient temperature, it is highly unlikely that changes (1), (2), or (3) could occur because of the nature and construction of the transducer; changes (4) and (5) would seem to be more likely to occur. Although changes in Δt could be due to any of the reasons given, it is most likely that suspension changes occurred (i.e., either suspension friction changes or pendulum/case relative position changes). The usefulness of fallthrough stop-to-stop travel time observation before and after testing was thus

*Schulz, G., *Method of Transfer Function Calculation and Distorted Data Correction*, AFWL Technical Report, Air Force Weapons Laboratory, Kirtland Air Force Base, New Mexico, to be published.

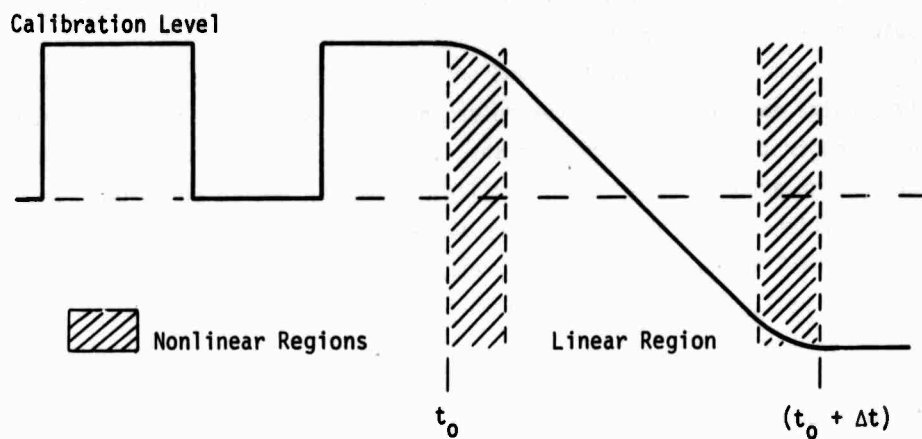


Figure 19. Pendulous Transducer 1-g Fallthrough Output

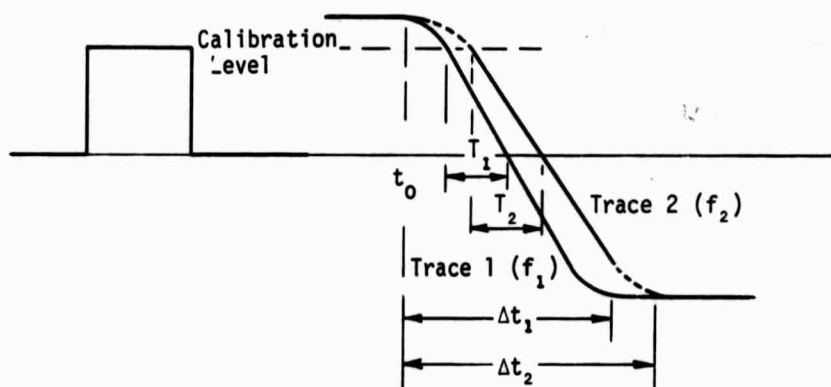


Figure 20. Pretest and Posttest 1-g Fallthrough (Example 1)

established. Obviously, two fallthroughs may have the same Δt but may also have different symmetries within the Δt interval. In this case, it is evident that suspension changes did occur.

Further examination of pretest and posttest fallthrough calibration data may give additional evidence of transducer changes. Again referring to figure 20 and noting that because of the increase in Δt after testing the transducer has either increased in suspension friction or damping due to pendulum/case relative position (as established by the suspension system), we can examine the calibration level equivalent for both pretest (trace 1) and posttest (trace 2) fallthrough. For pretest data, the calibration level equivalent is

$$ngT_1 \text{ in ft/sec}$$

For posttest data, it is

$$ngT_2 \text{ in ft/sec}$$

where

$n = 1$ for a horizontal transducer

$n = 2$ for a vertical transducer

T_1 = time required during pretest fallthrough for transducer output to go from calibration level to zero

T_2 = time required during posttest fallthrough for transducer output to go from calibration level to zero

Notice that when both traces have identical symmetry

$$f_1\left(\frac{\Delta t_1}{\Delta t_2} t\right) = f_2(t)$$

the ratio of the pretest calibration level equivalent to pretest Δt is equal to the ratio of the posttest calibration level equivalent to posttest Δt .

$$\frac{ngT_1}{\Delta t_1} = \frac{ngT_2}{\Delta t_2}$$

When this equality is not realized, differences in transducer output symmetry occur (fig. 21). In this case, $\Delta t_1 = \Delta t_2$ and $T_1 = 2T_2$. From examination of the calibration level equivalent ratios

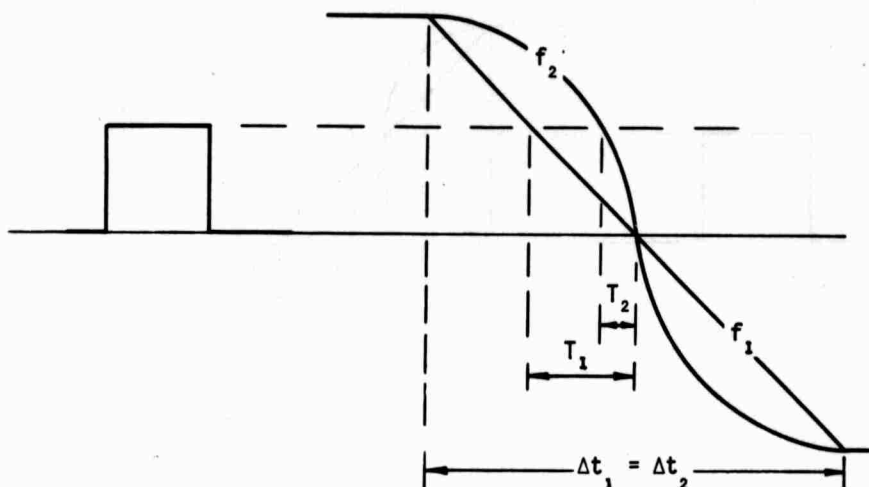


Figure 21. Pretest and Posttest 1-g Fallthrough (Example 2)

$$\text{Ratio 1} = \frac{ngT_1}{\Delta t_1}$$

$$\text{Ratio 2} = \frac{ngT_2}{\Delta t_2} = \frac{ngT_1}{2\Delta t_1}$$

it is obvious that the different symmetries of f_1 and f_2 are responsible for the factor of 2 difference in the two ratios. It is also obvious that anytime there is a difference between pretest and posttest calibration level equivalent Δt ratios, a difference in symmetry will exist between the pretest and posttest fallthroughs; it is not as obvious, however, that different symmetries may occur even when pretest and posttest ratios are the same. Figure 22 illustrates this; however, based on numerous fallthrough tests, this symmetry is unlikely to occur. Notice that $T_1 = T_2$ and $\Delta t_1 = \Delta t_2$. Therefore, the calibration level equivalents/ Δt ratios are the same for both f_1 and f_2 ; however, there is a noticeable difference between the symmetries of the two functions. So, just as equal pretest and posttest Δt s do not necessarily prove that no suspension changes occurred during dynamic testing, equal pretest and posttest

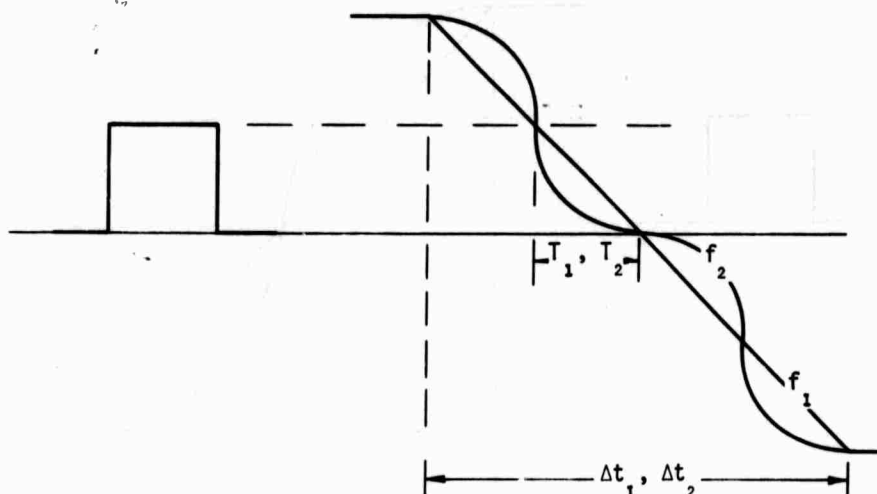


Figure 22. Pretest and Posttest 1-g Fallthrough (Example 3)

calibration level equivalents/ Δt ratios do not prove that no differences in fallthrough data symmetries exist.

In analyzing pretest and posttest fallthrough data, the following assumptions were made:

- (1) When pretest Δt and posttest Δt were not equal (or nearly equal), transducer friction or transducer damping, or both, changed during the test.
- (2) When pretest and posttest calibration level equivalents/ Δt ratios were not equal, transducer response symmetry changed during the test.

SECTION VII TEST RESULTS

1. SIGNAL CONDITIONER FAST RISE TIME DATA

Results of signal conditioner testing (table V and figures 23 through 30) indicate that the long lines did not severely degrade the performance of any of the signal conditioner systems. Although the Sparton FM system was driven into bounded oscillation during the long-line test, it should be remembered that this system was not designed for field use. The purpose of this system was to obtain laboratory data using short lines between the transducer and the signal conditioner. The EG&G signal conditioner is matched to a corresponding transducer, but it was tested independently of this transducer. The large negative spike in the long-line testing was thought to be due to contact bounce of an internal calibrate relay. Since this contact was present during short-line testing, it is possible that relay closure time may also have affected the signal conditioner response. At any rate, short-line testing indicated that the EG&G signal conditioner is capable of passing up to 860 Hz. Carrier noise was evident during this testing as it was in the actual transducer dynamic testing. The signal conditioner systems which were compatible with the OX-type velocity transducers had f_{CH} limits between 250 and 3000 Hz.

The Natel system frequency response was not affected by long lines. However, the long lines did cause the 9-percent overshoot to double and did generate a 5.5-percent peak-to-peak noise level; no noise was seen in the short-line testing.

The WES system frequency response was not affected by long lines. However, a 3-percent peak-to-peak noise level was observed during long-line testing; no appreciable noise was observed in the short-line testing.

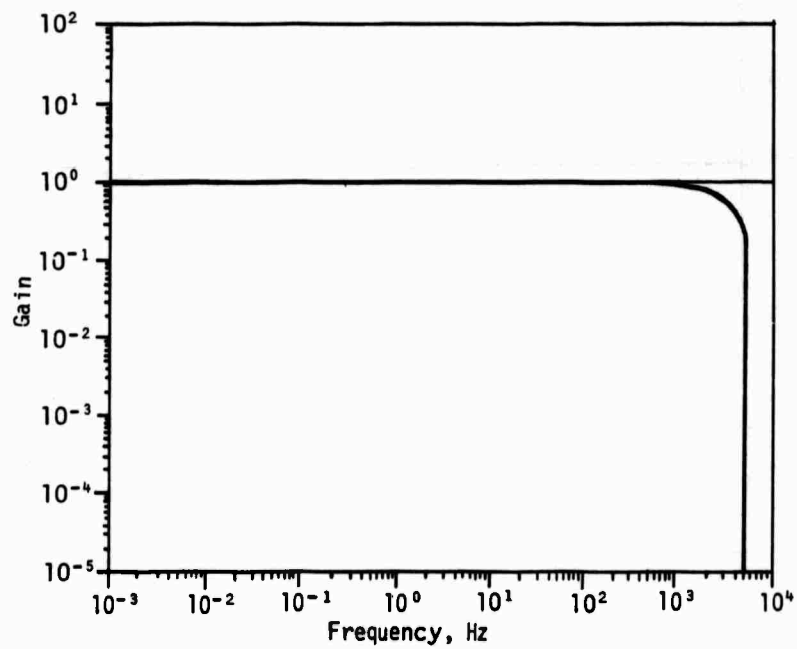
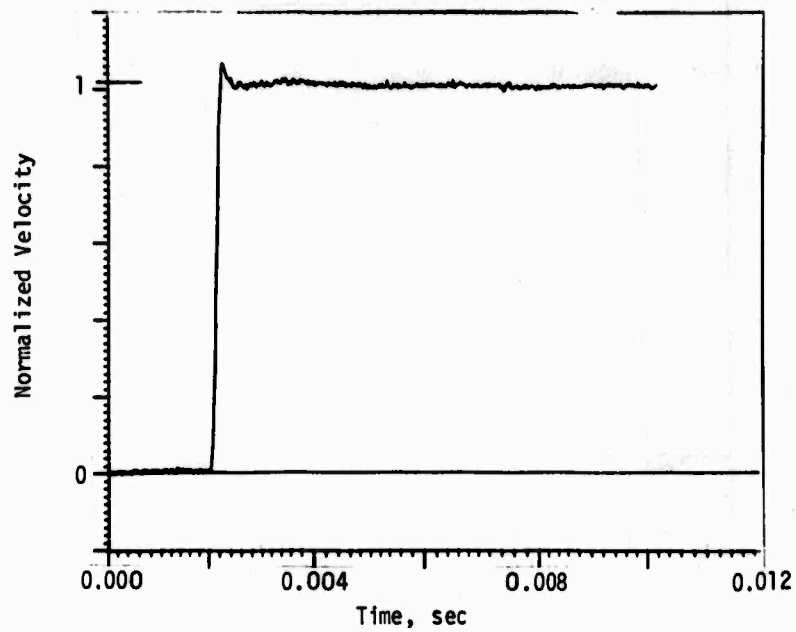
The Crescent 3-kHz system frequency response was 290 Hz with both short and long lines. (No differences were observed in the two tests.) A low-frequency (147 Hz) damped oscillation was seen in both tests. The Crescent 10-kHz system had the same performance characteristics during both short- and long-line testing.

The CEC 1-118 system had a longer rise time and a lower f_{CH} during long-line testing than during short-line testing; however, the 3-kHz carrier content in the system output was lower during long-line testing. The CEC 1-113 system had a rise time of about 1.5 msec during both short- and long-line testing. No noise, overshoot, or ringing was observed in either test.

Table V
SUMMARY OF SIGNAL CONDITIONER TEST RESULTS

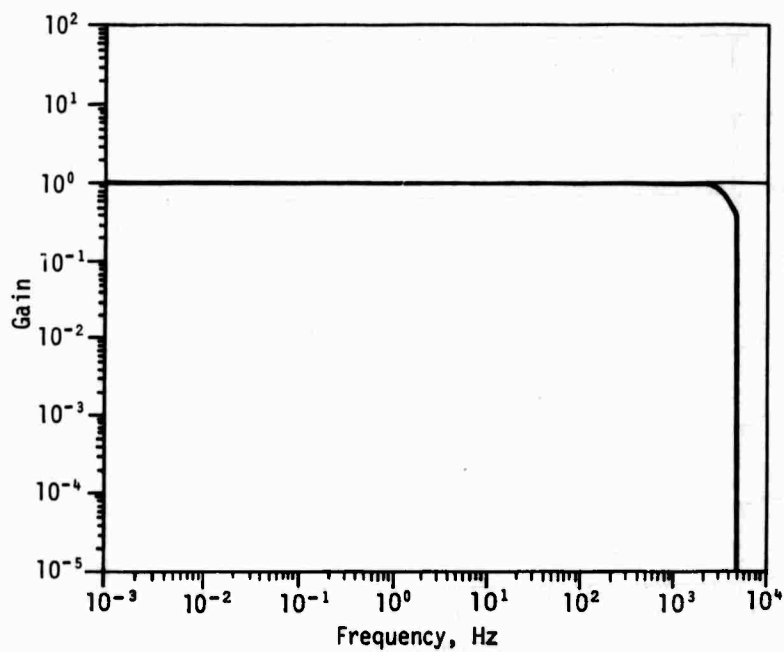
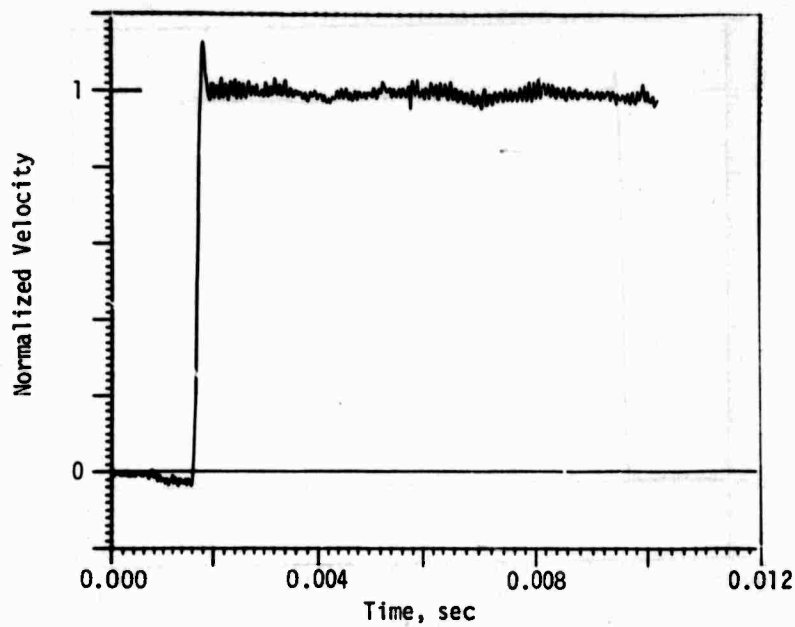
Signal Conditioner	Rise Time, msec	f_{CH} , Hz	Comments
Nate1			
Short Lines	0.14	2300	6% overshoot; no ring; no noise.
Long Lines	0.14	3000	13% overshoot; no ring; 5.5% peak-to-peak noise.
WES			
Short Lines	0.40	1100	13% overshoot; 22% 1160-Hz ring; no noise.
Long Lines	0.38	1100	14% overshoot; 21% 1040-Hz ring; 3% peak-to-peak noise.
Crescent (3 kHz)			
Short Lines	0.90	290	29% overshoot; 39% 147-Hz ring; initial positive drift.
Long Lines	0.92	290	24% overshoot; 30% 147-Hz ring.
Crescent (10 kHz)			
Short Lines	0.34	1200	Overdamped.
Long Lines	0.36	1200	Overdamped.
CEC 1-118			
Short Lines	1.36	300	Overdamped; 10% peak-to-peak carrier frequency.
Long Lines	1.60	250	Overdamped; 4% peak-to-peak carrier frequency.
CEC 1-113			
Short Lines	1.56	280	Overdamped.
Long Lines	1.54	280	Overdamped.
EG&G			
Short Lines	0.40	860	Carrier noise at 5.5% peak-to-peak; overdamped.
Long Lines	--	--	Initial high-magnitude spikes (possibly contact bounce).
Sparton 602 (F1)			
Short Lines	0.10	>5000	17% overshoot; 5000-Hz ring.
Long Lines*			

*System not designed for long lines.



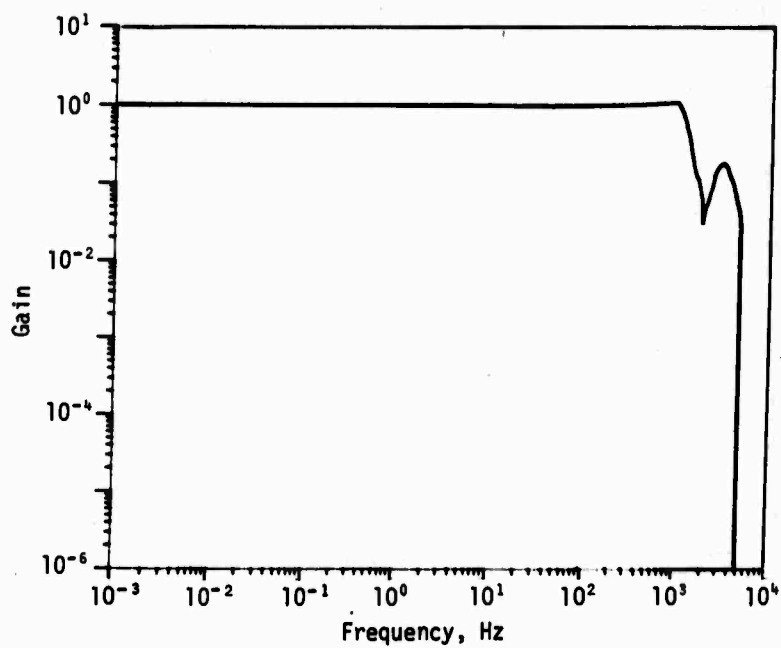
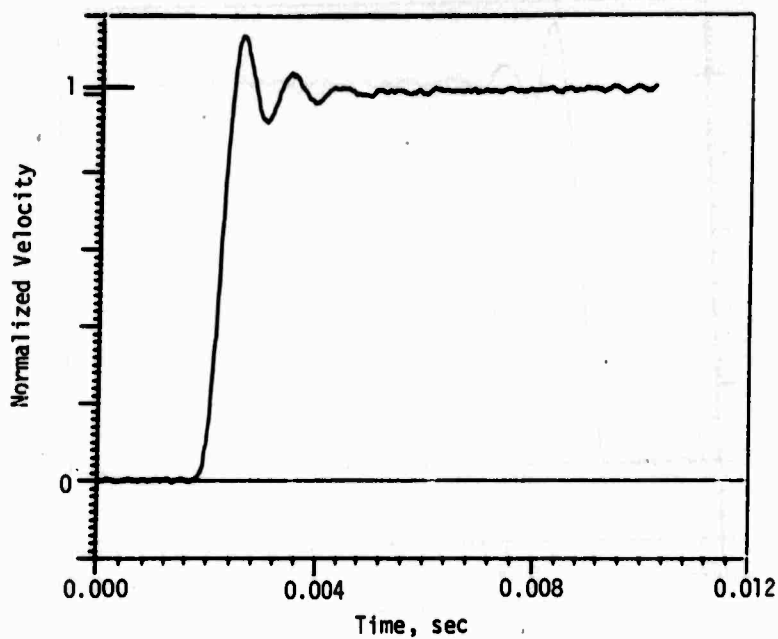
(a) Short Lines

Figure 23. Natel Fast Rise Time Test Data



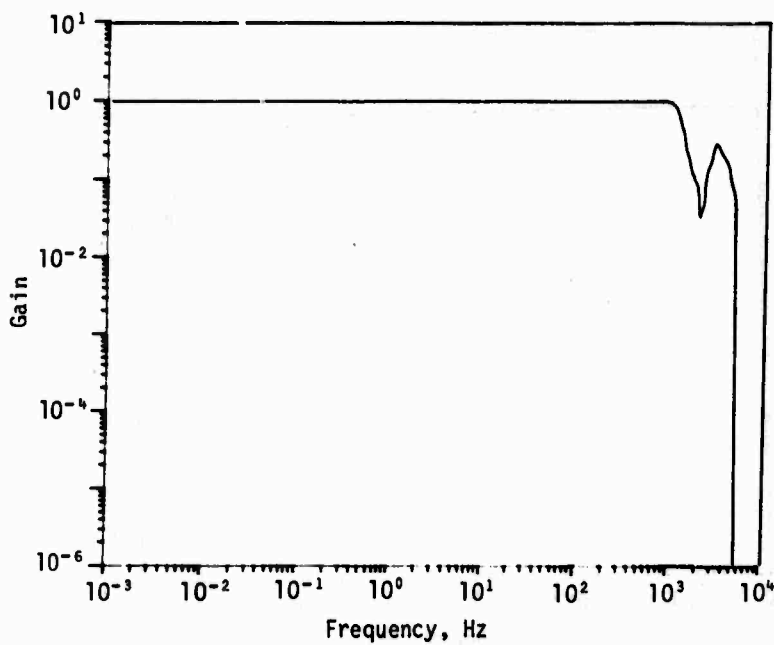
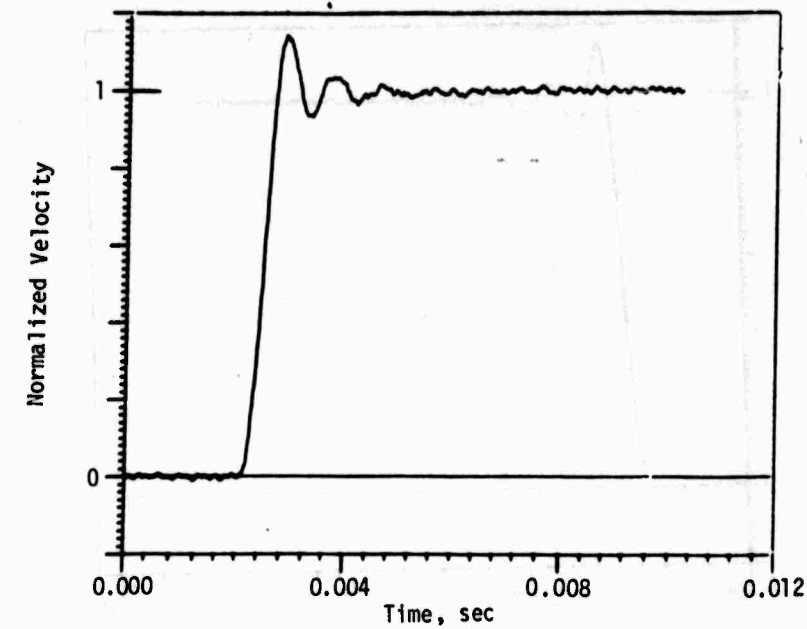
(b) Long Lines

Figure 23.---Concluded



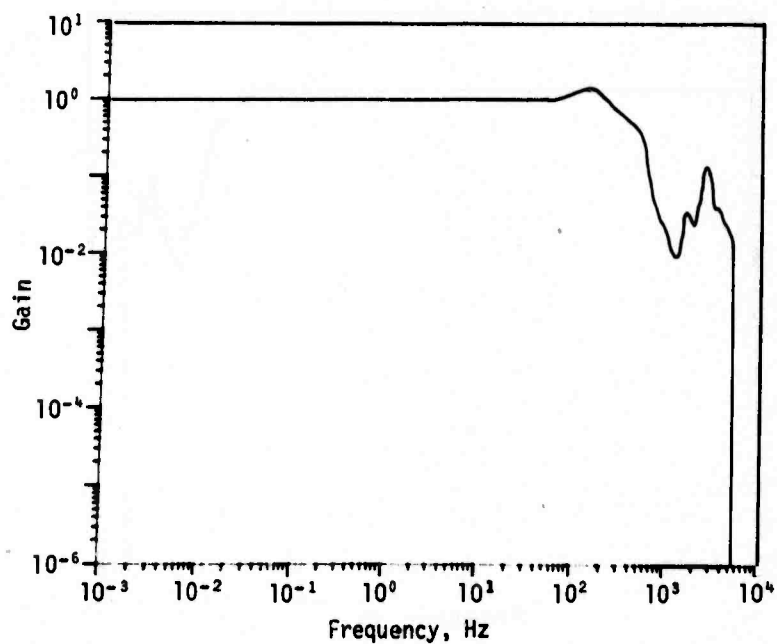
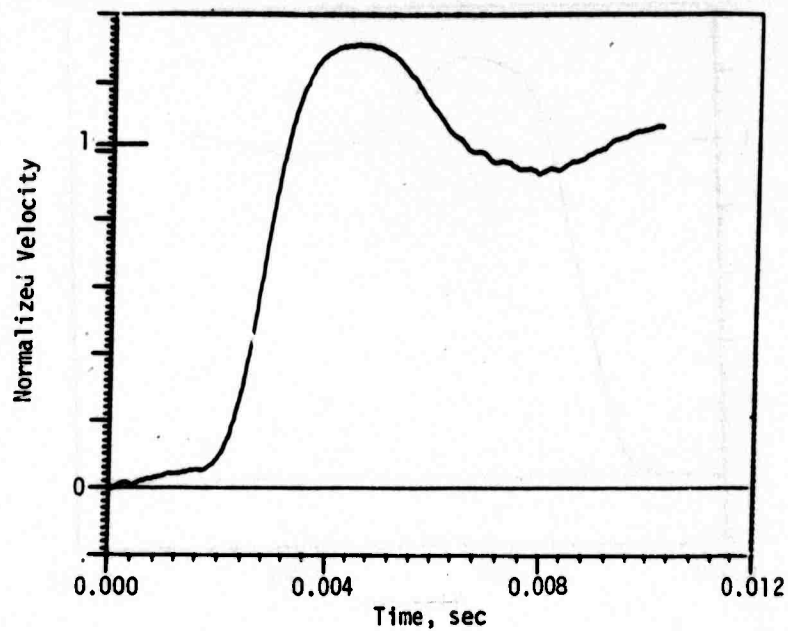
(a) Short Lines

Figure 24. WES Fast Rise Time Test Data



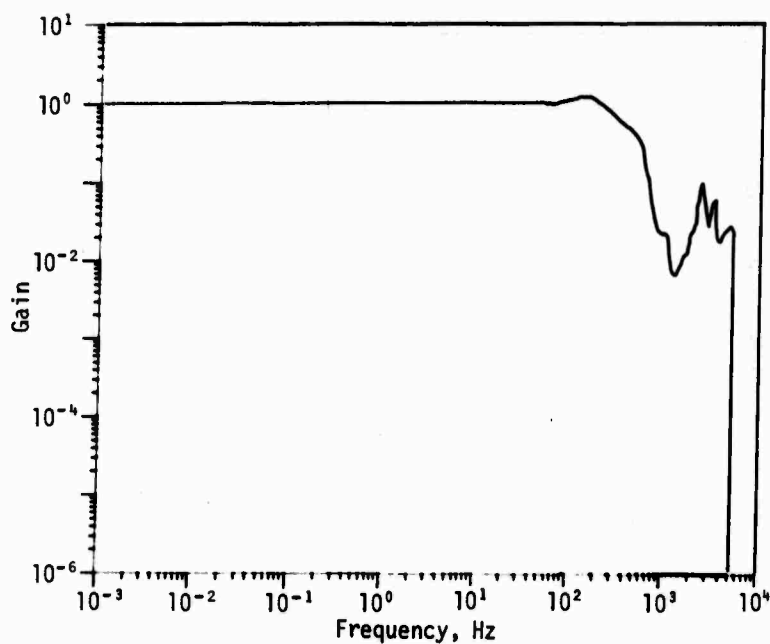
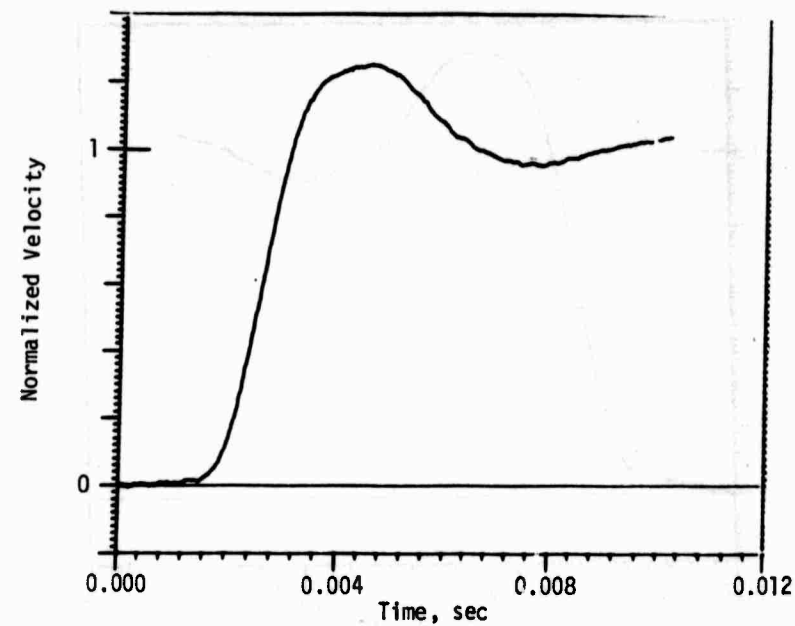
(b) Long Lines

Figure 24.---Concluded



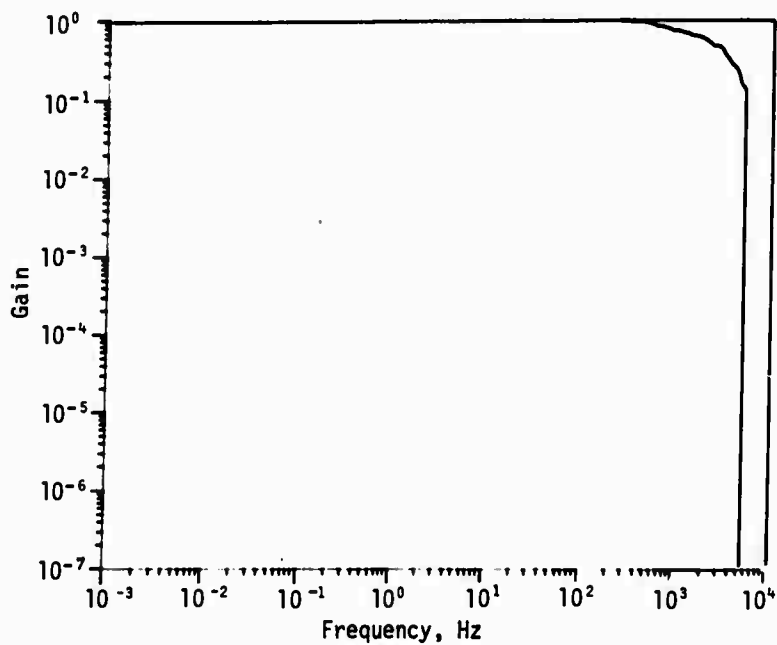
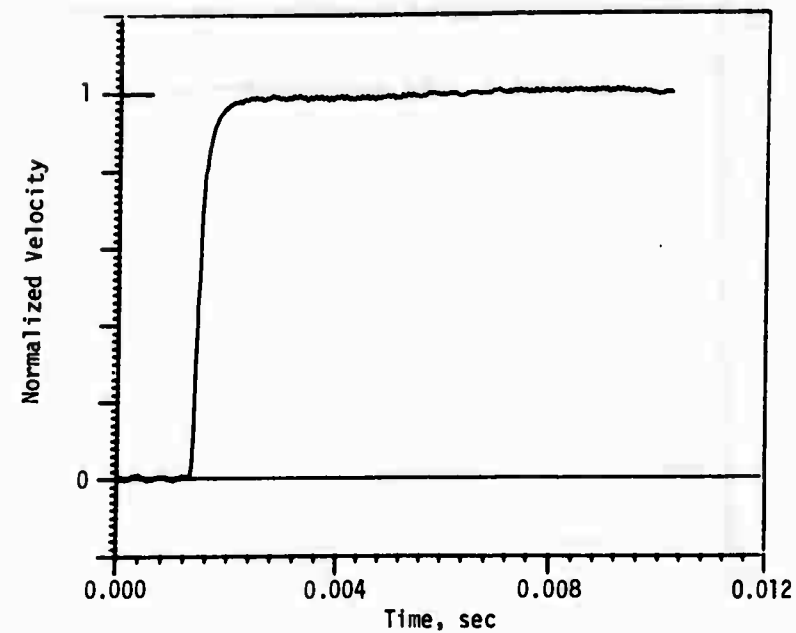
(a) Short Lines

Figure 25. Crescent (3 kHz) Fast Rise Time Test Data



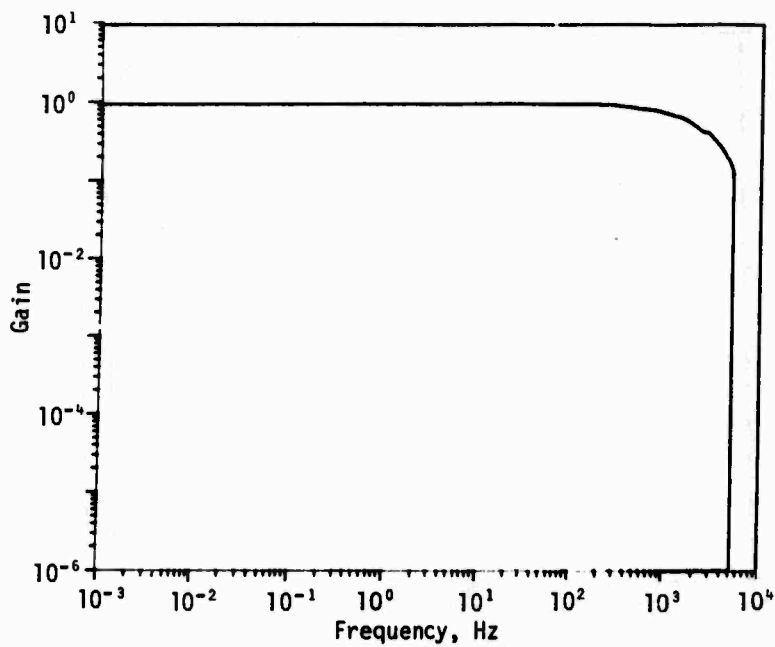
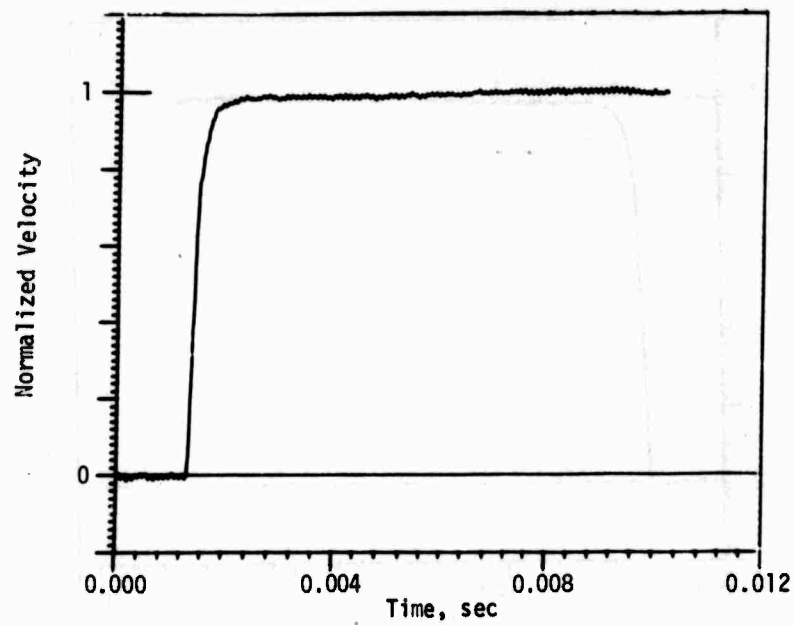
(b) Long Lines

Figure 25.---Concluded



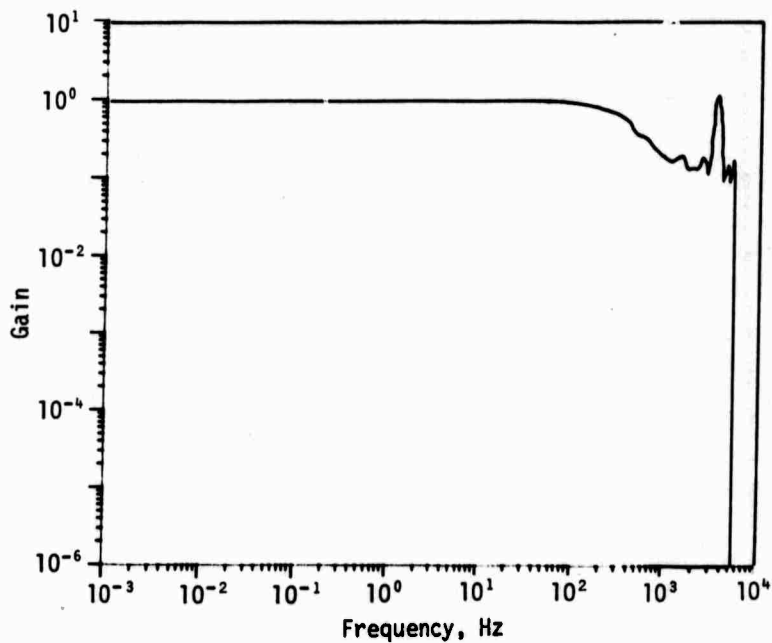
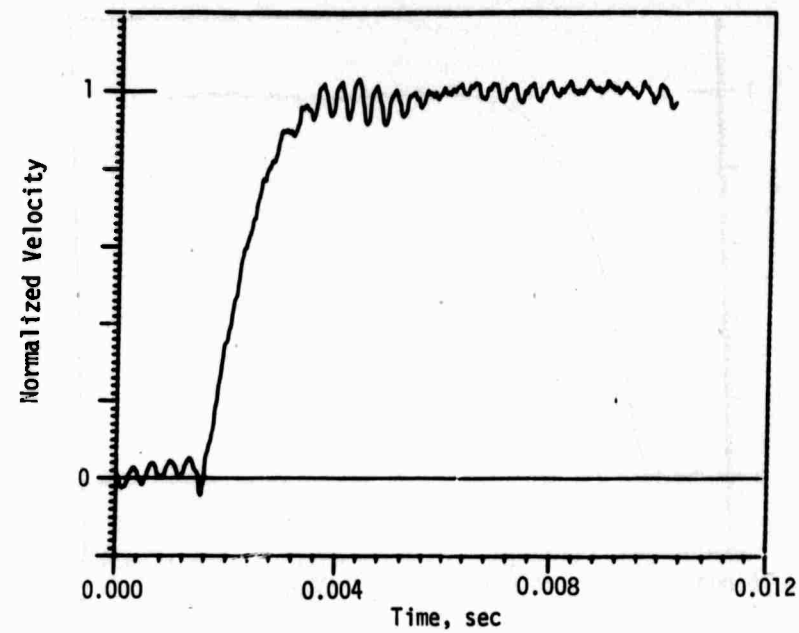
(a) Short Lines

Figure 26. Crescent (10 kHz) Fast Rise Time Test Data



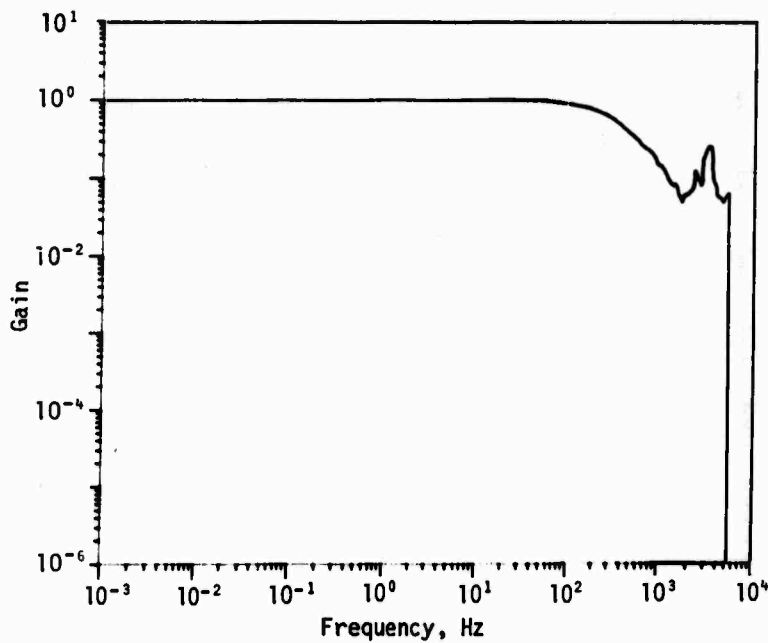
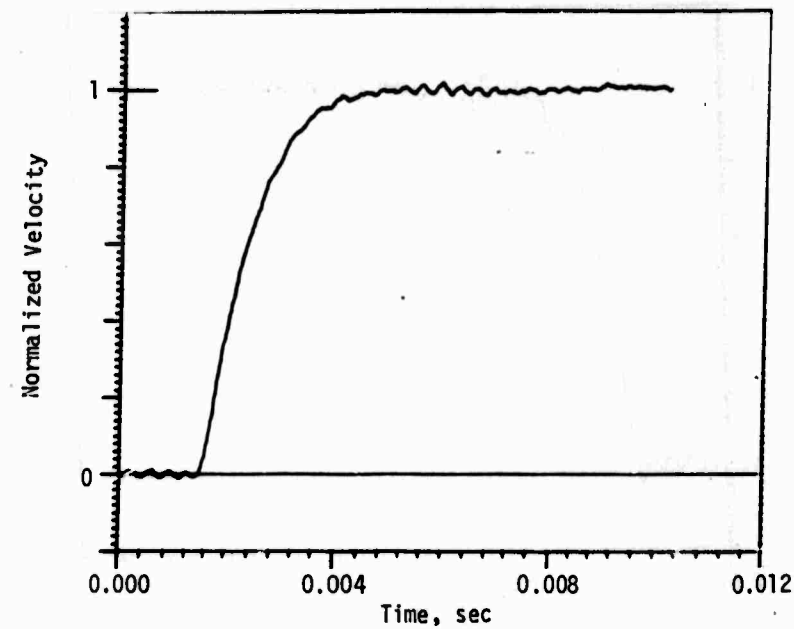
(b) Long Lines

Figure 26.---Concluded



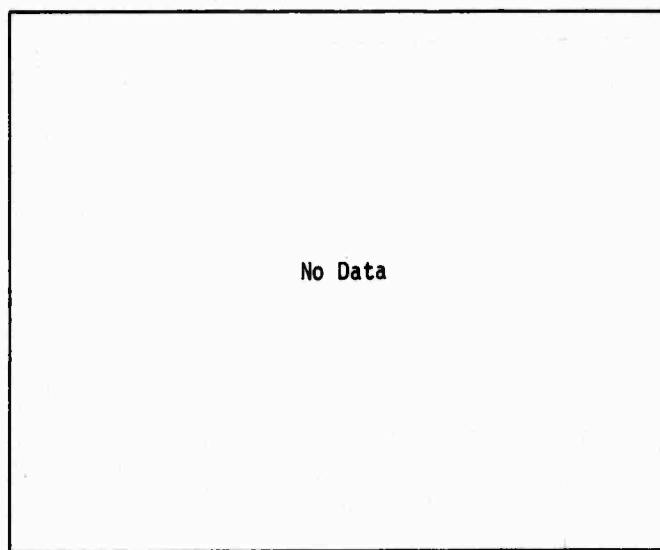
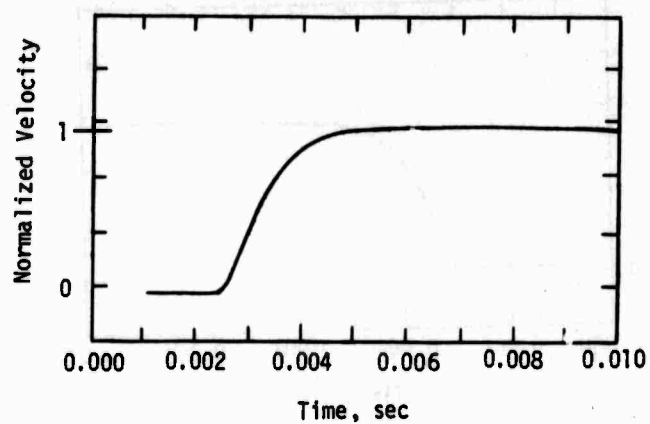
(a) Short Lines

Figure 27. CEC 1-118 Fast Rise Time Test Data



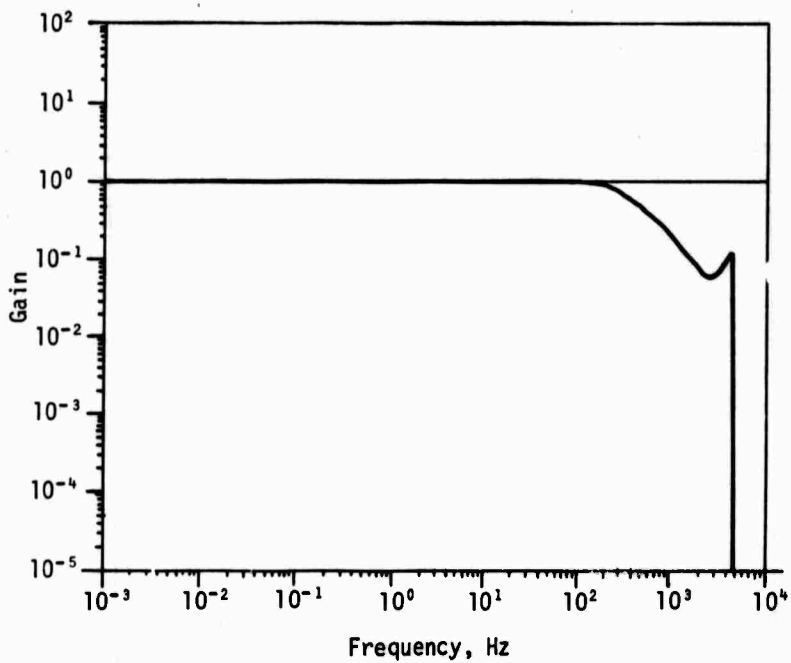
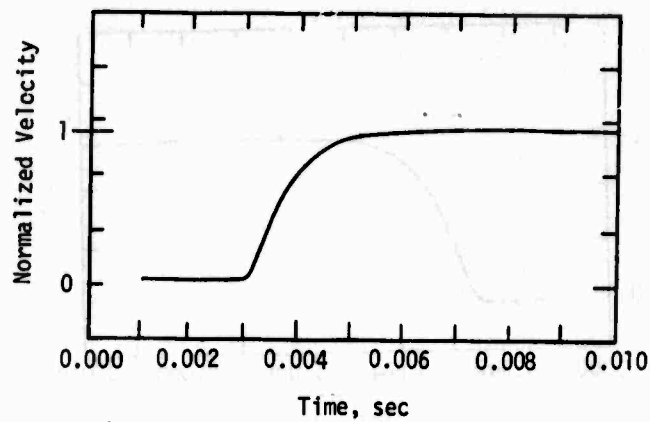
(b) Long Lines

Figure 27.---Concluded



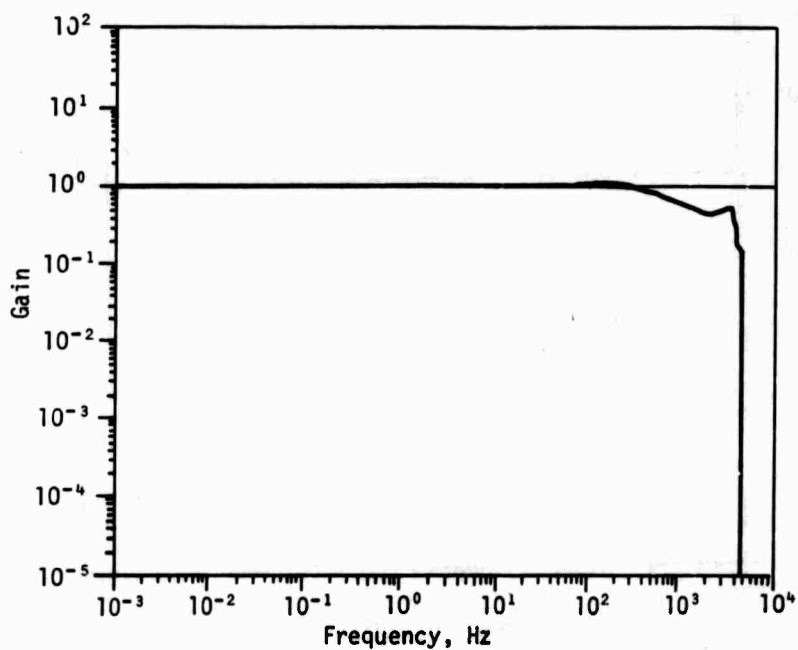
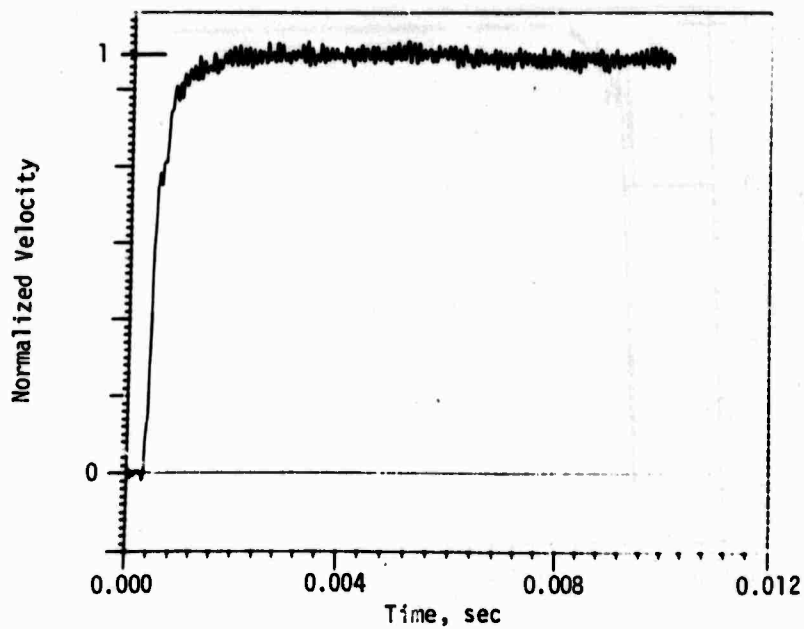
(a) Short Lines

Figure 28. CEC 1-113B Fast Rise Time Test Data



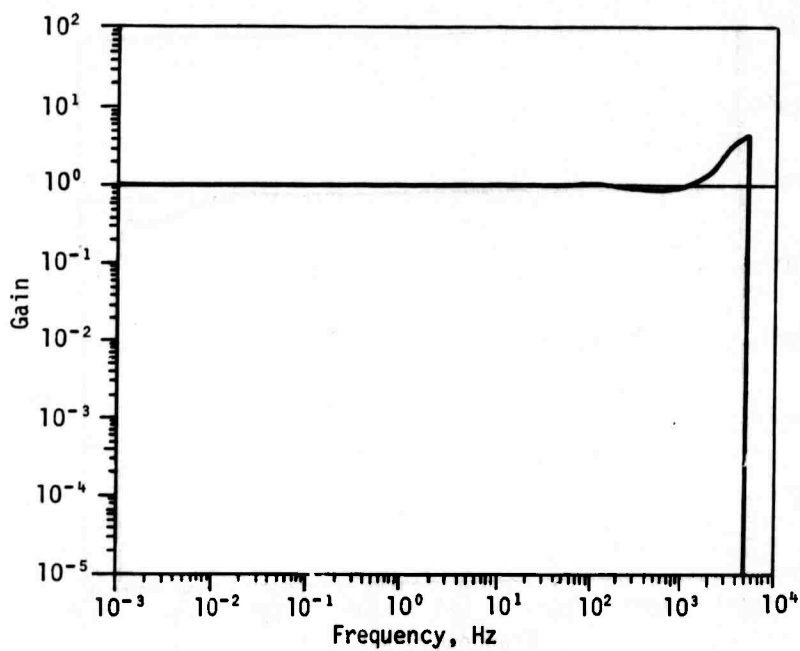
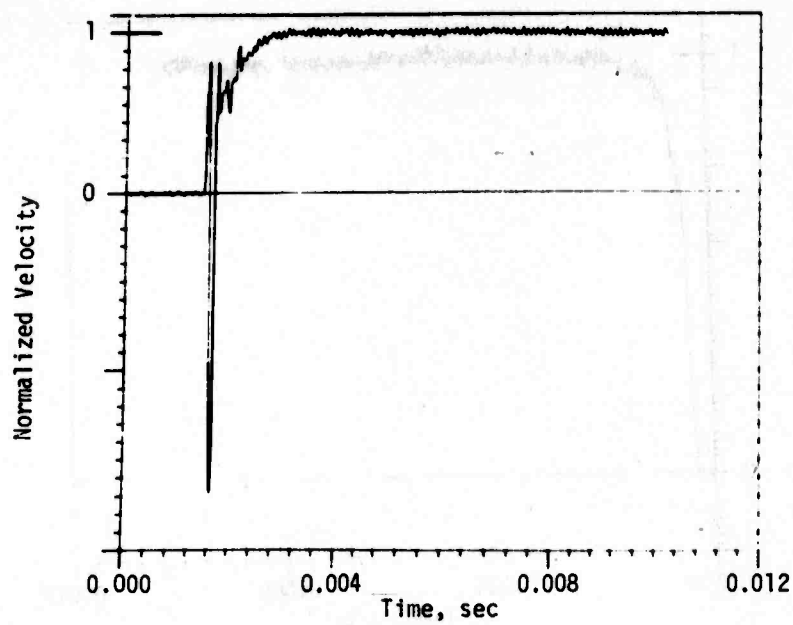
(b) Long Lines

Figure 28.---Concluded



(a) Short Lines

Figure 29. EG&G Fast Rise Time Test Data



(b) Long Lines

Figure 29.---Concluded

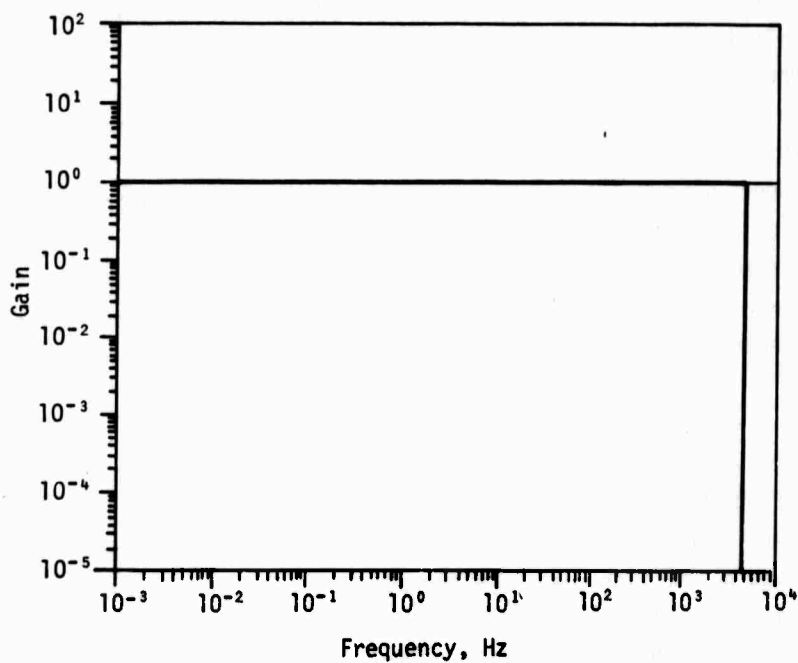
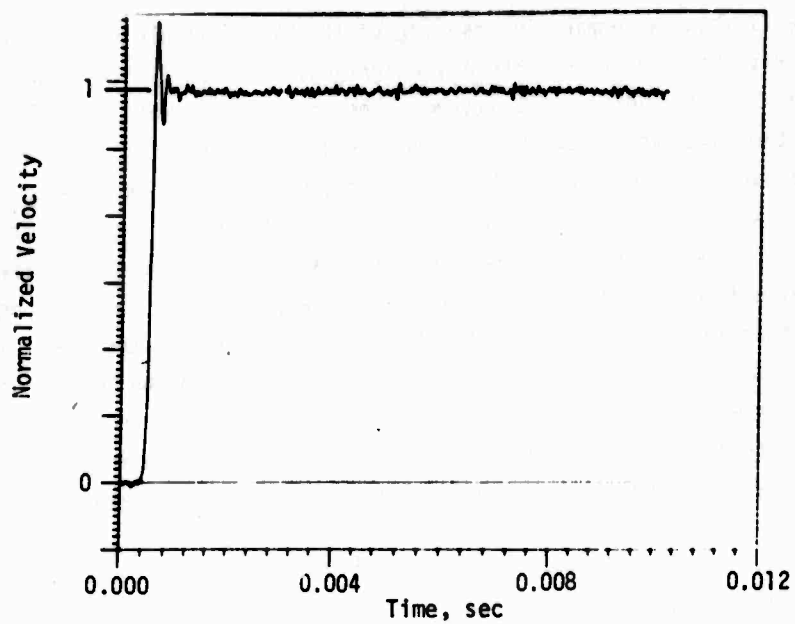


Figure 30. Sparton 602 (FM) Fast Rise Time Test Data (Short Lines)

Table VI shows a comparative ranking of the DX-compatible signal conditioners. Without grading and category weighting, it is of little value to compare the overall ranking of a system. The ranking was performed only to establish the relative performance of these signal conditioners. Different test objectives and conditions will dictate the relative weight of each category. For example, the Natel system appears to be the best system in this group if rise time and frequency response are the dominant factors in the particular velocity-measurement application. However, good frequency responses and rise times were also observed with the Crescent 10-kHz system, and with respect to noise and overshoot, this system was superior to the Natel. However, the Natel system would appear to be the system of choice because of its relatively high frequency response capabilities and because of the fact that, unlike the Crescent 10-kHz system, a reference phase adjustment capability is provided.

2. PENDULOUS TRANSDUCER DATA

Under high-g-level loads, all the DX-type velocity transducers exhibited a ringing output component which was nominally 2500 Hz. The source for this ringing component is not known for certain; it may be due to a mechanical resonance in the E-core. Results of the pendulous velocity transducer testing are given in table VII.

Since there were two reference accelerometers associated with each dynamic test and since all inputs were almost identical (except for amplitudes), the numerous reference input plots are not given. However, the typical input for all the dynamic tests is shown in figure 31 and all necessary information relating to rise time and amplitude is given in tabular form throughout this section.

a. Cibola

Data for the Cibola horizontal transducer are given in tables VIII and IX, and figures 32, 33, and 34.

These transducers had one common problem: the outer lock rings were loose and could not be tightened; the threads were apparently stripped. This resulted in a small oil leak which caused air bubbles inside transducer SN 002.

Transducer SN 003 was not used because the fallthrough test resulted in a very nonlinear output (approximately 25 percent of total output when measured from a straight line). This possibly was due to an increasing damping

Table VI
COMPARATIVE RANKING OF DX-COMPATIBLE SIGNAL CONDITIONERS

Overall Ranking	Signal Conditioner	Rating					
		Rise Time	f _{CH}	Noise	Overshoot	Ringling	Avg.
Short Lines							
1	Nate1	1	1	1	2	1	1.2
2	Crescent (10 kHz)	2	2	1	1	1	1.4
3	WES	3	3	1	3	2	2.4
4	CEC 1-118	5	4	2	1	1	2.6
5	CEC 1-113	6	6	1	1	1	3.0
6	Crescent (3 kHz)	4	5	1	3	2	3.0
Long Lines							
1	Crescent (10 kHz)	2	2	1	1	1	1.4
2	Nate1	1	1	4	2	1	1.8
3	WES	3	3	2	3	2	2.6
4	CEC 1-113	5	6	1	1	1	2.8
5	CEC 1-118	6	5	3	1	1	3.0
6	Crescent (3 kHz)	4	4	1	4	3	3.2

Table VII
SUMMARY OF PENDULOUS TRANSDUCER TEST RESULTS

Transducer	Rise Time, msec			Error Magnitude, %			Δt Change Magnitude, %			Cal Eq/ Δt Change Magnitude, %			f_{CH} (Calculated), (From FFT), Hz	f_{CH} (Calculated), (From FFT), Hz	f_{CH} (Calculated), (From FFT), Hz
	Low	Avg.	High	Low	Avg.	High	Low	Avg.	High	Low	Avg.	High			
Cibola Horizontal (CSV-V-25)	0.52	0.80	1.12	2.40	24.40	55.80	0.176	3.83	8.07						
CEC Horizontal (364137-0102)	1.24	1.35	1.44	2.27	10.70	19.20	0.000	2.44	4.90	0.000	4.33	9.00	971	330	2.94
Sparton Brass Horizontal (601-M-H-25L)	1.06	1.31	1.52	7.79	26.00	64.60	0.110	2.49	6.77	1.220	4.60	12.38	1149	252	4.56
Sparton Aluminum Horizontal (601-M-H-22)	1.20	1.45	1.62	3.90	13.15	22.40	0.220	3.45	7.50	0.330	2.95	6.39	1199	252	4.75
CEC Vertical (364142-0102)	1.06	1.30	1.48	6.18	11.60	20.80	0.790	5.56	15.90	0.166	2.30	4.50	949	310	3.05
Sparton Brass Vertical (601-M-V-25L)	1.20	1.45	1.70	5.56	9.50	19.50	0.114	3.94	7.31	1.470	3.91	6.80	1191	250	4.76
Sparton 604 Vertical	0.80	--	0.92	3.00	--	16.00	4.270	5.33	6.85	1.350	1.40	1.45	1460	380	3.84

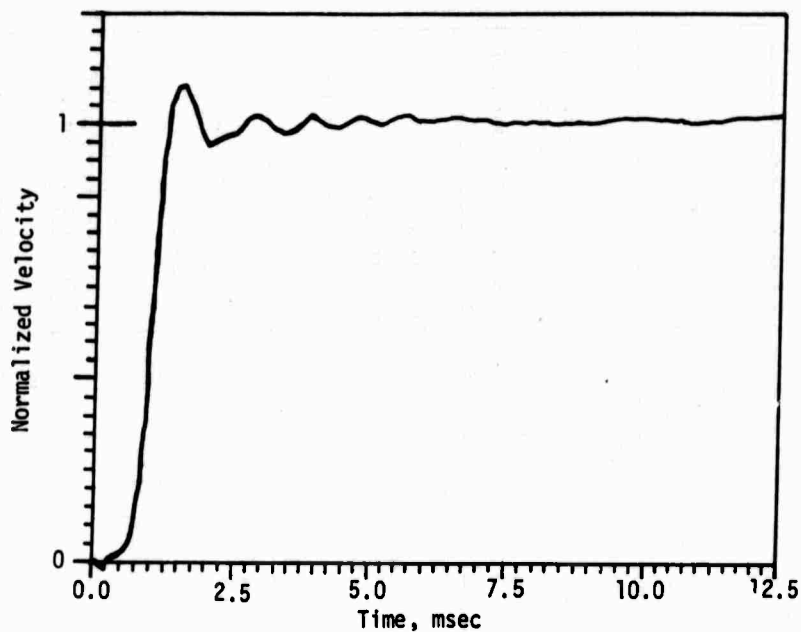


Figure 31. Typical Input for Dynamic Tests

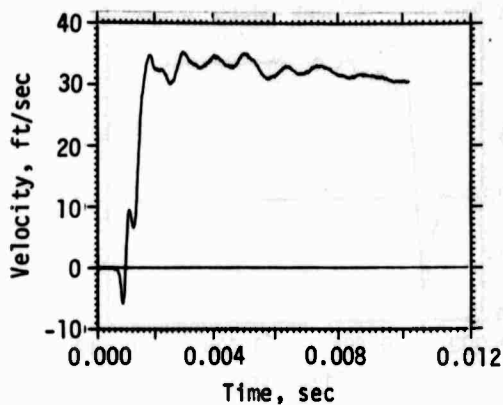
Table VIII

STATIC CALIBRATION FALLTHROUGH DATA
FOR CIBOLA TRANSDUCER

Test Series	Pre-Post Interval	Δt Change, %	Cal Eq/ Δt Change, %
1	Series	2.40	3.66
2	30°	-3.93	-4.55
	90°	8.06	2.68
	On Axis	0.18	0.97
	Series	4.03	-0.19
3	Short Lines	-1.93	3.97
	Long Lines	8.07	-2.48

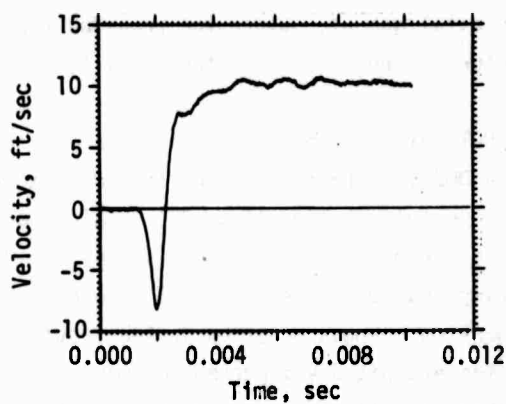
Table IX
DATA SUMMARY FOR CIBOLA TRANSDUCER TESTING

Test Series	Test	Dynamic Data					Static Data			Comments	
		Peak Input, g	Input Velocity Rise Time, msec	Output Velocity Rise Time, msec	Input Velocity, fps	Output Velocity, fps	Error, %	Δt	Cal Eq		Cal Eq/ Δt
1	Fallthrough	1000	0.400	1.08	10.00	9.00	-10.0	10.84	22.48	2.074	3120 Hz at 5 fps; initial negative 5 fps; loose pivots. Initial negative pulse of 3.5 fps.
	110-01-04	3000	0.232	0.62	21.00	30.50	45.2				
	110-01-05										
S/N 001	110-01-06 Fallthrough	1400	0.300	0.80	12.80	11.00	-21.9	11.11	23.90	2.150	
2	Fallthrough	4388	0.200		20.00			10.93	24.00	2.196	30° off axis. 90° off axis. Erroneous 1000-Hz signal; loose pivots.
	111-01-01										
	111-01-02	3650	0.240		23.00			10.50	22.00	2.096	
S/N 001	111-01-03 Fallthrough	4000	0.250	0.52	21.50	33.50	55.8	11.35	24.60	2.167	
3	Fallthrough	1220	0.280	0.68	10.80	9.60	-11.1	10.90	20.05	1.839	Initial negative pulse of 8.5 fps; loose pivots; bad transducer.
	112-01-02										
	Fallthrough							10.69	18.88	1.766	
S/N 002	112-01-03 Fallthrough	1400	0.240	1.12	11.68	11.44	- 2.4	10.29	26.09	2.536	2160 Hz at 1.6 fps; initial negative pulse of 8 fps; loose pivots; bad transducer.
	Fallthrough							11.12	27.50	2.473	



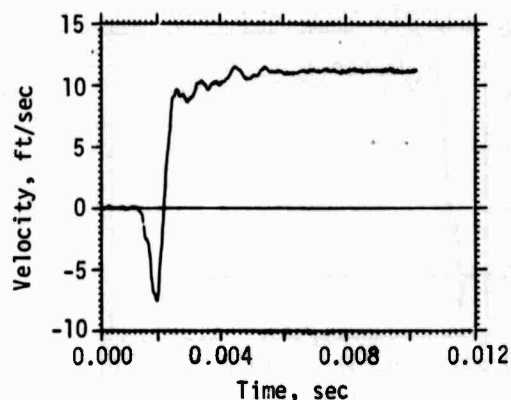
Test 111-01-03

Figure 32. Cibola Test Series 2 High-Level, Normal Data



Test 112-01-02

Figure 33. Cibola Test Series 3 Low-Level, Short-Line Data



Test 112-01-03

Figure 34. Cibola Test Series 3 Low-Level, Long-Line Data

ratio or an air bubble within the oil; however, it could also have been caused by a large E-core misalignment. Since the transducer could not be sent back to the manufacturer, and it was not taken apart, these causes are only speculative.

Transducer SN 001 was used for both series 1 and 2 testing. The output from transducer SN 002 (during fallthrough testing) had an offset step voltage at the end of the pendulum travel (fig. 35). This could have been caused by an air bubble in the oil or by excessive suspension friction.

Δt changes during transducer testing were 8 percent or less; this indicates that some suspension changes occurred during testing. Calibration level equivalents/ Δt ratios exhibited 4.5 percent changes or less; this is not alarming based on other pendulous transducer test results. An initial negative output trend was observed in all dynamic responses; this indicates E-core looseness or suspension problems. Rise times varied from 0.52 to 1.12 msec; these were much faster than the rise times for the other 3000-centistoke pendulous velocity transducers.

Error magnitude varied from 2.4 to 55.8 percent. Since the worst

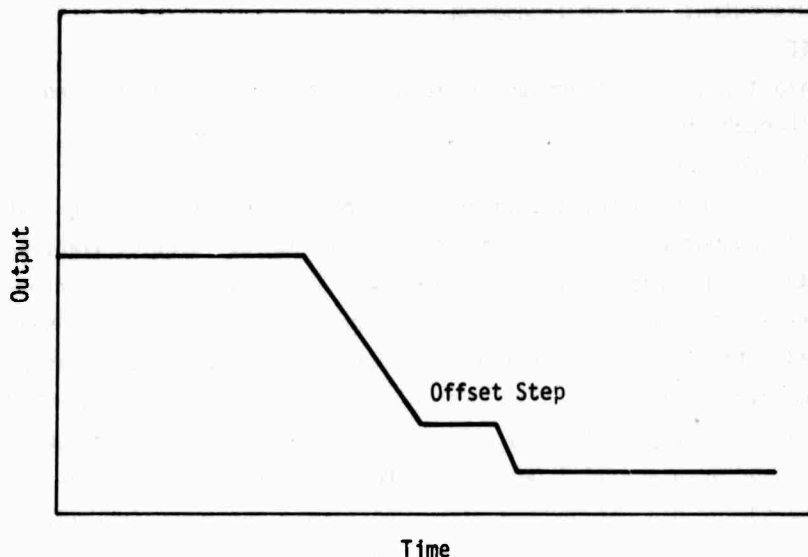


Figure 35. Cibola Transducer 1-g Fallthrough Output

error magnitude (55.8 percent) was observed after high-g-level, cross-axis testing, this transducer type appeared to have suffered from cross-axis shock. The low-g-level test after the 4000-g normal test exhibited a higher error (21.9 percent) than other low-g-level normal tests. Obviously, the samples used in this test program did suffer from both normal and cross-axis, high-g-level inputs.

Input/output time histories for tests 111-01-03, 112-01-02, and 112-01-03 are presented in figures 32, 33, and 34. Notice that in all three of these tests, the transducer responded to the 1000-Hz input component. The initial negative spike is obvious in all three of these tests also. Test 112-01-03 also shows some moderate 2160-Hz ringing. Rise time and frequency response were good for this transducer compared to the other pendulous transducers tested; but, relative to the other pendulous transducers, the overall performance of this transducer was not good. Oil leakage, nonlinear fallthroughs, shock sensitivity, and initial negative spikes severely limited the performance of this transducer. f_{CL} and f_{CH} could not be determined for this transducer because of nonlinear exponential fallthrough and negative spikes

in the dynamic outputs of the transducer.

b. CEC

Data for the CEC transducers are given in tables X and XI, and figures 36 through 40.

(1) Horizontal

The horizontal transducers performed fairly well during testing. The maximum Δt change was 4.9 percent, and the maximum calibration level equivalent Δt ratio change was 9.0 percent. This was a fairly large ratio change for the high-g-level, 30°-off-axis test. No subsequent significant changes were observed after this test. Ringing ranging from 2000 to 2780 Hz was observed in the dynamic testing. Time histories of tests 101-01-05 and 102-01-03 (figs. 36 and 37) show this clearly. During test 102-01-03 the transducer responded with good accuracy (4.3 percent). Thus, from the standpoint of accuracy, the transducer did not degrade after cross-axis testing. Test 101-01-05 also showed an accurate transducer response (9.73-percent error) after high-g-level, normal testing; this again demonstrated no accuracy deterioration after high-g-level, normal inputs. However, the high-frequency ring in the transducer output during test 102-01-03 had a greater magnitude than the rings in all other tests; this transducer ring magnitude may be increased after cross-axis, high-g-level inputs.

Rise times for this transducer were very closely grouped, 1.24 msec (min) and 1.44 msec (max), indicating a degree of consistency in the damping ratio of the three transducers tested.

Overall performance of this transducer was relatively good. No initial negative spikes were observed; transducer accuracy averaged 10.7 percent.

Low-frequency response was 0.00927 Hz. High-frequency response determined from exponential fallthrough testing was 971 Hz; high-frequency response determined by the fast Fourier transform modulus ratio was 330 Hz. The ratio of the high-frequency response three dB points was 2.94, i.e.,

$$\frac{f_{CH} \text{ (exponential fallthrough)}}{f_{CH} \text{ (fast Fourier transform modulus ratio)}}$$

(2) Vertical

Very small changes were observed in Δt and in the calibration level equivalents/ Δt ratios throughout the testing of the vertical

Table X
 STATIC CALIBRATION FALLTHROUGH DATA
 FOR CEC TRANSDUCERS

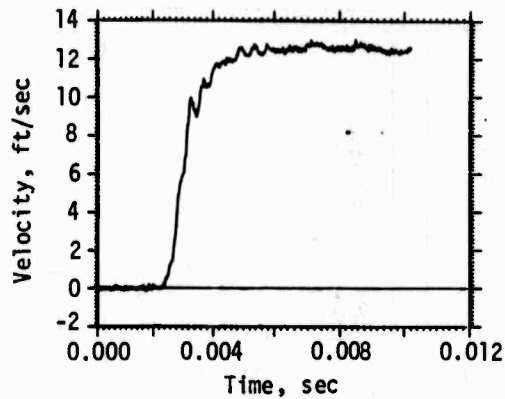
Test Series	Pre-Post Interval	Δt Change, %	Cal Eq/ Δt Change, %
Horizontal Transducers			
1	Series	- 3.23	0.00
2	30°	- 4.40	-9.00
	90°	1.82	3.78
	On Axis	4.90	2.30
3	Short Lines	- 1.31	-4.22
	Long Lines	1.33	2.20
Vertical Transducers			
1	Series	- 1.15	1.22
2	30°	- 4.24	0.17
	90°	0.79	0.19
	On Axis	4.71	4.13
	Series	1.37	4.50
3	Short Lines	3.49	-3.26
	Long Lines	15.90	3.36

Table XI
DATA SUMMARY FOR CEC TRANSDUCER TESTING

Test Series	Test	Dynamic Data					Static Data				Comments
		Peak Input, g	Input Velocity Rise Time, msec	Output Velocity Rise Time, msec	Input Velocity, fps	Output Velocity, fps	Error, %	Δt	Cal Eq	Cal Eq/ Δt	
Horizontal Transducers											
1 S/N 2003	Fallthrough 101-01-01	1550	0.300	1.40	15.00	17.25	15.0	6.51	15.40	2.366	2500 Hz; peak magnitude of 1.0 fps. 2600 Hz at 2 fps. 2360 Hz at 1.05 fps.
	101-01-03	4200	0.216	1.44	25.60	30.40	19.2				
	101-01-05	1150	0.320	1.40	10.80	11.85	9.7				
	Fallthrough							6.30	14.91	2.367	
2 S/N 2004	Fallthrough 102-01-01	3800	0.210		22.50			6.32	16.70	2.640	2000 Hz at 1.75 fps; 30° off axis. 90° off axis. 2000 Hz at 2.7 fps.
	Fallthrough 102-01-02	4275	0.230		23.88			6.04	14.40	2.380	
	Fallthrough 102-01-03	5350	0.200	1.36	24.50	25.60	4.3	6.15	15.20	2.470	
	Fallthrough							6.45	16.30	2.527	
3 S/N 2005	Fallthrough 103-01-02	1920	0.304	1.26	13.20	13.50	2.3	6.12	17.90	2.925	2600 Hz at 2.1 fps. 2780 Hz at 1.1 fps.
	Fallthrough 103-01-03	1230	0.296	1.24	10.20	11.60	13.7	6.09	18.60	3.054	
	Fallthrough							6.01	17.58	2.925	
	Fallthrough							6.09	17.39	2.860	

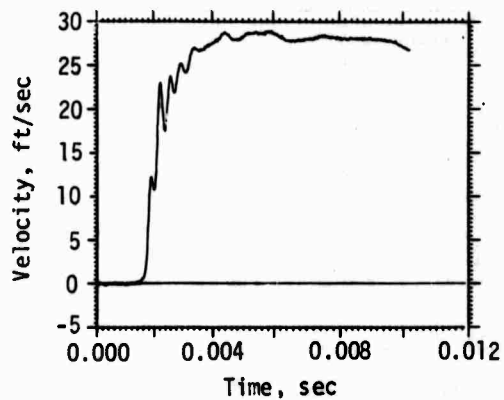
Table XI (Concl'd)

Test Series	Test	Dynamic Data					Static Data			Comments	
		Peak Input, g	Input Velocity Rise Time, msec	Output Velocity Rise Time, msec	Input Velocity, fps	Output Velocity, fps	Error, %	Static Data			
								Cal Eq	Cal Eq/ Δt		
Vertical Transducers											
1 S/N 2119	Fallthrough	920	0.290	1.24	9.40	10.50	11.7	3.05	14.80	4.850	2080 Hz at 0.5 fps. 2630 Hz at 1.2 fps. 2000 Hz at 0.35 fps.
	201-01-02	2700	0.240	1.48	19.20	23.20	20.8				
	201-01-03	950	0.280	1.06	9.70	10.30	6.2	3.02	14.80	4.909	
	Fallthrough										
2 S/N 2120	Fallthrough	3900	0.260		21.00			3.30	31.80	9.636	30° off axis. 52° off axis. 2000 Hz at 2.1 fps.
	202-01-01	3500	0.240		21.10			3.16	30.50	9.652	
	202-01-02	3600	0.220	1.32	21.00	23.00	9.5	3.19	30.80	9.670	
	Fallthrough						35	33.70	10.070		
3 S/N 2121	Fallthrough	910	0.380	1.36	9.70	10.60	9.3	2.67	17.40	6.068	2600 Hz at 0.5 fps. 2605 Hz at 0.4 fps.
	203-01-02							2.88	16.90	5.870	
	Fallthrough	920	0.320	1.36	9.20	10.20	10.9	2.80	16.20	5.780	
	203-01-03							3.25	19.40	5.974	



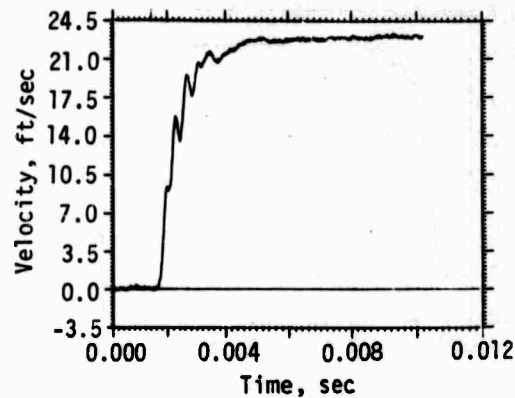
Test 101-01-05

Figure 36. CEC Horizontal Test Series 1 Low-Level, Post-High-g Data



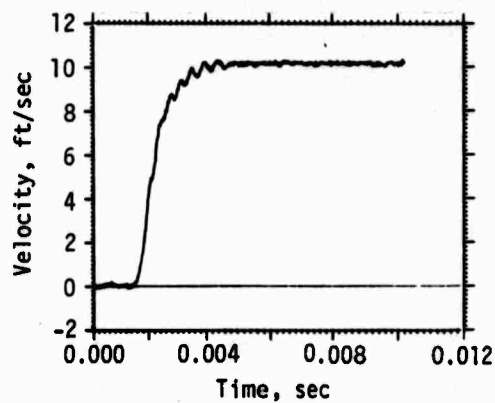
Test 102-01-03

Figure 37. CEC Horizontal Test Series 2 High-Level, Normal Data



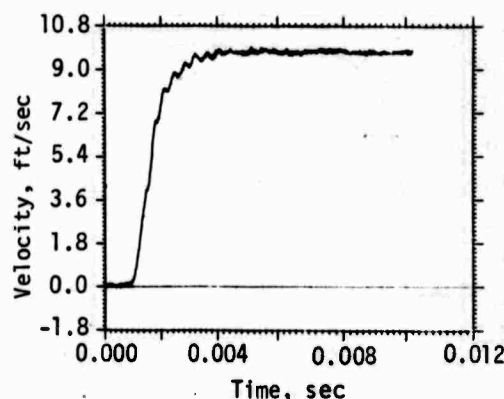
Test 202-01-03

Figure 38. CEC Vertical Test Series 2
High-Level, Normal Data



Test 203-01-02

Figure 39. CEC Vertical Test Series 3
Low-Level, Short-Line Data



Test 203-01-03

Figure 40. CEC Vertical Test Series 3
Low-Level, Long-Line Data

transducers. This transducer also performed fairly well during dynamic testing. Again, ringing at frequencies between 2000 and 2630 Hz was observed during all on-axis tests. Ringing magnitudes varied from a low of 0.35 to a high of 2.10 fps peak-to-peak. Rise times varied from a low of 1.06 to a high of 1.48 msec. Peak magnitude error, which occurred during the series 1 4000-g normal test, was 20.8 percent. The time histories from tests 202-01-03, 203-01-02, and 203-01-03 (figs. 38, 39, and 40) are presented primarily to show the good relative performance after cross-axis testing and almost identical long- and short-line performance. The average error for the vertical transducers was 11.6 percent. f_{CL} and f_{CH} determined from exponential fallthrough data were 0.0095 and 947 Hz, respectively; f_{CH} from the fast Fourier transform modulus ratio was 310 Hz. The ratio of the two f_{CH} points was 3.05. Note the consistency between these data and the corresponding data for the horizontal CEC transducer.

Relatively speaking, this transducer performed well. No evidence of shock deterioration was observed, no initial negative spikes were noted, and relatively good accuracy was obtained. High-frequency ringing,

however, was seen in all the testing.

c. Sparton Brass

Data for the Sparton brass transducers are given in tables XII and XIII, and figures 41 through 47.

(1) Horizontal

The maximum Δt change encountered during this testing was 6.77 percent. This result, which occurred during test series 2, indicates some suspension changes occurred during the cross-axis tests. The maximum calibration level equivalent/ Δt ratio change was seen after the high-g-level, 30°-cross-axis test (-12.88 percent). Figure 48 shows the pretest and posttest 30° fallthroughs for this transducer. Notice that the fallthroughs do not visually show a great deal of difference; but, when slope lines are drawn through the zero and calibration points and compared to the slope of a line drawn through the transducer stop points, a noticeable difference is seen in the two fallthroughs. This demonstrates the usefulness of the calibration level equivalent/ Δt ratio check to spot transducer parameter changes after a dynamic test. The fact that the transducer did undergo a change after the 30° test does not necessarily mean that transducer performance deteriorated or was impaired by the 30°-cross-axis testing.

Ringings were again observed in all tests during the initial rise at frequencies between 2500 and 2940 Hz at magnitudes of 1.1 to 3.0 fps peak-to-peak.

Test results for test 105-01-03 (fig. 44) are also presented to show the performance after cross-axis testing. Of particular interest in all tests was the high-frequency component of the transducer output. Nominal 2500-Hz ringings were observed in all tests during the initial rise.

Transducer rise time varied from 1.06 to 1.52 msec during the testing. Outputs were consistently low during test series 1 compared to those for the CEC transducer, which were consistently high. During test series 3, the Sparton brass horizontal transducer had high outputs (positive errors); the CEC transducers had high outputs in all tests.

The Sparton brass horizontal transducer performed better than the Cibola transducer but not as well as the CEC horizontal transducer. There was no obvious deterioration in performance after normal, high-g-level shock

Table XII

STATIC CALIBRATION FALLTHROUGH DATA
FOR SPARTON BRASS TRANSDUCERS

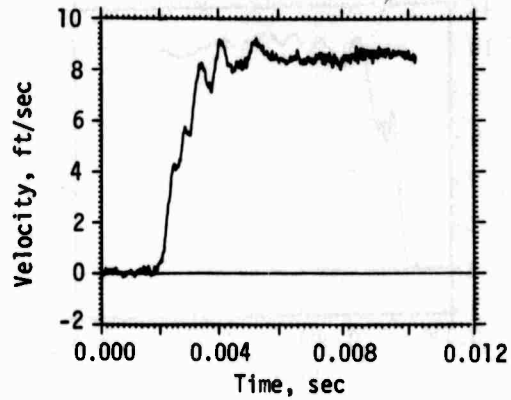
Test Series	Pre-Post Interval	Δt Change, %	Cal Eq/ Δt Change, %
Horizontal Transducers			
1	Series	-3.93	- 2.96
2	30°	4.00	-12.38
	90°	0.11	4.26
	On Axis	2.55	5.56
	Series	6.77	- 3.56
3	Short Lines	-0.97	1.89
	Long Lines	1.48	- 4.93
Vertical Transducers			
1	Series	3.81	2.61
2	30°	4.38	1.47
	90°	2.33	- 1.82
	On Axis	-2.27	5.27
	Series	4.38	4.86
3	Short Lines	0.11	4.52
	Long Lines	7.31	- 6.80

Table XIII
DATA SUMMARY FOR SPARTON BRASS TRANSDUCER TESTING

Test Series	Test	Dynamic Data						Static Data			Comments
		Peak Input, g	Input Velocity Rise Time, msec	Output Velocity Rise Time, msec	Input Velocity, fps	Output Velocity, fps	Error, %	Δt	Cal Eq	Cal Eq/ Δt	
Horizontal Transducers											
1 S/N 3594	Fallthrough							9.16	19.20	2.096	2500 Hz at 2 to 0.6 fps. 2500 Hz at 3 fps. 2500 Hz at 1.3 fps.
	104-01-01	1080	0.380	1.32	11.85	8.60	-27.5				
	104-01-02	3680	0.240	1.12	22.25	18.50	-21.6				
	104-01-03 Fallthrough	1609	0.380	1.42	13.30	10.40	-21.6	8.80	17.90	2.034	
2 S/N 3595	Fallthrough							9.01	20.30	2.253	30° off axis. 90° off axis. 2940 Hz at 1.5 fps.
	105-01-01	4500	0.230		23.80						
	105-01-02	5000	0.240		25.00			9.37	18.50	1.974	
	105-01-03 Fallthrough	4600	0.120	1.06	15.80	26.00	64.6	9.38	19.30	2.058	
3 S/N 3596	Fallthrough							9.62	20.90	2.173	2500 Hz at 1.1 fps. 2500 Hz at 1.2 fps.
	106-01-02	1000	0.344	1.44	11.70	12.60	7.8	8.23	22.20	2.697	
	106-01-03	1240	0.328	1.52	13.40	15.10	12.7	8.15	22.40	2.748	
	Fallthrough							8.10	22.70	2.802	
								8.22	21.90	2.664	

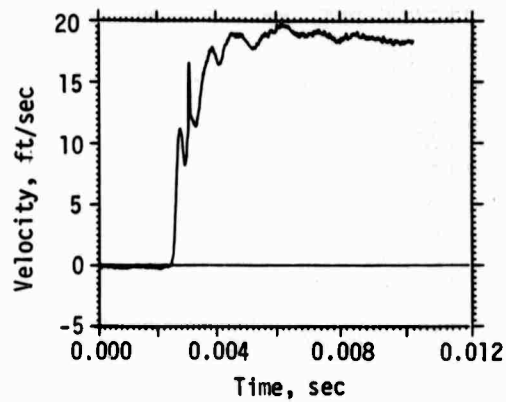
Table XIII (Concl'd)

Test Series	Test	Dynamic Data					Static Data				Comments
		Peak Input, g	Input Velocity Rise Time, msec	Output Velocity Rise Time, msec	Input Velocity, fps	Output Velocity, fps	Output Velocity, Error, %	Static Data			
								Δt	Cal Eq	Cal Eq/ Δt	
Vertical Transducers											
1 S/N 3597	Fallthrough										
	204-01-01	950	0.400	1.44	9.40	8.60	- 8.5	4.20	15.60	3.710	1660 Hz at 1.6 fps.
	204-01-02	2763	0.256	1.20	21.60	20.40	- 5.6				2280 Hz at 4.36 fps.
	204-01-03 Fallthrough	1000	0.400	1.46	10.00	9.20	- 8.0	4.36	16.60	3.807	1670 Hz at 3.6 fps.
2 S/N 3598	Fallthrough										
	205-01-01	3860	0.230		20.90			4.11	32.10	7.810	30° off axis.
	Fallthrough							4.29	34.00	7.925	90° off axis.
	205-01-02 Fallthrough	3500	0.224		19.50			4.39	34.10	7.780	
S/N 3598	205-01-03 Fallthrough	3800	0.300	1.70	20.50	24.50	19.5	4.29	35.10	8.190	1560 Hz at 3.3 fps.
3 S/N 3599	Fallthrough										
	206-01-02	930	0.280	1.42	9.60	8.90	- 7.9	4.40	17.50	3.980	1550 Hz at 2.2 fps.
	Fallthrough							4.40	18.30	4.160	
	Fallthrough							4.38	14.80	3.380	
S/N 3599	206-01-04 Fallthrough	1000	0.320	1.45	10.60	9.80	- 7.6	4.70	14.80	3.150	1550 Hz at 2.2 fps.



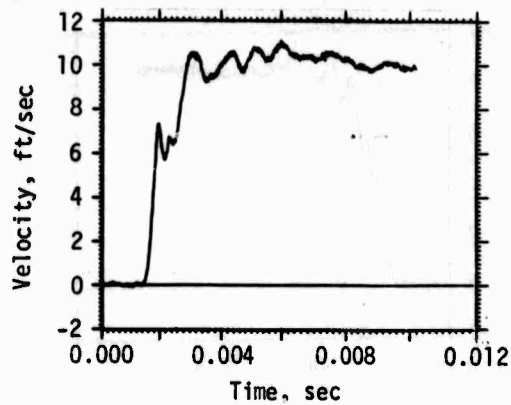
Test 104-01-01

Figure 41. Sparton Brass Horizontal Test Series 1
Low-Level, Pre-High-g Data



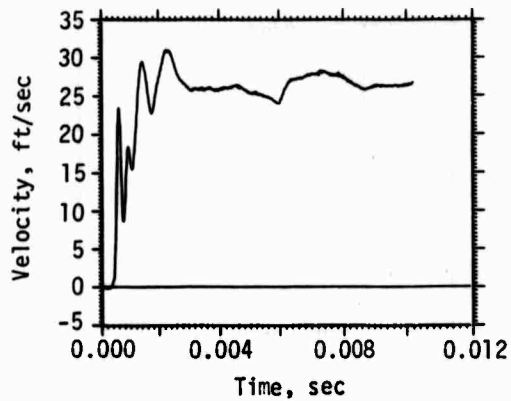
Test 104-01-02

Figure 42. Sparton Brass Horizontal Test Series 1
High-Level, Normal Data



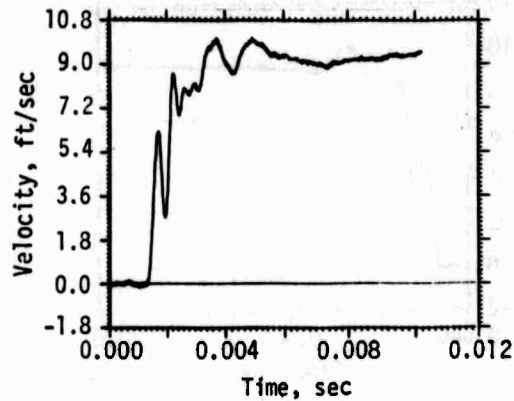
Test 104-01-03

Figure 43. Sparton Brass Horizontal Test Series 1
Low-Level, Post-High-g Data



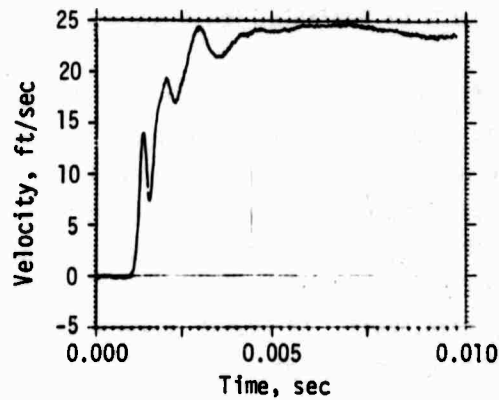
Test 105-01-03

Figure 44. Sparton Brass Horizontal Test Series 2
High-Level, Normal Data



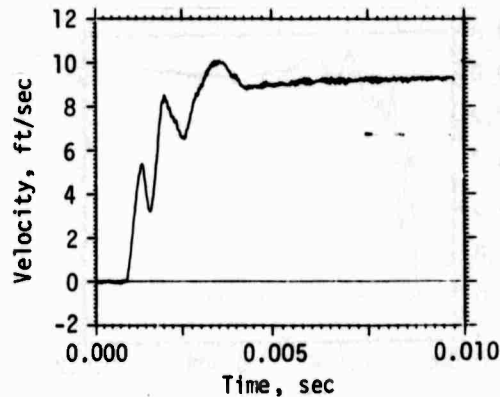
Test 204-01-03

Figure 45. Sparton Brass Vertical Test Series 1
Low-Level, Post-High-g Data



Test 205-01-03

Figure 46. Sparton Brass Vertical Test Series 2
High-Level, Normal Data



Test 206-01-02

Figure 47. Sparton Brass Vertical Test Series 3
Low-Level, Short-Line Data

loading; however, as seen in figure 44, the cross-axis test transducer had an unusually large magnitude of variable high-frequency ringing after cross-axis testing.

f_{CL} and f_{CH} determined from exponential fallthrough testing were 0.0078 and 1149 Hz, respectively; f_{CH} determined from the fast Fourier transform modulus ratio was 252 Hz. In comparison with the CEC horizontal transducer, this transducer had a slightly broader calculated passband, but actual high-frequency cutoff observed in the dynamic testing was 252 Hz (78 Hz lower than that for the CEC transducer). The f_{CH} ratio for this transducer was 4.56 Hz--a greater deterioration of high-frequency response during dynamic testing than that for the CEC transducer.

(2) Vertical

The maximum Δt and calibration level equivalent (Δt ratio) changes, 7.31 and -6.80 percent respectively, occurred during long-line testing. Compared to the other transducers, these changes were not excessively high.

Ringing was observed during all tests, and as was the case

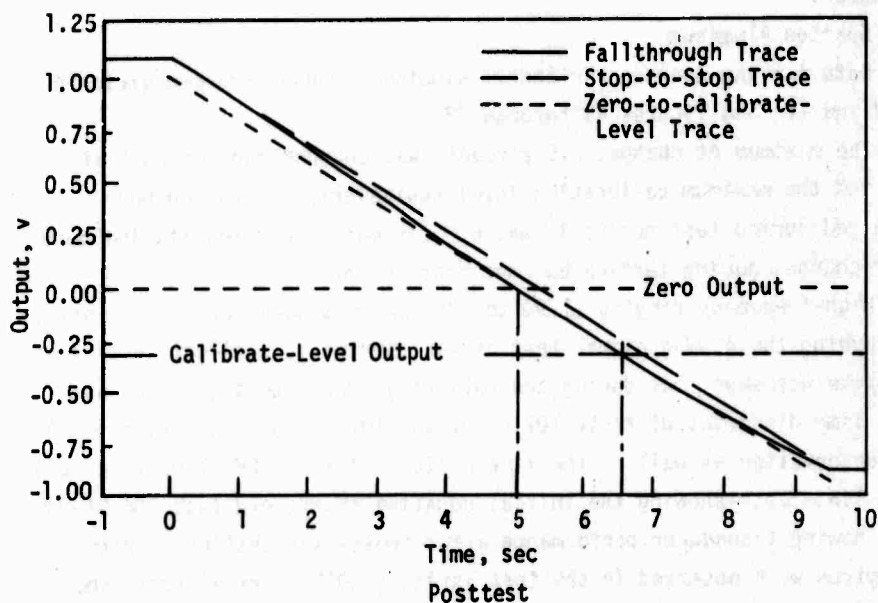
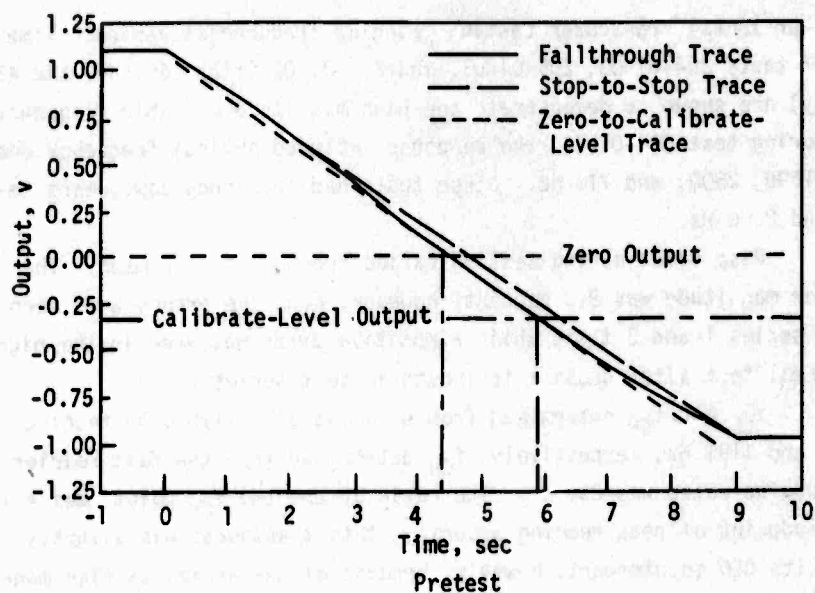


Figure 48. 30° Test Fallthroughs for Sparton Brass Transducer

during the horizontal transducer testing, ringing frequencies varied. Time histories of tests 204-01-03, 205-01-03, and 206-01-02 (figs. 45, 46, and 47, respectively) are shown to demonstrate the high magnitude variable frequency ringing. During test 204-01-03, the response included obvious frequency components of 1500, 2500, and 715 Hz. Other tests had frequency components between 790 and 2800 Hz.

Rise times during testing varied from 1.2 to 1.7 msec. The average error magnitude was 9.5 percent; however, negative errors were seen in all test series 1 and 3 tests while a positive error was seen in the high-g-level, normal test after cross-axis inputs in test series 2.

f_{CL} and f_{CH} determined from exponential fallthrough testing were 0.0076 and 1191 Hz, respectively; f_{CH} determined from the fast Fourier transform modulus ratio was 250 Hz. The ratio of the two f_{CH} points was 4.76. From the standpoint of peak reading accuracy, this transducer was slightly better than its CEC counterpart; however, because of the anomalous high magnitude variable frequency ringing and the substantially higher f_{CH} degradation, overall performance of this transducer was poorer than that of the CEC vertical transducer.

d. Sparton Aluminum

Data for the Sparton horizontal aluminum transducers are given in tables XIV and XV and figures 49 through 52.

The maximum Δt change, 7.5 percent, was encountered during test series 1, and the maximum calibration level equivalent/ Δt ratio change, which occurred during test series 3, was 6.3 percent. Both results indicate transducer changes during testing but not drastic ones.

High-frequency ringing (1790 to 2260 Hz) was seen during all tests.

During the 4000-g normal test of test series 1, a slight initial negative spike was seen, but during the following 1000-g tests, it was not observed. Time histories of tests 107-01-02 and 107-01-03 (figs. 49 and 50) show this observation as well as the time history of test 109-01-03 (fig. 52) --the long-line test--showing the initial negative spike, and test 108-01-03 (fig. 51) showing transducer performance after cross-axis testing. Initial negative spikes were observed in the test series 1 4000-g normal test, and both test series 3 tests.

Rise times for this transducer varied from 1.20 to 1.62 msec. The average error magnitude was 13.15 percent, with all tests indicating positive

Table XIV
STATIC CALIBRATION FALLTHROUGH DATA
FOR SPARTON ALUMINUM TRANSDUCER

Test Series	Pre-Post Interval	Δt Change, %	Cal Eq/ Δt Change, %
1	Series	7.50	3.23
2	30°	-3.13	-3.99
	90°	-0.22	1.17
	On Axis	-2.23	1.50
	Series	-5.50	4.00
3	Short Lines	1.37	0.33
	Long Lines	-2.82	-3.16

errors as did both CEC transducers.

f_{CL} and f_{CH} determined from exponential fallthrough data were 0.0075 and 1199 Hz, respectively; f_{CH} from the fast Fourier transform modulus ratio was 252 Hz. The f_{CH} ratio was 4.75.

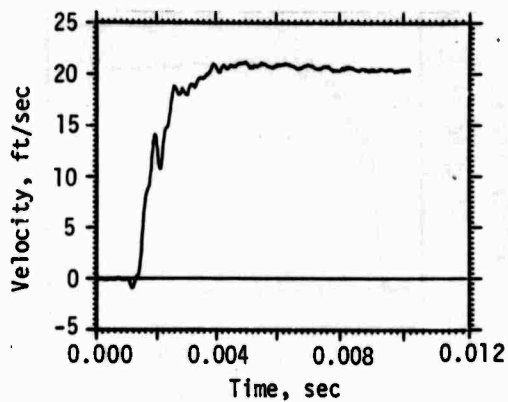
In terms of error, this transducer performed fairly well, but it had a slightly higher average error than did the CEC horizontal transducer. In terms of transducer ring magnitude and the anomalous spike observed in the three tests, this transducer did not perform nearly as well as the CEC transducer. The low-frequency cutoff point, f_{CL} , was slightly better than that for the CEC transducer, but high-frequency cutoff as well as dynamic f_{CH} degradation was poorer.

During cross-axis testing, the observed error did not indicate transducer degradation; however, the magnitude of the high-frequency ring in the 4000-g normal test of test series 2 was substantially higher than that in the 4000-g normal test of test series 1. This observation suggests that cross-axis testing may have worsened the high-frequency ring anomaly.

Table XV

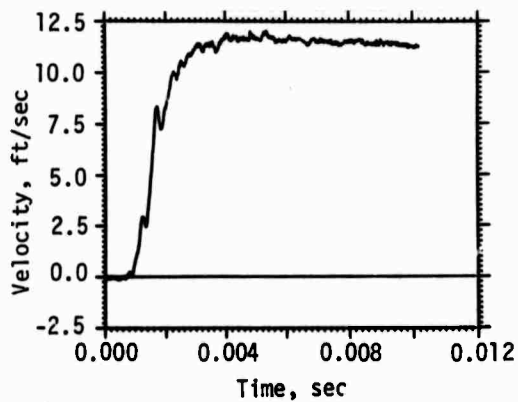
DATA SUMMARY FOR SPARTON ALUMINUM TRANSDUCER TESTING

Test Series	Test	Dynamic Data						Static Data			Comments
		Peak Input, g	Input Velocity Rise Time, msec	Output Velocity Rise Time, msec	Input Velocity, fps	Output Velocity, fps	Error, %	Δt	Cal Eq	Cal Eq/ Δt	
1 S/N 2881	Fallthrough	1300	0.400	1.20	13.20	15.20	15.1	8.65	22.26	2.573	2175 Hz at 7 fps. Slight initial negative output = 1.2 fps; 2500 Hz at 3.6 fps. 1850 Hz at 1.4 fps.
	107-01-01	3200	0.224	1.56	20.30	24.40	20.2				
	107-01-02										
2 S/N 2881	107-01-03	1300	0.260	1.40	12.50	15.30	22.4	9.30	24.70	2.656	2260 Hz at 1.5 fps; 30° off axis. 90° off axis. 2000 Hz at 4 fps.
	Fallthrough										
	Fallthrough							9.26	25.45	2.748	
	108-01-01							8.97	23.68	2.640	
	Fallthrough	4700	0.200		22.50			8.95	23.91	2.671	
3 S/N 2882	108-01-03	4450	0.200	1.60	25.50	29.50	15.7	8.75	23.00	2.629	1790 Hz at 1.4 fps; initial negative output. 2160 Hz at 2.4 fps; initial negative 4.8 fps.
	Fallthrough										
	Fallthrough	1520	0.255	1.62	12.80	13.30	3.9	8.74	18.34	2.098	
	109-01-02							8.86	18.53	2.091	
	Fallthrough	1440	0.320	1.32	12.04	14.72	11.0	9.56	29.68	3.105	
	109-01-03							9.29	27.94	3.007	
	Fallthrough										



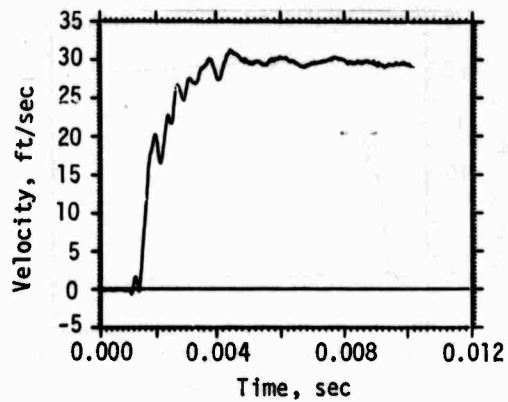
Test 107-01-02

Figure 49. Sparton Aluminum Test Series 1
High-Level, Normal Data



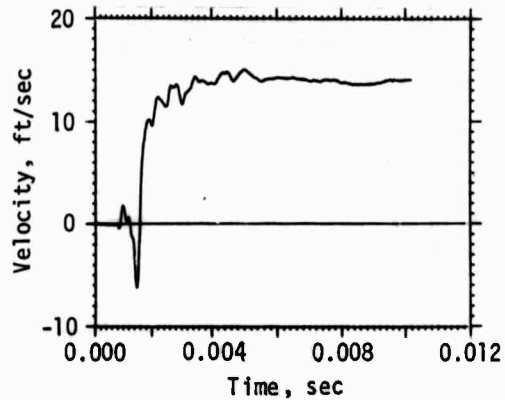
Test 107-01-03

Figure 50. Sparton Aluminum Test Series 1
Low-Level, Post-High-g Data



Test 108-01-03

Figure 51. Sparton Aluminum Test Series 2
High-Level, Normal Data



Test 109-01-03

Figure 52. Sparton Aluminum Test Series 3
Low-Level, Long-Line Data

e. Sparton 604

Data for the Sparton 604 vertical transducer are given in tables XVI and XVII, and figures 53 and 54.

Only two Sparton 604 transducers were received and both had oil leaks upon receipt from the manufacturer. They were sent back for repair. One transducer still had an oil leak when received the second time; only test series 3 tests were performed on the remaining transducer.

The Sparton 604 transducer performed fairly well, but it did exhibit a large amount of nonlinearity during 2-g fallthrough testing. In terms of accuracy, this transducer averaged a magnitude error of 9.5 percent. A small amount of transducer ring was observed at a nominal 4000-Hz frequency. This is interesting since this ringing frequency is noticeably higher than DX-type transducer ringing frequencies. Since this transducer is quite different in physical size and natural frequency (4.4 Hz) from conventional DX-type transducers, some clue may be offered as to why ringing occurs in nearly all pendulous-type transducers. These possibilities should be explored in future transducer test programs. It should be noted, however, that the Natec system gain is about 9 dB down at 4000 Hz (i.e., 65 percent of the amplitude of this frequency component is attenuated).

Another important difference seen in this transducer response as compared to conventional DX-type transducers was rise times. These were extremely short--0.800 and 0.924 msec for tests 209-01-02 and 209-01-03, respectively. (Rise times of transducers with 3000-centistoke damping oil are about 1.4 msec.) Because of the higher damping ratio during exponential fallthrough, the f_{CH} calculated was 1460 Hz; this is much higher than the calculated f_{CH} for DX-type transducers (971 to 1199 Hz). f_{CL} was 0.0133 Hz; this is about 0.0006 Hz higher than that for DX-type transducers. f_{CH} determined from the fast Fourier transform modulus ratio was 380 Hz; this is also higher than the dynamic f_{CH} observed in DX-type transducers. Because of the increased passband capabilities, this transducer was superior in terms of high-frequency response to any DX-type transducer tested. Low-frequency cutoff, f_{CL} , however, was about one octave higher than that for DX-type transducers. The f_{CH} ratio was 3.84; this is better than that for Sparton DX-type transducers but still not as low as that for CEC transducers.

Since only one transducer was available for testing, it is difficult to weigh the performance of this transducer against DX-type transducers. Test

Table XVI

STATIC CALIBRATION FALLTHROUGH DATA
FOR SPARTON 604 TRANSDUCER

Test Series	Pre-Post Interval	Δt Change, %	Cal Eq/ Δt Change, %
3	Short Lines	6.85	1.45
	Long Lines	4.27	1.35

results do show, however, that this transducer has the poorest f_{CL} capabilities of any of the DX-type transducers, but better dynamic f_{CH} capabilities. A linearity problem was also evident during fallthrough calibrations.

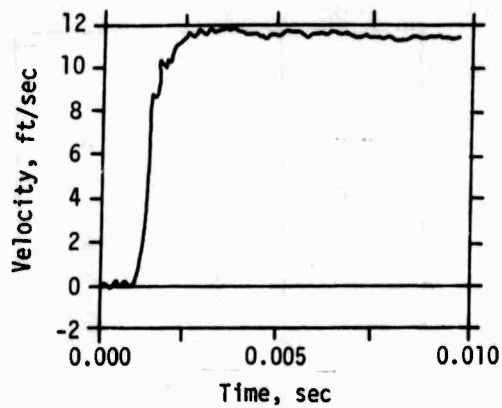
f. Sparton 602 (FM)

Data for the Sparton 602 (FM) transducer are given in figure 55. Transducer output did not resemble the input. Therefore, tabular data for this transducer are not included. Long-line testing could not be conducted because the signal conditioner went into oscillation. It should be noted, however, that the signal conditioner was only designed for laboratory short-line testing.

Only two test transducers were received. The fallthrough test on transducer SN 3592 had a nonlinear output (fig. 56a). This nonlinearity seemed to indicate the possibility of loose pivots. The transducer output during the low-frequency test was also nonlinear (fig. 56b). After the test series 1 dynamic tests, the posttest 1000-g fallthrough indicated transducer failure (fig. 56c). The transducer output during this test seemed to indicate a mechanical nonlinearity and an internal coil failure.

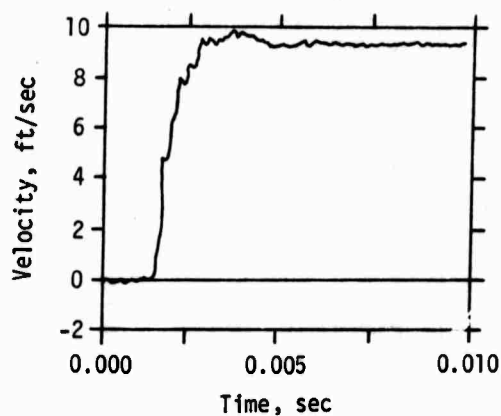
Table XVII
DATA SUMMARY FOR SPARTON 604 TRANSDUCER TESTING

Test Series	Test	Dynamic Data						Static Data			Comments
		Peak Input, g	Input Velocity Rise Time, msec	Output Velocity Rise Time, msec	Input Velocity, fps	Output Velocity, fps	Output Error, %	Δt	Cal Eq	Cal Eq/ Δt	
3	Fallthrough							3.91	18.90	4.830	4180 Hz at 0.4 fps.
	209-01-02	1240	0.267	0.800	10.00	11.60	16.0				
	Fallthrough							4.18	19.90	4.760	
	Fallthrough							3.94	14.60	3.710	
S/N 3607	209-01-03	1100	0.296	0.924	9.80	9.50	- 3.0				3780 Hz at 0.4 fps.
	Fallthrough							4.10	15.00	3.660	



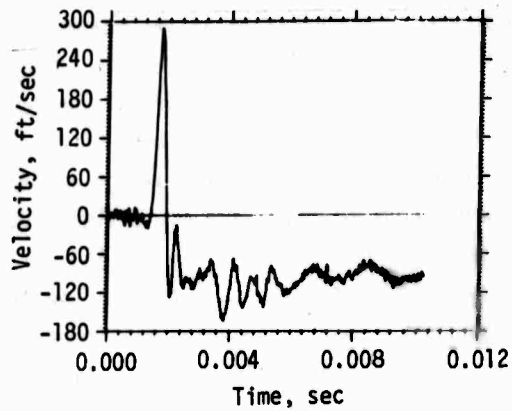
Test 209-01-02

Figure 53. Sparton 604 Test Series 3
Low-Level, Short-Line Data



Test 209-01-03

Figure 54. Sparton 604 Test Series 3
Low-Level, Long-Line Data



Test 128-08-01

Figure 55. Sparton 602 (FM) Test Series 1
Low-Level, Normal Data

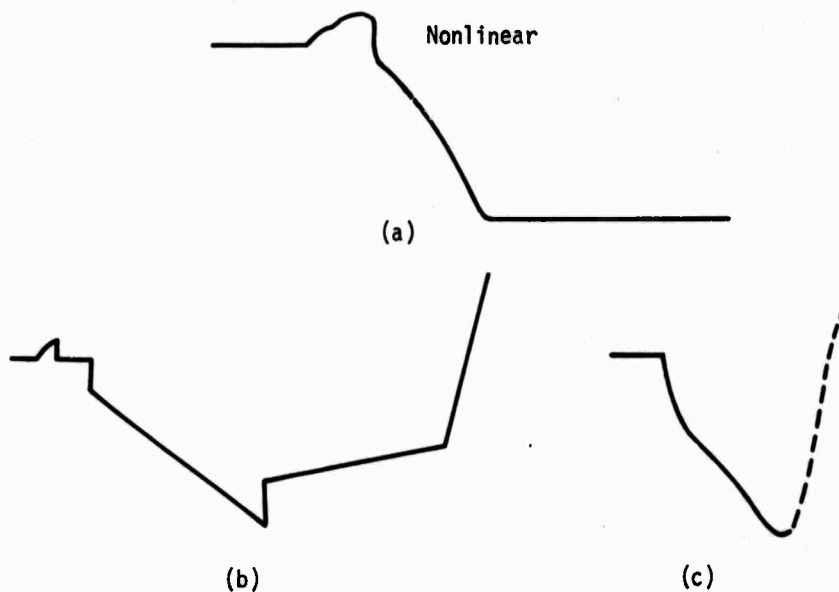


Figure 56. Sparton 602 (FM) Transducer 1-g Fallthrough Output

In order to investigate the cause of the extremely poor performance of these transducers, they were turned over to Physics International by Captain Darrell J. Newell for examination. Upon examination by Mr. Ed Eckert of Physics International, the following conditions were observed:

- (1) SN 3592 - The coil was broken loose from the plastic coil carrier and the pendulum suspension had at least 0.1 in. of side slop.
- (2) SN 3593 - Suspensions were extremely tight. The free-swinging pendulum (without surrounding oil) decayed to half-amplitude oscillation in three to four cycles*.

3. LINEAR TRANSDUCER DATA

Table XVIII gives a tabulation of rise time, error magnitude, and frequency cutoff points for all the linear transducers tested.

a. EG&G

The EG&G transducer can be used in either a vertical or horizontal operating mode by performing a simple mechanical nulling procedure for the mode desired. Since the transducers, as received, were nulled for vertical measurements, vertical testing was done first; the same transducers were then adjusted for horizontal operation. Because of previous vertical cross-axis testing, the cross-axis transducer was not tested horizontally. Dynamic data for these transducers are given in table XIX, and figures 57 through 60.

During linear velocity transducer testing, the EG&G transducer performed better in terms of error magnitude as a horizontal transducer. This transducer also exhibited a high f_{CL} (compared to the pendulous transducers) and failed after 90°-cross-axis testing.

(1) Horizontal

Transducer SN 026 was used for test series 1 and 3 horizontal testing. Test series 2 cross-axis tests were not performed on the horizontal sled track because this same transducer (SN 025) was tested on the vertical drop tower. Transducer SN 024 was improperly adjusted for horizontal mechanical null and thus was not used. The top outer lock ring was adjusted, but the setscrews were not tightened. Also, the inner bushing was loose and

* Physics International has an acceptable limit of 16 to 28 cycles to half amplitude on a free-swinging pendulum.

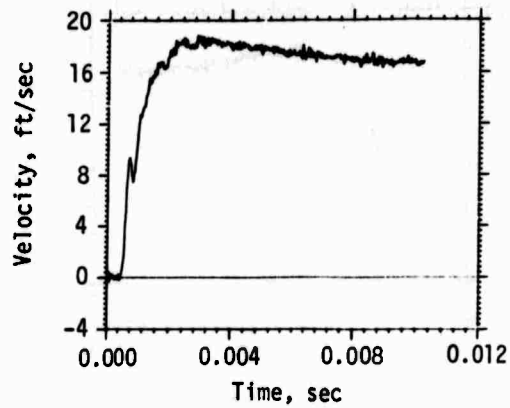
Table XVIII
SUMMARY OF LINEAR TRANSDUCER TEST RESULTS

Transducer	Rise Time, msec			Error Magnitude, %			f_{CL} (Calculated), Hz	f_{CH} (Calculated), Hz	f_{CH} (From FFT), Hz	f_{CH} (Calculated) f_{CH} (From FFT)
	Low	Avg.	High	Low	Avg.	High				
EG&G - 100 (Horizontal)	0.72	1.02	1.20	1.15	6.55	11.60	0.058	1722	300	5.74
Setra - 151 (Horizontal)	0.28	0.46	0.64	18.20	36.58	56.00	--	*	1200	*
Endevco (Horizontal)							*	*	*	*
EG&G - 100 (Vertical)	1.20	1.37	1.60	11.00	20.96	35.00	0.058	1722	215	7.99
Setra - 151 (Vertical)	0.16	0.32	0.56	0.86	20.52	34.30	--	*	1900	*
Endevco (Vertical)							*	*	*	*

* Exponential falloff or FFT could not be obtained.

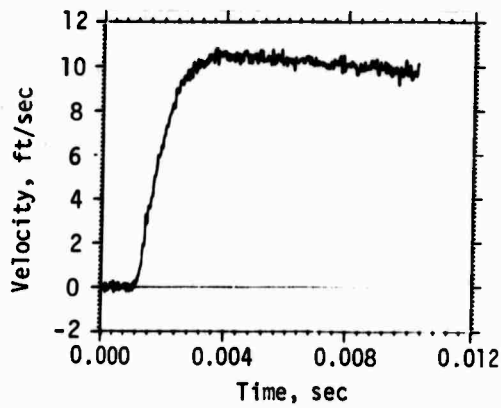
Table XIX
DYNAMIC DATA SUMMARY FOR EG&G TRANSDUCER TESTING

Test Series	Test	Dynamic Data					Static Data				Comments
		Peak Input, g	Input Velocity Rise Time, msec	Output Velocity Rise Time, msec	Input Velocity, fps	Output Velocity, fps	Output Velocity, Error, %	Static Data			
								Δt	Cal Eq	Cal Eq/Δt	
Horizontal Transducers											
1	124-00-01	700	0.360	1.20	8.70	8.80	1.15				Carrier at 0.8 fps; good output.
S/N 026	124-00-03	3500	0.168	1.20	18.60	18.20	- 2.15				High frequency component during rise; 2800-Hz ring.
	124-00-04	950	0.350	1.12	9.50	10.60	11.60				Carrier noise at 0.8 fps.
3	125-00-01	800	0.430	1.04	11.50	12.80	11.30				Carrier at 0.6 fps peak-to-peak.
S/N 026	125-00-02	1120	0.248	1.30	11.40	12.00	5.26				Carrier at 0.6 fps, peak-to-peak.
Vertical Transducers											
1	116-00-02	940	0.260	1.60	8.70	7.20	-17.24				Carrier noise at 1.5 fps.
S/N 024	116-00-03	4700	0.260	1.40	17.40	15.60	-10.30				Carrier at 0.8 fps; 2500 Hz at 3.2 fps.
	116-00-04	1125	0.288	1.40	9.00	8.01	-11.00				Carrier noise at 1.32 fps.
2	117-00-03	2829	0.266		17.60						30° off axis.
S/N 025	117-00-04	4000	0.220		17.50						90° off axis. (Transducer went bad after 90° test)
3	118-00-01	1080	0.240	1.28	7.83	9.40	20.60				Carrier noise at 1.7 fps.
S/N 026	118-00-02	1000	0.232	1.20	7.70	10.40	35.00				Carrier noise at 0.9 fps.



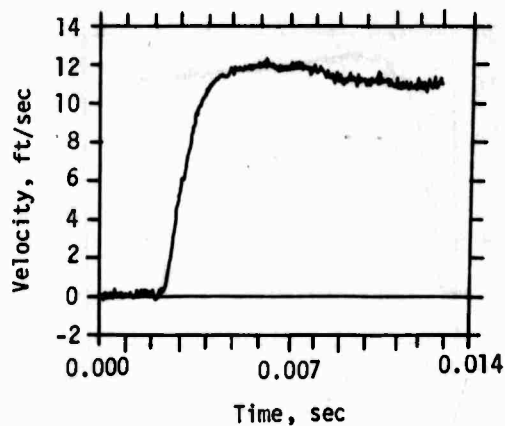
Test 124-00-03

Figure 57. EG&G Horizontal Test Series 1
High-Level, Normal Data



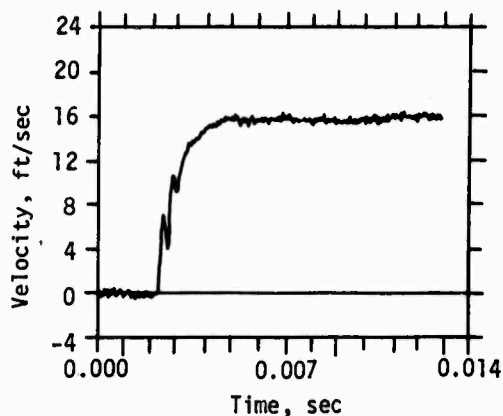
Test 124-00-04

Figure 58. EG&G Horizontal Test Series 1
Low-Level, Post-High-g Data



Test 125-00-02

Figure 59. EG&G Horizontal Test Series 3
Low-Level, Long-Line Data



Test 116-00-03

Figure 60. EG&G Vertical Test Series 1
High-Level, Normal Data

a small amount of oil leaked out.

During horizontal testing, the EG&G transducer had an average rise time of 1.02 msec. Since this was noticeably lower than the rise times encountered during vertical testing, it may be speculated that (at least for the test series 1 transducer) rise time was affected by the null adjustment made between vertical and horizontal testing, or that the mode of operation itself (vertical or horizontal) influenced the rise-time capabilities.

During test series 1, a carrier frequency signal component was noted with a peak-to-peak value of about 10 percent of peak velocity. In the first two tests of this series, transducer error was 1.15 and -2.15 percent. During the last test series 1 test, the error was 11.6 percent; this indicates that the transducer may have been damaged during the previous high-g-level test.

During test series 3, carrier content with a peak-to-peak magnitude of 0.6 fps (about 5 percent of peak velocity) was again observed. The errors were 11.30 and 5.26 percent for short- and long-line testing, respectively.

Data from tests 124-00-03, 124-00-04, and 125-00-02 (figs. 57, 58, and 59) are presented to show high-g-level test results, transducer performance after high-g-level testing, and long-line test results, respectively.

f_{CL} and f_{CH} determined from exponential falloff data were 0.058 and 1722 Hz, respectively. The calculated f_{CH} was 300 Hz in the test series 1, high-g-level test and 190 Hz in the test series 3, short-line test.

Transducer performance during horizontal testing was fairly good in terms of accuracy with a 6.55-percent average. A moderate amount of carrier noise was observed.

(2) Vertical

Figure 60 shows the transducer performance during test series 1, 4000-g, normal testing. A nominal 2500-Hz ring was apparent during the initial rise time.

During test series 1, errors were consistently negative --ranging between -10.3 and -17.24 percent. Carrier noise was noted and a nominal 2500-Hz signal with a 0.8-fps peak-to-peak amplitude was seen during the rise time of the high-g-level test.

The test series 2 transducer failed after the high-g-level, 90°-cross-axis test. When this transducer was turned opposite its normal

(at rest) axis and held in that position, the output went to only ≈ 0.33 v, but the electrical calibrate signal went to 1.0 v. When the transducer was brought back to its normal position, the output would not come back to zero, unless the transducer was moderately tapped.

During test series 3, errors were 20.6 and 35.0 percent for short- and long-line testing, respectively.

The average rise time during testing was 1.37 msec. f_{CL} and f_{CH} from exponential fallthrough were 0.058 and 1722 Hz, respectively. f_{CH} determined from the fast Fourier transform modulus ratio was 215 Hz.

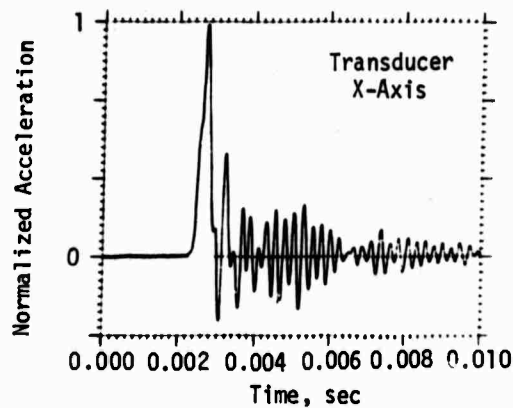
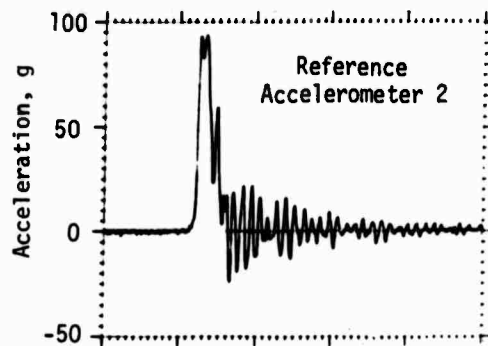
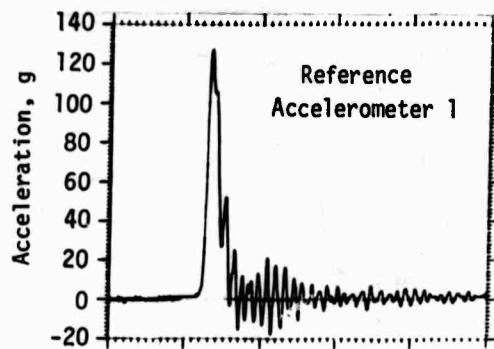
Transducer performance during vertical testing was not good. The average error magnitude was high (20.96 percent), and the transducer failed during cross-axis testing. A moderate amount of carrier frequency component was observed in all on-axis tests. From the standpoint of rise time, f_{CH} , and error magnitude (in particular), transducer performance in the horizontal mode was noticeably better than that in the vertical mode.

b. Endevco

The Endevco system had an inconvenient calibration procedure and noticeable long-term drift errors but excellent rise-time capabilities and good reproduction of input waveform patterns. Error analysis could not be performed because of calibration problems. Time histories for test 122-00-07 are shown in figure 61.

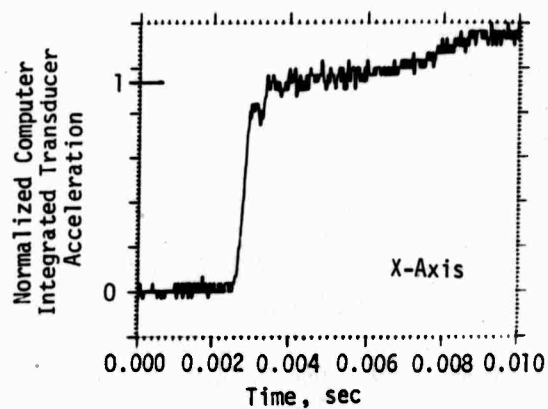
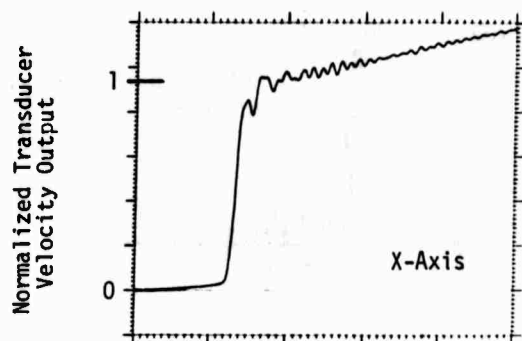
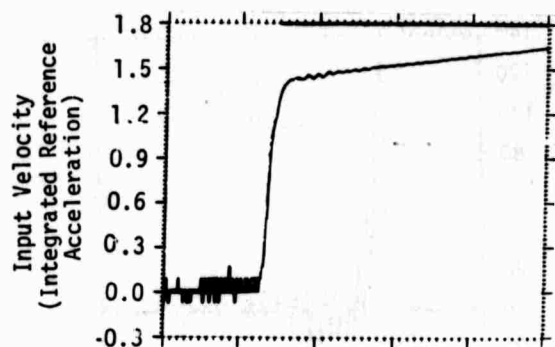
Since the Endevco triaxial transducer has a maximum g-level rating of 150 g, it could not be tested on the sled track and still maintain the required acceleration pulse width of less than 0.5 msec. It was desirable to achieve input acceleration pulse widths at 150 g between 0.25 and 0.50 msec so as to be consistent with the overall program objectives. (Typical pulse widths at minimum sled-track pressures were approximately 5.0 msec at 150 g.) Therefore, since there is more control at low-g-level inputs on the drop tower and since the Endevco transducer is triaxial and can be tested in the horizontal or vertical mode, it was retested on the drop tower. Acceleration input pulse widths of 0.5 msec at 110 g on the drop tower were obtained.

One problem encountered with this system was the method of calibration relating to the velocity output signal. There were six outputs on the signal conditioner: three of them were input acceleration, and the other three were integrated input acceleration to obtain an output velocity signal. An electrical calibrate signal was provided for the acceleration channels;



Test 122-00-07

Figure 61. Endevco 150-g, Normal Data



Test 122-00-07

Figure 61.---Concluded

this allowed the dynamic peaks to be accurately determined. However, velocity output channels do not have the same type of calibrate signals since their outputs are dependent on the integrated acceleration signal. In a normal test, a simulated square-wave electrical acceleration calibrate signal is initiated for approximately 1 sec. The velocity channel will integrate this calibrate signal and reach saturation almost immediately upon generation of this signal. Therefore, the calibrate signal on the velocity channel cannot be related back to feet per second. Since the acceleration calibrate signal of one channel is directly related to the velocity output data of another channel, it is difficult to relate these two signals because of possible differences in tape deck gains and inherent digitizing problems. Therefore, the Endevco transducer outputs were only compared to the reference accelerometers with regard to visual observation of noise level, patterns, and comparison to the integrated reference input acceleration.

The Endevco transducer acceleration output had a slightly higher ringing output (fig. 61). The pulse shape was very similar to the reference accelerometer outputs and the noise level was approximately 12 percent of the total output signal. The digitized data relating integrated reference acceleration and the transducer velocity output signal were almost identical in wave shape except for noise level and drift slope angle. Input rise time was 0.48 msec; output rise time was 0.52 msec. These rise times were very close.

A zero baseline drift test was also performed to determine the percentage of output voltage drift with time. The signal conditioner was zeroed and then released just prior to this test. The output versus time was recorded on Polaroid film. Ten percent of maximum output was reached in approximately 3 sec: this is well within the specification limits.

It would be desirable to have a single square-wave pulse, of known amplitude and representing a fixed foot-per-second level, for a calibrate signal for the velocity channel so that the data could be accurately determined in the field or in the computer laboratory. At the present time these data can be determined, but with considerable effort and time. Also, the zero baseline drift on the velocity channel necessitates holding the zero pushbutton switch until a few seconds prior to the actual test. If this is not done, the output will reach saturation before the input signal is generated, or the data acquisition system may saturate because of the additional dc-voltage

shift. Initiation and release of the zero switch can be troublesome under certain test conditions and may not be practical.

c. Setra

The Setra transducers had a system output boundary below the rated capability of the horizontal transducer, relatively large amounts of noise, and an inconvenient calibration procedure. Data for the Setra transducers are given in table XX, and figures 62 through 66.

(1) Horizontal

During test series 1, the Setra horizontal transducer exhibited moderate amounts of noise and fairly large negative errors (-18.2 to -56.0 percent). All 4000-g tests exceeded the transducer capability of 16.6 fps, but all outputs appeared to be bounded at about 9 fps. Time histories of tests 119-00-01, 119-00-03, and 119-00-04 (figs. 62, 63, and 64) show an apparent transducer maximum output boundary of 9 fps. The rated transducer velocity input capability (16.6 fps) was exceeded only in the test series 1, high-g-level, normal input test (test 119-00-03).

Transducer SN 904 was not considered usable after the cross-axis tests. A normal 5000-g and a normal 1000-g test were generated after the cross-axis tests to determine survivability. However, many spikes were observed in the output signal. Prior to test series 2, transducer SN 904 was used for test series 3. This transducer could not be used with 4000 ft of cable; thus, the long-line test could not be run. The error in short-line testing was -23.79 percent with peak-to-peak noise at 1.1 fps.

During exponential fallthrough testing, inadequate data were generated because of obvious ac coupling in the Setra signal conditioner; so, no f_{CH} or f_{CL} limits could be established from exponential fallthrough data. Fast Fourier transform modulus ratios from the dynamic data showed f_{CH} for this transducer to be 1200 Hz.

Performance of this system was not good because of high error magnitudes, cross-axis test failures, and the inability of the transducer to function properly with long lines. In addition, calibration procedures were not compatible with many field test requirements.

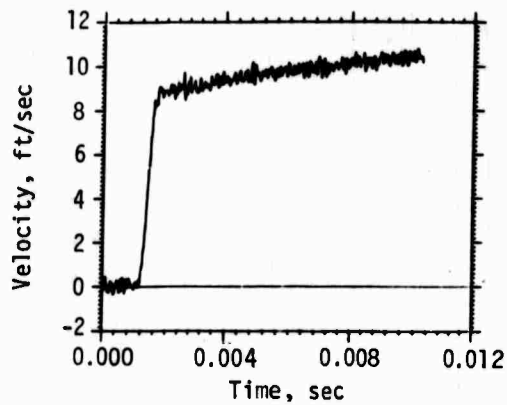
(2) Vertical

Since only two transducers were available, transducer SN 906 was used in test series 1 and 2. During test series 1, transducer errors varied from 4.86 to -34.30 percent. It should again be noted, however, that

Table XX

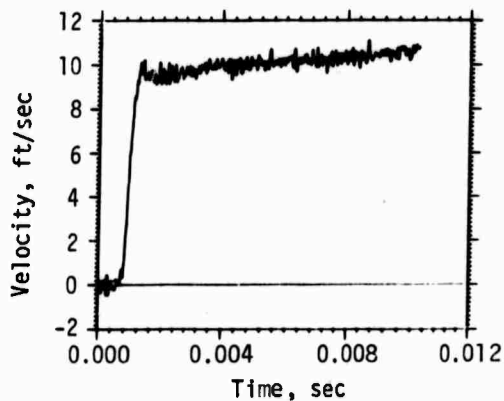
DYNAMIC DATA SUMMARY FOR SETRA TRANSDUCER TESTING

Test Series	Test	Dynamic Data					Static Data			Comments	
		Peak Input, g	Input Velocity Rise Time, msec	Output Velocity Rise Time, msec	Input Velocity, fps	Output Velocity, fps	Error, %	Δt	Cal Eq		Cal Eq/ Δt
Horizontal Transducers											
1 S/N 903	119-00-01	2000	0.280	0.64	14.4	9.1	-36.80			Overranged; noise at 0.6 fps. Noise at 1.2 fps.	
	119-00-03	3300	0.176	0.36	20.4	9.0	-56.00				
	119-00-04	1400	0.320	0.36	11.0	9.0	-18.20				
2 S/N 904	120-00-01	3700	0.120		19.6					30° off axis. 90° off axis. Overranged.	
	120-00-02	4150	0.120	0.64	21.6						
	120-00-03	3600	0.240		21.2	11.0	-48.20				
3 S/N 904	121-00-02	1340	0.274	0.28	11.4	8.7	-23.70			Noise at 1.0 fps.	
Note: Could not run transducer with long lines because of oscillations.											
Vertical Transducers											
1 S/N 906	113-00-01	1260	0.360	0.16	9.2	7.4	-19.60			Noise at 0.6 fps; fairly good pattern. Overranged. Carrier noise at 0.6 fps; best Setra shot.	
	113-00-02	4000	0.216	0.24	24.5	16.1	-34.30				
	113-00-03	1277	0.200	0.44	11.6	11.7	0.86				
2 S/N 906	114-00-01	6178	0.150		23.0					30° off axis. 90° off axis. Overranged; negative spikes.	
	114-00-02	6000	0.130		24.0						
	114-00-03	4900	0.240	0.56	24.3						
3 S/N 905	115-00-02	1140	0.241	0.28	9.8	12.6	28.50			Good shot; percentage error for peak only--the rest looked very close.	
	115-00-03	1275		0.24	9.1						



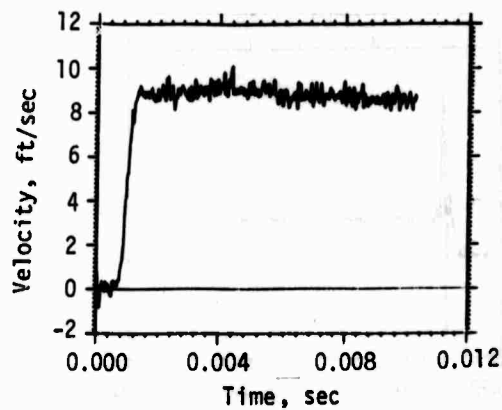
Test 119-00-01

Figure 62. Setra Horizontal Test Series 1
Low-Level, Pre-High-g Data



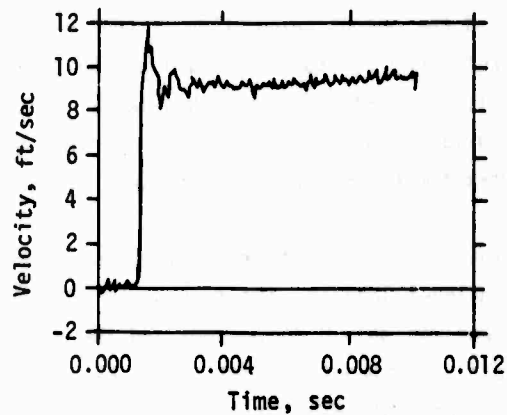
Test 119-00-03

Figure 63. Setra Horizontal Test Series 1
High-Level, Normal Data



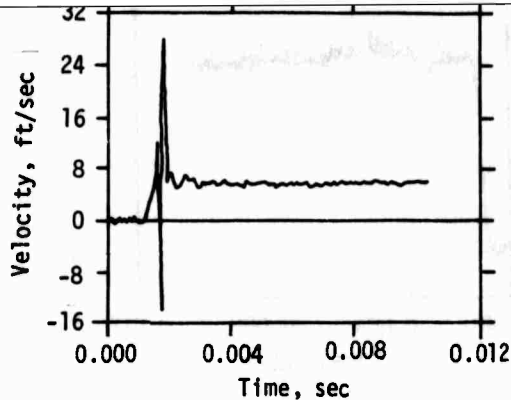
Test 119-00-04

Figure 64. Setra Horizontal Test Series 1
Low-Level, Post-High-g Data



Test 113-00-03

Figure 65. Setra Vertical Test Series 1
Low-Level, Pre-High-g Data



Test 114-00-03

Figure 66. Setra Vertical Test Series 2
High-Level, Normal Data

the transducer input exceeded the output capability of the transducer in the high-g-level tests. Therefore, the transducer should not be criticized for excessively high error magnitude in any of the high-g-level tests. During all high-g-level tests, high-level output spikes were observed, but again it should be remembered that maximum transducer velocity input (16.6 fps) was exceeded.

Of special interest was the third test in test series 1. In this test, conducted after high-g-level loading, the transducer performance was outstanding. Transducer error was only 0.86 percent and the output, except for 1.6-fps peak-to-peak noise, matched the input almost exactly. Transducer performance in this test was the best of all transducers in the entire test program.

After test series 2 cross-axis testing, transducer outputs contained high-g-level spikes; however, maximum input velocity was greatly exceeded.

During test series 3, transducer error was 28.5 percent for the short-line testing; but the output velocity profile matched the input velocity very well.

After the 1000-g, long-line test, transducer SN 905 malfunctioned. The neutral at-rest transducer output remained at 2.5 v (only occurred when long lines were connected); with short lines, the output went back to zero. Although the output contained oscillations, the transducer functioned during the long-line test.

One undesirable feature of this transducer was the calibrate signal output. The time necessary for output stabilization after the calibrate signal is initiated (3 min) and the output voltage magnitude relating to time can cause several problems when these transducers are used in the field.

The level of output swing 1 sec after engaging of the shunt calibrations can be somewhat difficult to determine accurately (fig. 67). The difference between the 1-sec magnitude level and the reference magnitude level is the simulated velocity signal. When this calibrate signal is retrieved from a tape recorder, oscillograph, oscilloscope, etc., an accurate time readout is necessary. Also, the stabilization period of 3 min after the calibrate signal is initiated makes it impossible to calibrate these transducers 15 to 20 sec prior to a field test. Both the horizontal and vertical velocity transducers were calibrated in the same way.

Overall performance of this transducer was good except for high magnitude errors. Except for scale factor variations, output velocity patterns very closely matched input velocity in all low-g-level tests. Rise time average was 0.32 msec, and f_{CH} from the fast Fourier transform modulus ratio was 1900 Hz; both were better than those for the Setra horizontal transducer.

The time history of test 113-00-03 (fig. 65) demonstrates the extremely good performance after high-g-level, normal loading, and the time history of test 114-00-03 (fig. 66) demonstrates the spikes observed when transducer velocity input capabilities were exceeded.

4. DAMPING FLUID TEST DATA

The damping fluid test results are shown in figures 68 through 72. Time lags resulting from digital plot start-time errors are evident. Data tabulation is given in table XXI.

The damping ratio determined from exponential fallthrough data varied almost linearly with oil viscosity (fig. 73). A close approximation of the damping ratio is

$$h \approx 26.52 + (\text{oil centistoke rating} - 500) \times 0.0467$$

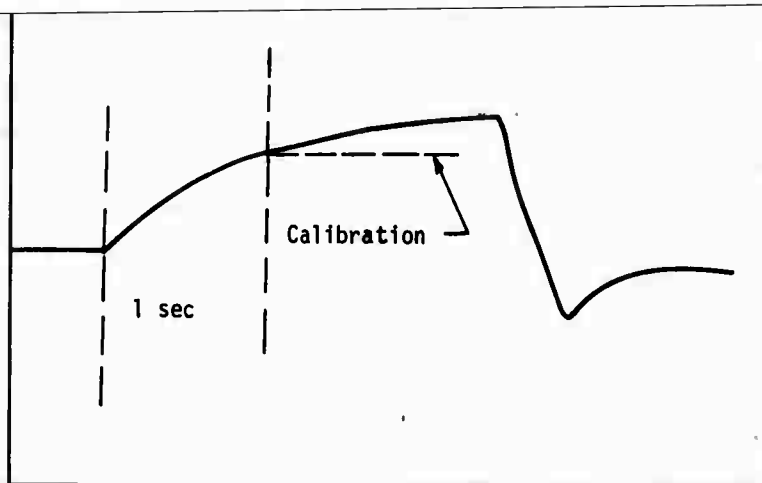


Figure 67. Typical Setra Transducer Calibration Output

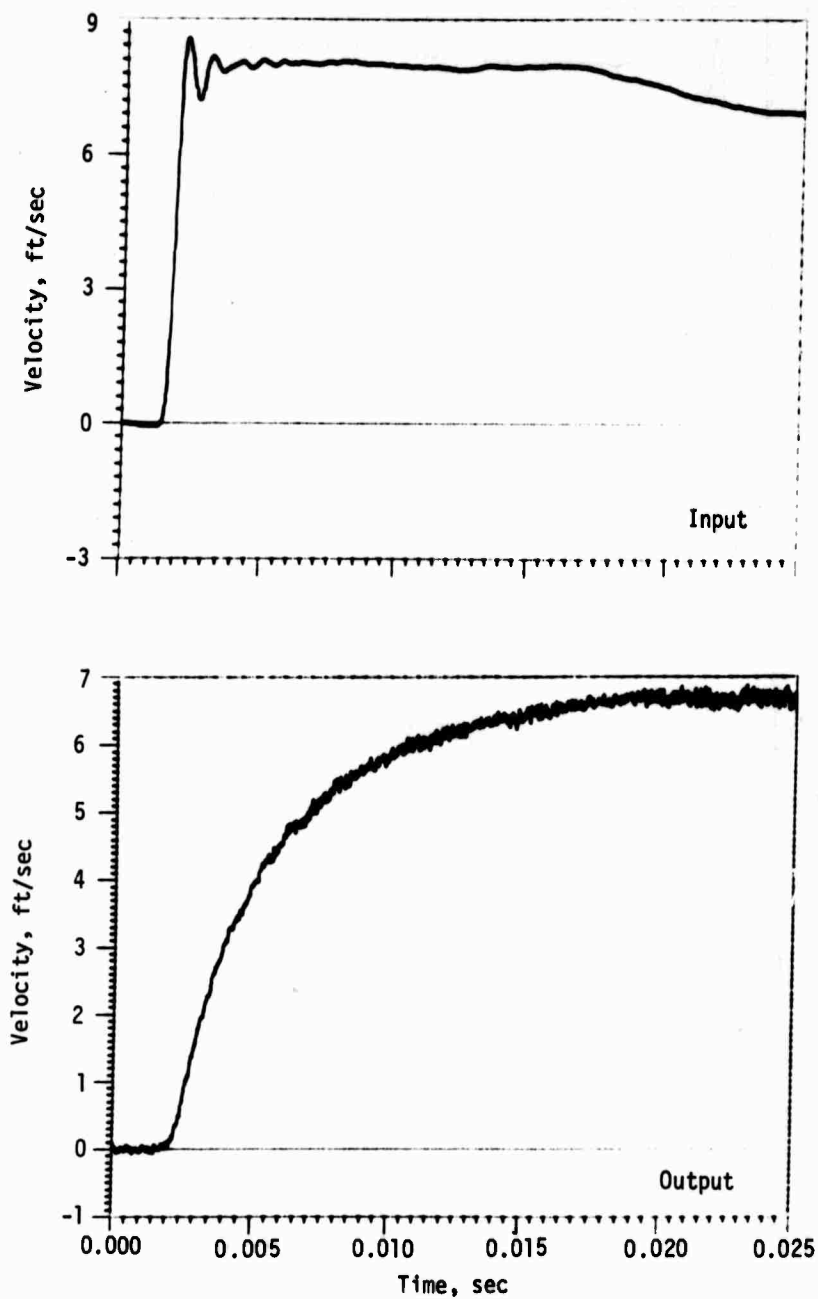
As expected, the high- and low-frequency response limits improved as oil viscosity was increased. In addition, the transducer scale factor appeared to be fairly linear with the centistoke value of the oil fill. Figure 74 shows velocity/voltage ratio versus oil centistoke rating. Velocity/voltage ratio is the transducer output in feet per second for a bridge imbalance equal to the bridge supply voltage. A close approximation for transducer velocity output per voltage ratio output is

$$\frac{V}{VR} = \text{oil centistoke rating}$$

where

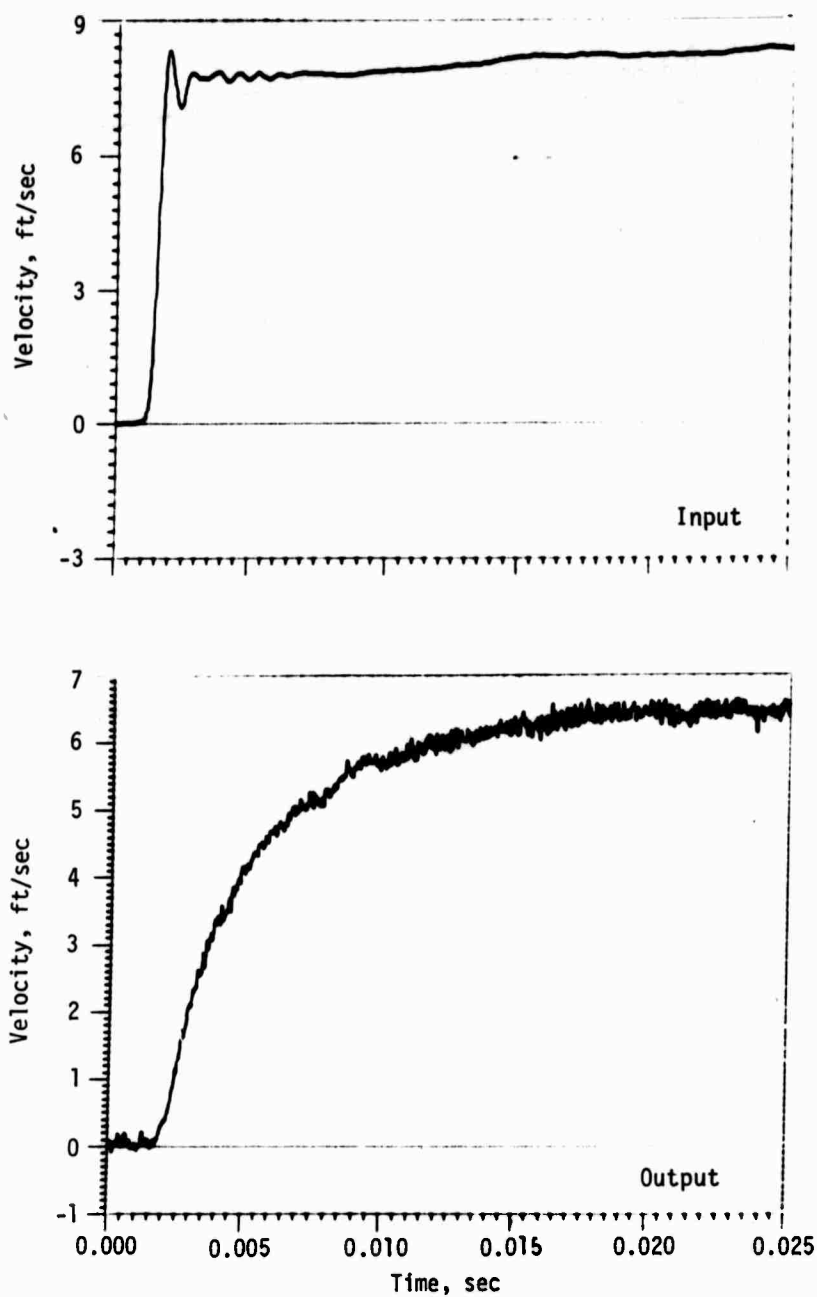
V/VR is velocity output per voltage ratio in feet per second.

From these test observations, a number of simple rules can be developed which will allow the user to closely estimate many of the properties of a CEC horizontal DX-type transducer, knowing only the centistoke value of the damping oil. Since DX-type velocity transducers have a natural frequency of 3 Hz,



(a) Short Lines

Figure 68. CEC Transducer Response with 500-Centistoke Damping Oil



(b) Long Lines

Figure 68.---Concluded

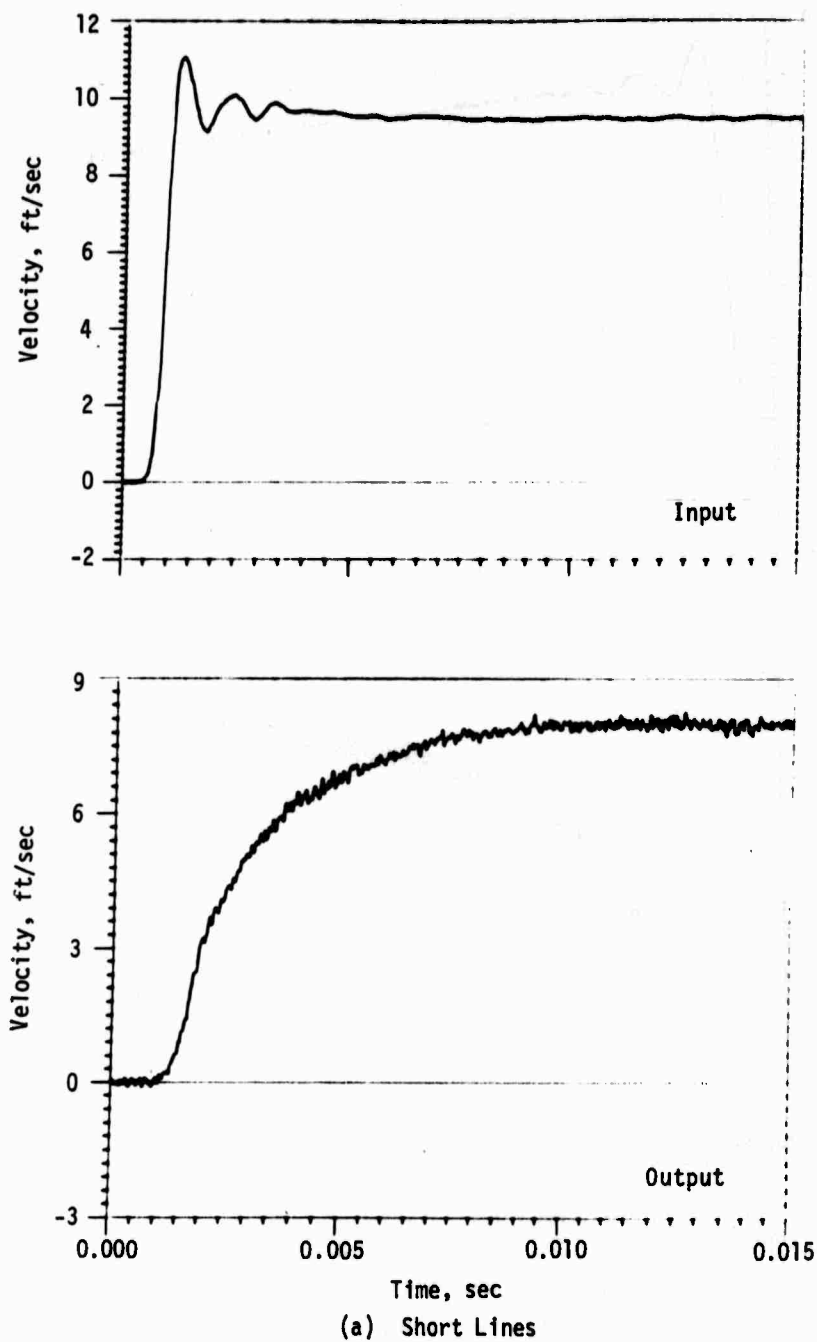
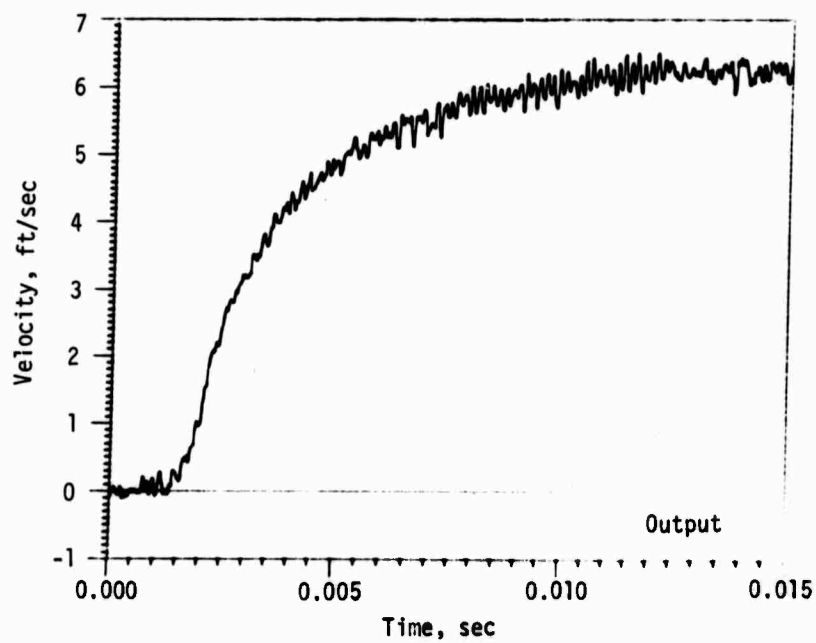
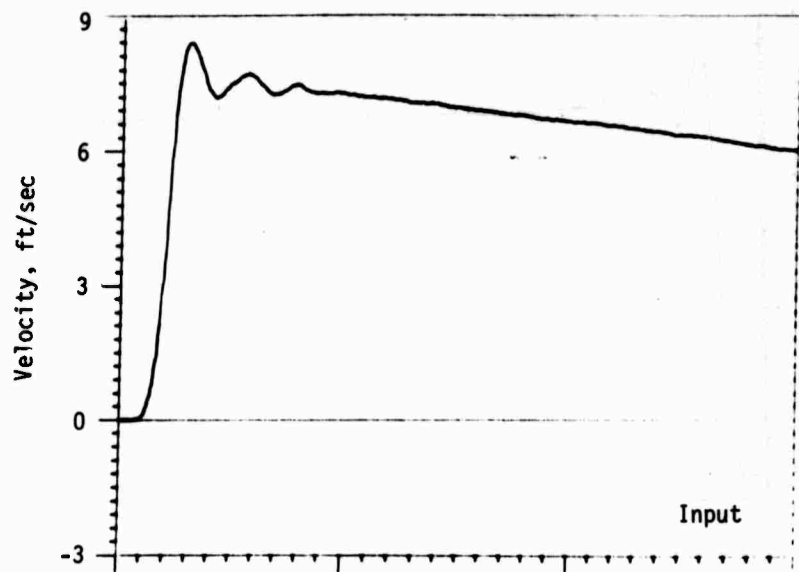
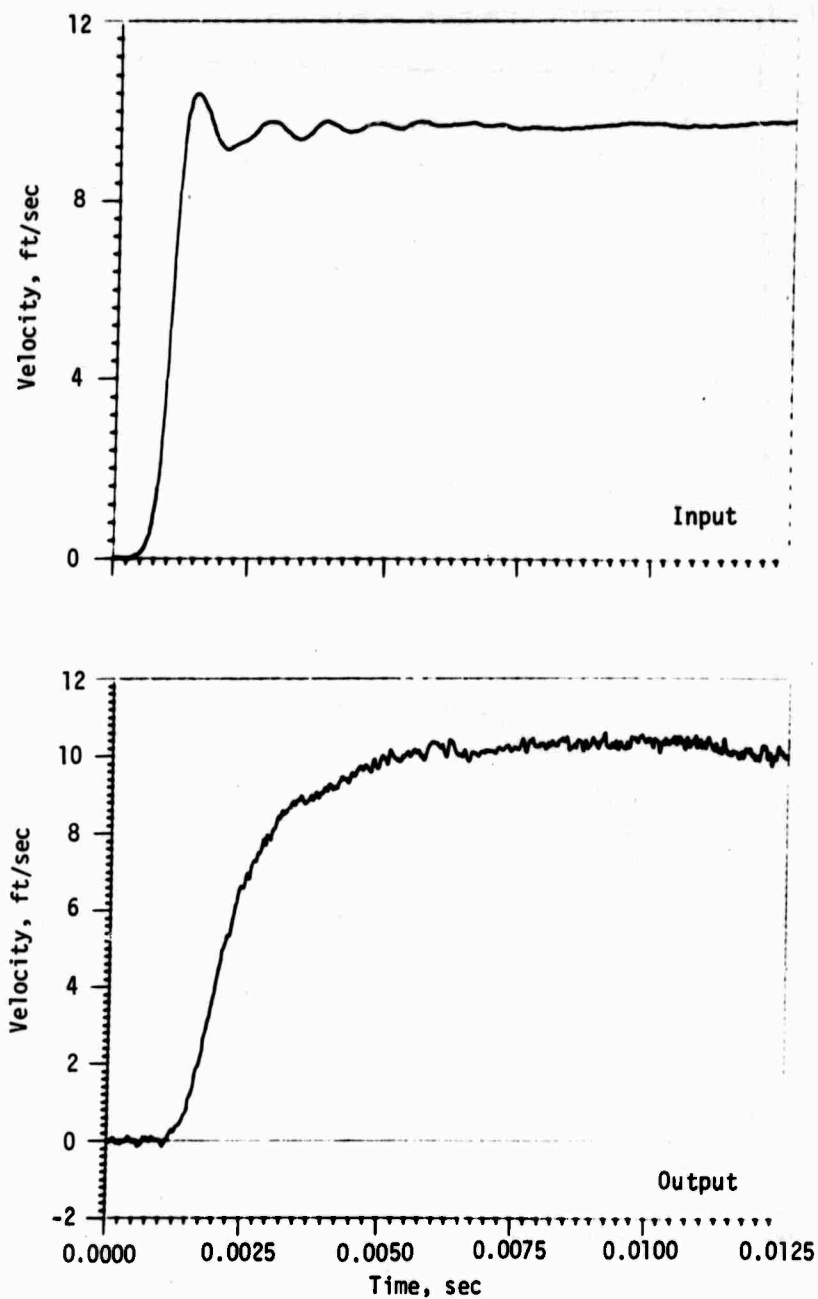


Figure 69. CEC Transducer Response with 1000-Centistoke Damping Oil



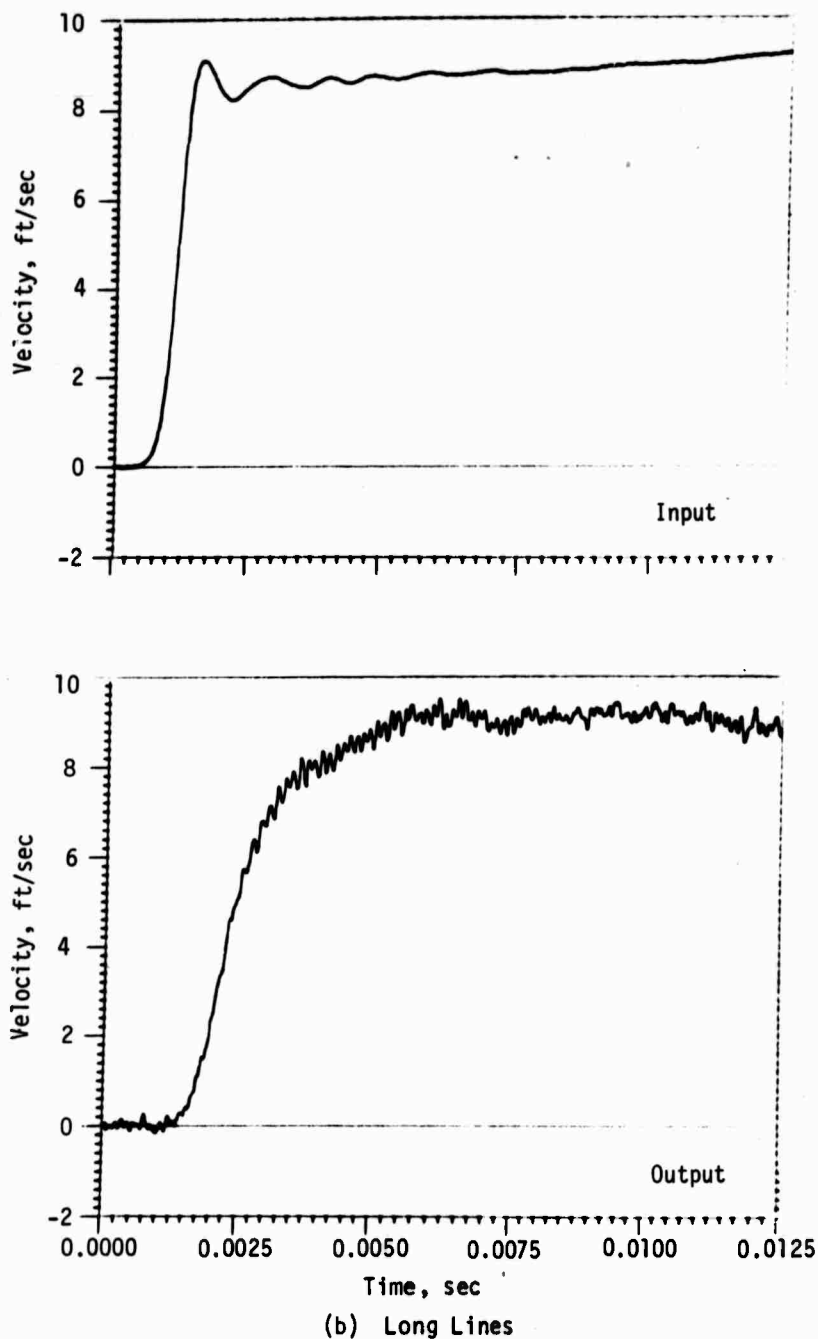
(b) Long Lines

Figure 69.---Concluded



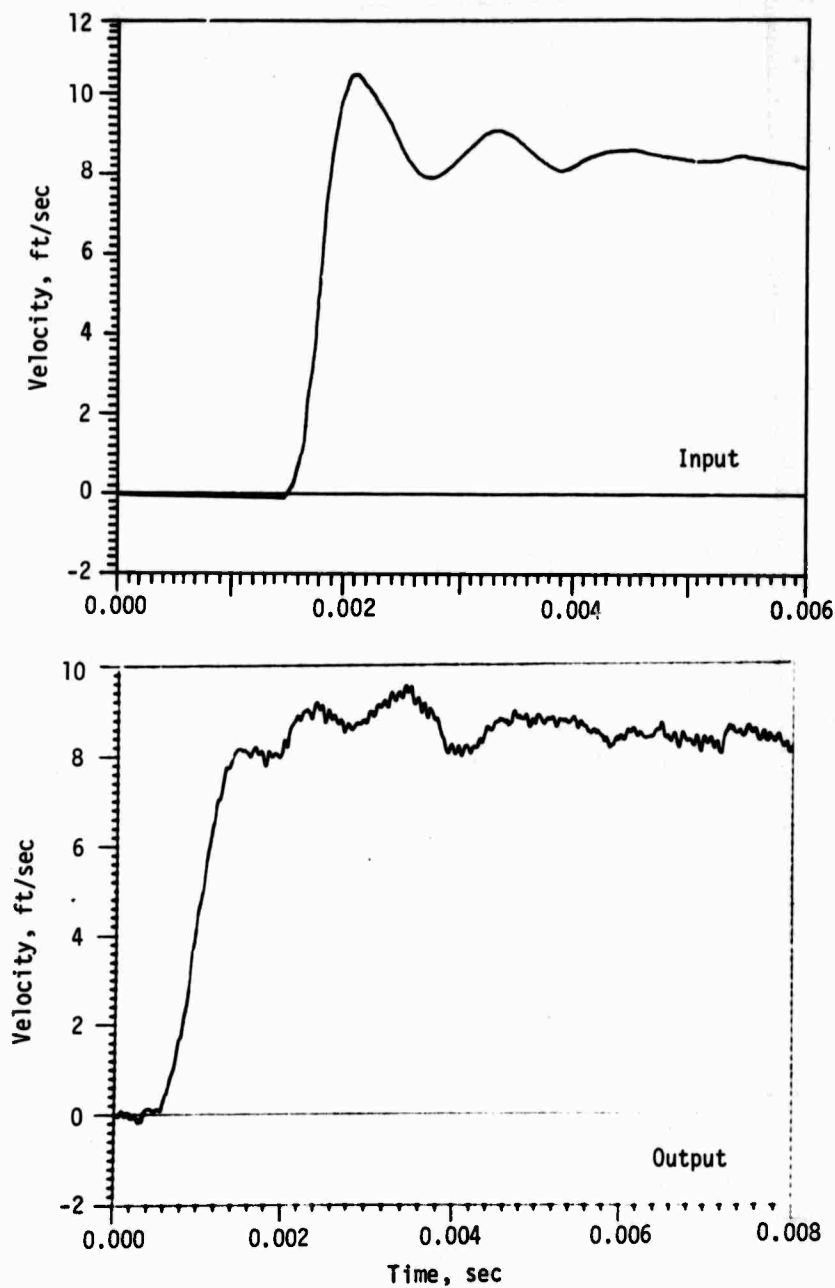
(a) Short Lines

Figure 70. CEC Transducer Response with 2000-Centistoke Damping Oil



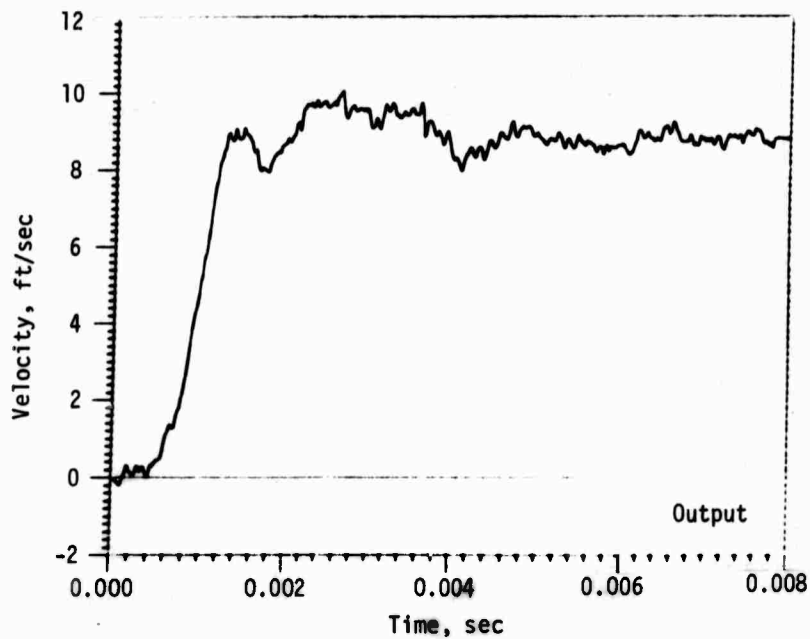
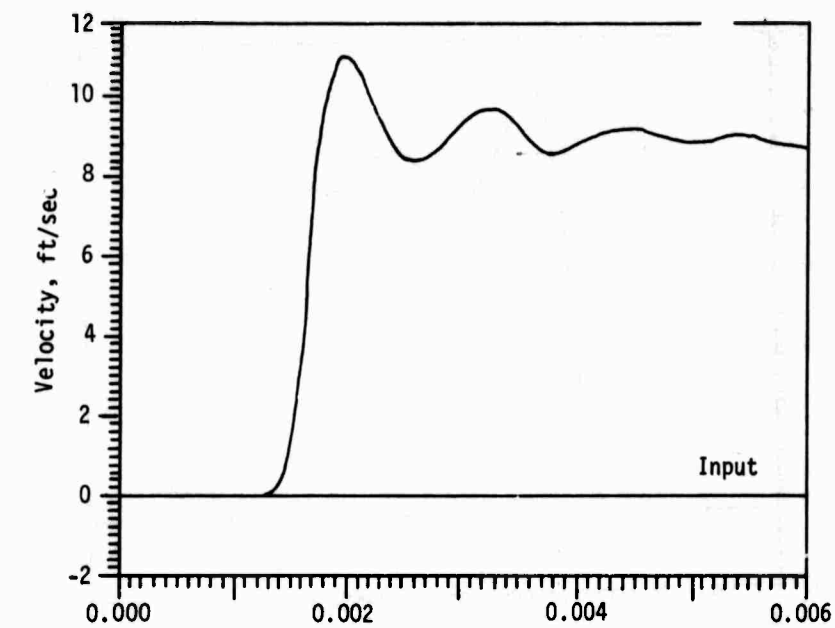
(b) Long Lines

Figure 70.---Concluded



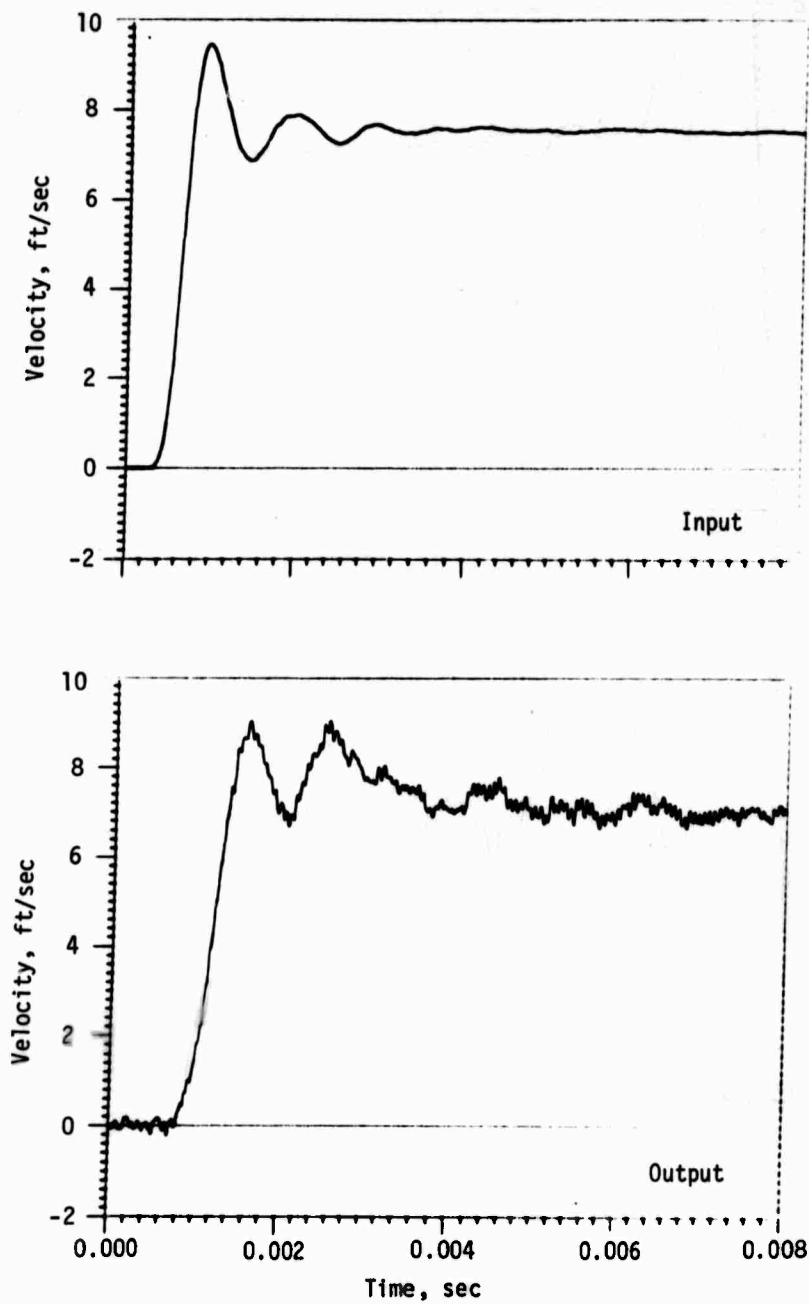
(a) Short Lines

Figure 71. CEC Transducer Response with 5000-Centistoke Damping Oil



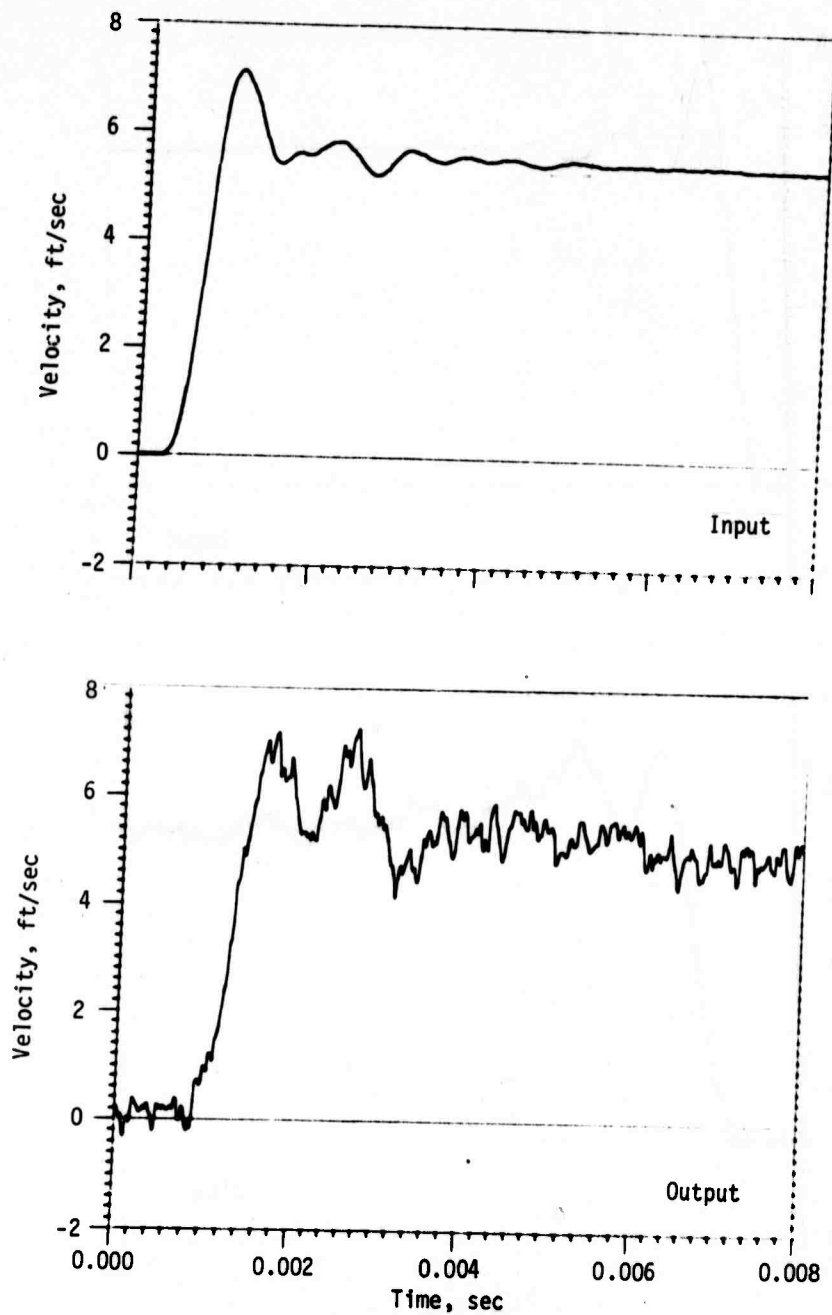
(b) Long Lines

Figure 71.---Concluded



(a) Short Lines

Figure 72. CEC Transducer Response with 7500-Centistoke Damping Oil



(b) Long Lines

Figure 72.---Concluded

Table XXI
SUMMARY OF DAMPING FLUID TEST RESULTS

Transducer S/N	Oil Centistoke Rating	Droop, sec	Damping Ratio	f_{CL} (Calculated)	f_{CH} (Calculated)
1820	500	1.95	26.52	0.5650	159.12
2108	1000	4.00	54.64	0.0275	327.87
2054	2000	8.00	108.90	0.0137	633.40
1770	5000	18.40	250.24	0.0060	1501.00
2235	7500	25.80	350.88	0.0043	2105.00

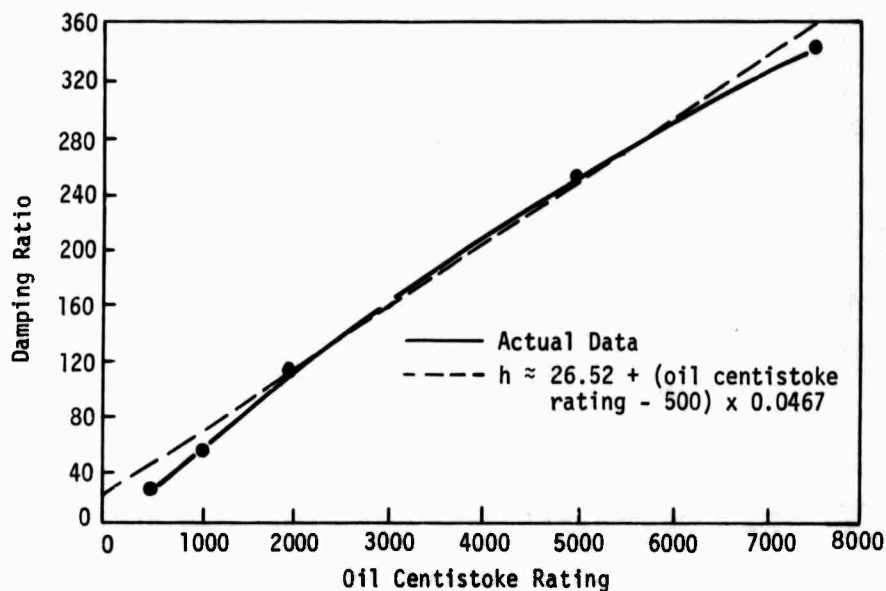


Figure 73. Damping Ratio versus Oil Centistoke Rating for CEC Horizontal Transducer

the following rules may be applied to determine specific transducer properties:

(1) Damping Ratio

$$\text{From } h \approx 26.52 + (\text{oil centistoke rating} - 500) \times 0.0467$$

$$h \approx (\text{oil centistoke rating} + 67.9) 0.0467$$

(2) Scale Factor

$$\text{From } \theta = \frac{\omega_n}{2gh} V$$

$$\text{scale factor} = \frac{6.27}{\text{oil centistoke rating} + 67.9} \text{ rad sec/ft}$$

$$\text{scale factor} = \frac{359}{\text{oil centistoke rating} + 67.9} \text{ degree sec/ft}$$

If for example $\pm 5^\circ$ is the full-scale pendulum travel desired

$$\frac{5(\text{oil centistoke rating} + 67.9)}{359} \approx \text{full-scale positive velocity output}$$

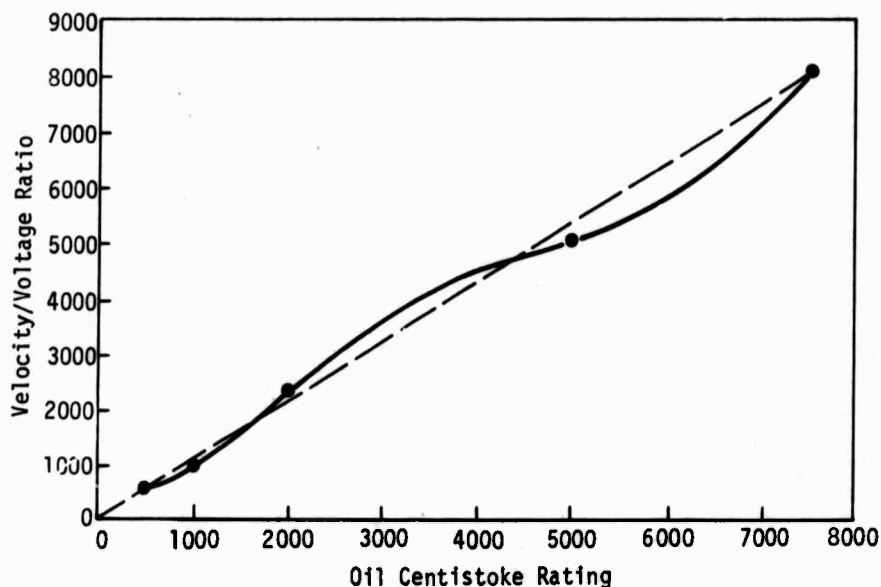


Figure 74. Velocity/Voltage Ratio versus Oil Centistoke Rating for CEC Horizontal Transducer

(3) Droop

From $h = 13.6 \delta t$ (See appendix V.)

$$\delta t = \frac{h}{13.6} = \frac{(\text{oil centistoke rating} + 67.9) 0.0467}{13.6}$$

$$= 3.43 (\text{oil centistoke rating} + 67.9) \times 10^{-3} \text{ sec}$$

(4) Low-Frequency Response

$$\text{From } f_{CL} \approx \frac{1}{2h} f_n$$

$$f_{CL} \approx \frac{32.1}{(\text{oil centistoke rating} + 67.9)}$$

(5) High-Frequency Response

$$\text{From } f_{CH} \approx f_n 2h$$

$$f_{CH} \approx 0.28 (\text{oil centistoke rating} + 67.9)$$

(6) Shunt Calibrate Equivalence

Where R is bridge completion resistor value and R_c is calibrate shunt resistor value,

$$\frac{R + R_c}{R + 2R_c} - 0.5(\text{oil centistoke rating}) \sim \text{calibrate equivalence (fps)}$$

SECTION VIII

ANALYSIS OF LOW- AND HIGH-FREQUENCY CUTOFF

The high-frequency cutoff values determined from the exponential fallthrough data were much higher than the cutoff values obtained from the fast Fourier transform modulus ratios using the dynamic test data. This same observation has been made by others at CERF and AFWL using 1- and 2-g fallthrough instead of exponential fallthrough data. The CEC transducers tested had a high-frequency cutoff ratio of 3 (i.e., the ratio of f_{CH} determined from exponential fallthrough data to f_{CH} determined from dynamic testing). For the Sparton transducers tested, this ratio was nominally 4.7. No explanation can be given for this; however, it should be the subject of future investigations.

The Sparton 604 velocity transducer with a natural frequency of 4.4 Hz had both high and low cutoff frequencies that were higher than those of the 3-Hz pendulous transducers tested. This was expected since calculated transducer cutoffs are directly proportional to the natural frequency of the transducer. The upper cutoff frequency of this transducer determined from the dynamic data was also higher than the dynamic f_{CH} for the 3-Hz transducers. By increasing the natural frequency of the transducer by a factor of 1.47, Sparton increased the upper cutoff frequency and frequency passband by a factor of approximately 1.52. The upper frequency cutoff for the Sparton 604 transducer exceeds the upper frequency cutoff for the Sparton 601 transducer by 130 Hz. This is a significant improvement in high-frequency response. However, a penalty is paid in low-frequency capability to achieve this improvement. In the 3-Hz transducers, low-frequency cutoff occurs at about 0.0075 Hz. The Sparton 604 transducer had a low-frequency cutoff of 0.0133 Hz ($1.77 \times$ the Sparton 601 f_{CH}). However, in terms of frequency differential, low-frequency cutoff increased only 0.006 Hz.

The DX velocity transducers had a low-frequency cutoff of 0.01 Hz or less during testing. If this low-frequency capability is in excess of the required low-frequency capability, it becomes feasible to substantially raise the natural frequency of the transducer to improve f_{CH} and pay the few thousandth Hertz low-cutoff frequency penalty. Consider a pendulous velocity transducer exactly like the DX type except with a natural frequency of 9 Hz and a damping ratio of 525 (three times the nominal natural frequency and damping ratio of a DX transducer with 3000-centistoke oil). This transducer will have the same velocity

range as its DX counterpart since

$$\theta = \frac{\omega_n}{2gh} V$$

in the passband. $f_{CL} = 0.00857$ Hz, and $f_{CH} = 9449$ Hz computed from

$$f_{CL} = \frac{\omega_n}{2\pi} (\sqrt{h^2 + 1} - h)$$

and

$$f_{CH} = \frac{\omega_n}{2\pi} (\sqrt{h^2 + 1} + h)$$

If the dynamic f_{CH} is 1/3 of the f_{CH} calculated above, this transducer will have a passband between 0.00857 and 3149 Hz. Low-frequency cutoff is the same as that for the DX type transducer, but f_{CH} is 9 times that of the DX transducer. This transducer has the same velocity range and the same f_{CL} as the standard DX transducer, but f_{CH} is 9 times that of the standard velocity transducer. Therefore, by increasing the natural frequency and the damping ratio by the same factor, a pendulous velocity transducer can have a substantial increase in passband without paying penalties in transducer sensitivity and low-frequency cutoff capability. To increase the natural frequency of the transducer, the pendulum may be shortened. By doing this, the overall length of the transducer is decreased and the maximum pendulum/case velocity is decreased; this may cause the transducer's damping ratio to be more nearly constant, and since pendulum mass is reduced, so are suspension forces. These factors make the high natural frequency even more attractive.

SECTION IX

CONCLUSIONS AND RECOMMENDATIONS

1. DYNAMIC TESTING

A large amount of dynamic data was generated, and these results can provide the transducer user with new and beneficial information. One example is a potential method for determining transducer changes that occur after dynamic testing. However, it should be noted that this method still needs further investigation, but the possibility of its being a useful working tool is excellent. Another example is the potential advantages of using higher viscosity damping fluids in pendulous-type transducers than are normally considered. This also needs further investigation. Pursuing these potentials was not within the scope of this effort; however, if a concentrated effort were generated, many benefits may possibly be realized.

With certain design modifications and improvements, many of the systems not recommended for field use could be substantially improved. Based on the limited testing in this effort, the following overall conclusions are made:

- (1) For most field applications, the CEC transducer with the appropriate signal conditioner is the system of choice. The signal conditioner system chosen should be capable of passing frequencies at least as high as the f_{CH} of the transducer*.
- (2) Based on the abbreviated testing of the CEC transducer with various damping oil viscosities, 5000- and 7500-centistoke oil fills appear to yield better transducer performance in terms of accuracy and input pattern reproduction at a nominal 10-fps input velocity than transducers filled with lower viscosity damping oils (including the extensively tested 3000-centistoke oil fill). Although these highly damped transducers were not tested with high-g-level or higher velocity inputs, it is likely that transducer performance at velocities

* Modified Crescent (10 kHz), Natel (6 kHz), or WES system for 3000-centistoke oil-filled transducers.

in excess of 10 fps may also be superior to lower-damped transducers. Because of this potential, further investigation of highly overdamped transducers is strongly recommended.

a. Signal Conditioners

During signal conditioner testing, the FM transducer signal conditioner had the highest f_{CH} of all the conditioners tested. Of the DX-compatible signal conditioners tested, the Natel, the Crescent 8303 (modified), and the WES systems had high-frequency cutoff capabilities well in excess of DX transducers with 3000-centistoke oil. Of these three, all of which performed well, the Natel is the only unit that provides reference phase adjustment*.

b. Pendulous Transducers

(1) Cibola

The Cibola transducer with the stripped locking threads and consequent oil leakage had anomalous negative output spikes, poor fallthrough patterns, and a high amount of degradation to on-axis and cross-axis shock. Therefore, overall performance was relatively poor, and this transducer is not recommended for any velocity application.

(2) CEC

The CEC transducers had consistent positive errors with the worst-case error of 20.8 percent occurring after cross-axis shock testing. Besides consistent error polarity, rise times and ringing frequency magnitudes were consistent. No negative spikes were observed and no obvious degradation was noted after normal and cross-axis high-g-level inputs. The useful pass-band for these transducers was nominally 0.009 to 320 Hz. Overall performance of this transducer was very good. For most test conditions, this transducer, with the proper signal conditioner, appears to be the system of choice.

(3) Sparton (Brass)

Error polarity varied from transducer to transducer during testing with the worst-case error magnitude of 64.6 percent occurring after cross-axis testing. No negative output spikes were observed, but horizontal transducer

*This adjustment is not necessary if input/output phase differentials are low. Testing of DX transducers with long and short lines using signal conditioners without reference phase adjustment capabilities suggests that for these line lengths, the input/output phase differential is low enough to yield good data without this adjustment.

ringing was present at a nominal 2500 Hz. Variable ringing frequencies and amplitudes were observed in the vertical transducers. The useful passband for these transducers was approximately 0.0076 to 250 Hz. Overall performance of this transducer was good. Although the CEC transducer is recommended for most applications, it would be advisable to use the Sparton brass transducer where low-frequency response (with 3000-centistoke oil) is the dominant consideration in the velocity data acquisition.

(4) Sparton (Aluminum)

Errors during testing were consistently positive, with the worst-case error of 22 percent occurring during normal high-g-level testing. Negative spikes were observed in some tests. No obvious error degradation was evident after cross-axis testing, but high-frequency ringing magnitude increased. Ringing frequency variations were also observed. The useful passband was 0.0075 to 250 Hz. Overall performance of this transducer was fair except for the negative spikes. Because of this, both the Sparton brass and the CEC transducers are deemed superior. With the lower transducer mass (aluminum versus brass), this transducer could be soil density matched with smaller canisters than conventional brass DX transducers. If the performance had been better, this feature would make this transducer highly desirable for field use; however, this transducer is not recommended for velocity measurements mainly because of the large negative spikes.

(5) Sparton 604

Since Sparton 604 testing was limited, the transducer was not thoroughly evaluated. Error polarity varied in the two dynamic tests. No negative spikes were observed, but nonlinear fallthrough and a low-magnitude ring at about 4000 Hz were observed. Good rise times and high f_{CH} were exhibited. The useful passband for this transducer was 0.0133 to 380 Hz. Although this transducer had a greater f_{CH} capability than conventional DX velocity transducers with 3000-centistoke damping oil, it cannot be recommended for field use primarily because of oil leakage in addition to the deficiencies mentioned above.

(6) Sparton 602 (FM)

The Sparton 602 (FM) transducers tested were mechanically defective. Overall performance of this transducer was extremely poor. Although the transducer signal conditioners showed potential for passing frequencies in excess of 5000 Hz, this velocity system is not recommended because of

severe defects observed in the two transducers tested.

c. Linear Transducers

(1) EG&G

The EG&G system had error polarities which varied with the worst-case error magnitude of 35 percent. This system, capable of both horizontal and vertical measurements, performed well from the standpoint of error in horizontal measurements. (Worst-case error magnitude was 11.6 percent.) The transducers tested rang during test series 1, high-g-level testing only at 2500 to 2800 Hz; this occurred during both horizontal and vertical tests.

No negative spikes were observed; however, the transducer failed after the 90° cross-axis test.

Rise times were fairly consistent at about 1.0 to 1.2 msec except for the nominal 1.6-msec rise time of the vertical transducer in test series 1. The useful passband of this transducer was 0.058 to 300 Hz horizontal and 0.058 to 215 Hz vertical. Overall performance of this transducer was fair. Except for the relatively high f_{CL} and cross-axis shock failure, performance was good.

The heater capability may make this transducer more desirable for field use if calibration and field ambient temperatures are subject to variations; however, testing to determine this was beyond the scope of this effort. If this is advantageous, it must be weighed against the nominal maximum 100-w/channel power requirement.

This transducer is not recommended for field application primarily because of cross-axis failure; however, if temperature problems are anticipated in field testing, further investigation of this transducer may be advisable.

(2) Setra

During Setra transducer testing, error polarity was consistently negative. Although the transducer was capable of inputs of 16.6 fps, the horizontal transducer output never exceeded about 9 fps even though inputs were generally well above this level. Worst error magnitude for this transducer was 36.8 percent.

No ringing was observed during testing; however, much noise was seen (sometimes in excess of 10 percent of peak output). No negative spikes were observed except when the transducer was overranged. Rise times were very short, ranging from 0.16 to 0.64 msec. Because the

exponential fallthrough could not be performed, f_{CL} and f_{CH} could not be calculated; f_{CH} from the fast Fourier transform was 1200 Hz horizontal, and 1900 Hz vertical.

Relative to the other transducers tested, this system had excellent rise time and f_{CH} capabilities; however, the overall performance was poor because of (1) an apparent upper system output saturation level far below the rated specification, (2) the low signal-to-noise ratio, and (3) the inconvenient calibration procedure. Therefore, this system is not recommended for field use, particularly because of the calibration procedure.

(3) Endevco

Because of calibration problems, high quantizing errors occurred in the digitized output data. Therefore, the fast Fourier transform would have been meaningless. Because of the calibration problems and the low-g-level inputs required, it was difficult to thoroughly evaluate this transducer.

Since input and output patterns were very similar, the system apparently can reproduce inputs of the type encountered during this test program, and since input and output rise times were also very close, the high-frequency response of this system is probably very high. Although the drift rate was within the manufacturer's specifications, it could seriously affect long-time history data.

Relative overall performance of this system was good for the parameters of interest which could be compared with those of the other transducers. The DX-type transducers with 3000-centistoke damping oil are obviously superior to this transducer for low-frequency or long-time applications. Because of the nature of this measurement, it is essential that this system be zeroed shortly before the test is initiated. The manual three-axis zeroing capability is convenient for laboratory tests but could be a drawback in an actual field test where many velocity channels are required. To minimize the effects of zero offset during a field test, all channels must be simultaneously zeroed before the test is initiated. This involves eliminating zero-sequencing problems to assure that all channels have completed the zeroing procedure at the same time.

Another potential field problem is accelerometer selection. To insure the best possible data from a system of this type, subsystems (accelerometers and signal conditioners) must not only be selected and scaled for maximum anticipated velocities, but also for maximum anticipated accelerations.

This transducer is conditionally recommended for short-time use

in field applications where both nominal peak velocities and acceleration levels are well defined before the test and where operators are available to initiate zeroing at the proper time. Also, it is recommended that an additional study of this system be made using an improved calibration procedure for the velocity channel to evaluate the transducer for errors, before it is applied.

d. Damping Fluid

The transducer passband of oil-damped transducers improves with increased oil viscosity, while transducer sensitivity decreases. The transducer scale factor is nearly linearly proportional to the centistoke rating of the damping oil used. With nominal peak velocities of 10 fps, highly overdamped DX-type transducers (5000 and 7500 centistoke) have less peak velocity error, and their output patterns more closely match the input patterns than do those of the less highly damped transducers. Even with the decrease in signal noise ratio due to decreased sensitivity, data quality is noticeably better.

During this testing it was found that many important parameters for CEC horizontal transducers can be closely estimated knowing only the transducer natural frequency of 3 Hz and the centistoke rating of the damping oil.

2. SLED TRACK

Although the sled track velocity reference system was reliable and adequate for this test program, several modifications to enhance its versatility and to improve the time and cost of data acquisition are needed. (The necessity of integrating the reference acceleration to obtain velocity also requires computer time which adds to the time and cost of each test.) Therefore, it is recommended that an on-line reference velocity system be incorporated as part of the sled track. One way to obtain a highly accurate velocity measurement would be to utilize a doppler laser system. Velocity transducer data could then be analyzed and compared within minutes of the dynamic test.

3. EXPONENTIAL FALLTHROUGH

The usefulness of the exponential fallthrough test technique was demonstrated in this test program in establishing system damping ratios, transducer droop, and high and low cutoff frequencies of compatible velocity transducers.

It should be noted that the results of these tests are useful only for the damping encountered at relatively low pendulum/case angular velocities.

4. Δt AND CALIBRATE LEVEL EQUIVALENT/ Δt RATIO TECHNIQUES

Δt and calibrate level equivalent Δt ratio techniques developed in this test program are theoretically substantiated, and with the limited applications during this program, thus demonstrate potential value in establishing DX-transducer suspension changes after dynamic testing. However, more work on these techniques is required to better relate their numerical values to transducer changes. As demonstrated, the cause of an approximate calibrate level equivalent/ Δt ratio change of 10 percent is difficult to detect without visual aids.

APPENDIX I OPERATING PRINCIPLES OF TRANSDUCER SYSTEMS

1. PENDULOUS TRANSDUCERS

A pendulous-type velocity transducer is basically a highly overdamped seismic system. Mechanically, this system consists of a pendulum suspended in a case filled with damping oil (fig. 75). The governing equation for this mechanical system is

$$\ddot{\theta} + 2h\omega_n\dot{\theta} + \omega_n^2\theta = \frac{\omega_n^2\ddot{x}}{g}$$

where

θ = angle between gravity unit vector and pendulum axis vector

x = case displacement

h = system damping ratio

ω_n = 2π times natural frequency of pendulum

g = acceleration of gravity

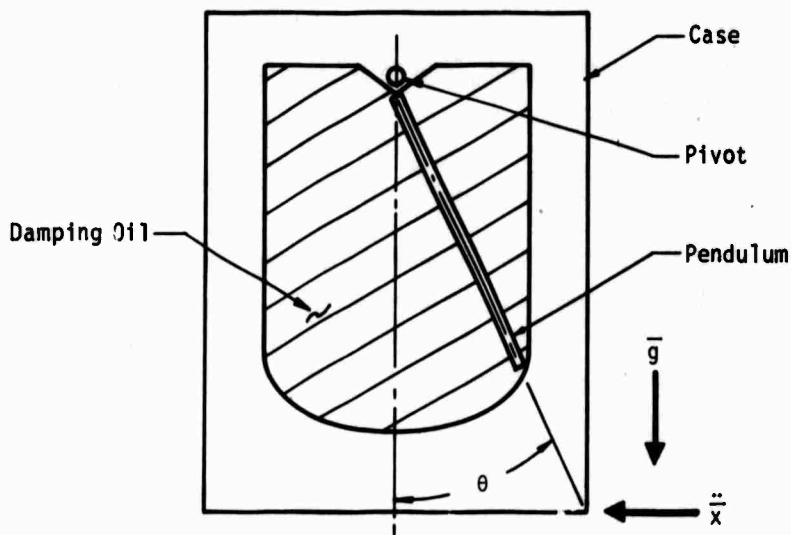


Figure 75. Horizontal Pendulous Transducer Mechanics

when the case displacement is orthogonal to both the gravity vector and the pendulum pivot axis and when there is no angular rotation of the transducer case. (See appendix III.) It is assumed in this development that h , ω_n , and g are constant. The transfer function for θ in terms of x is

$$\frac{\theta(s)}{\dot{x}(s)} = \frac{\omega_n^2}{g} S / (S^2 + 2h\omega_n S + \omega_n^2)$$

where S is the Laplace operator, $\theta(s)$ is the Laplace transform of θ , and $X(s)$ is the Laplace transform of X .

To examine the transfer function for θ in terms of X for a steady-state sinusoidal input ($X = k \sin \omega t$), the transfer function becomes

$$\frac{\theta(\omega)}{\dot{x}(\omega)} = \frac{\frac{\omega_n^2}{g} j\omega}{-\omega^2 + 2jh\omega_n\omega + \omega_n^2}$$

From this transfer function, it is evident that the pendulous velocity transducer has both high- and low-frequency limitations. For the input frequency where $\omega = \omega_n$

$$\theta(\omega) = \frac{\omega_n}{2gh} \dot{x}(\omega)$$

and $\omega_n/2\pi$ is midband frequency and $\omega_n/2gh$ is midband gain. For any frequency $\omega/2\pi$ satisfying the inequality

$$|\omega_n^2 - \omega^2| \ll |2h\omega_n\omega|$$

$\theta(\omega) \approx \frac{\omega_n}{2gh} \dot{x}(\omega)$ and the transducer is operating within its passband. Passband is considered to be the frequency range between a low frequency ($\omega_{CL}/2\pi$) and a high frequency ($\omega_{CH}/2\pi$). At both of these frequencies, the magnitude of the gain is 0.707X midband gain (3dB down from midband gain). For the pendulous transducer model, at ω_{CL}

$$2h\omega_n\omega_{CL} = \omega_n^2 - \omega_{CL}^2$$

$$\frac{\omega_{CL}}{2\pi} = \frac{\omega_n}{2\pi} \left(\sqrt{h^2 + 1} - h \right)$$

and at ω_{CH}

$$2h\omega_n\omega_{CH} = \omega_{CH}^2 - \omega_n^2$$

$$\frac{\omega_{CH}}{2\pi} = \frac{\omega_n}{2\pi} \left(\sqrt{h^2 + 1} + h \right)$$

$$f_{CL} = \frac{\omega_n}{2\pi} \left(\sqrt{h^2 + 1} - h \right) = \text{lower cutoff frequency}$$

$$f_{CH} = \frac{\omega_n}{2\pi} \left(\sqrt{h^2 + 1} + h \right) = \text{upper cutoff frequency}$$

A vertical velocity transducer is similar to a horizontal velocity transducer, except for its orientation and the addition of a 1-g spring (fig. 76). The 1-g spring is designed and attached such that the vertical spring force on the pendulum is nearly equivalent to a 1-g constant, thus canceling out gravitational forces on the pendulum and forcing the pendulum angle, θ , to be zero

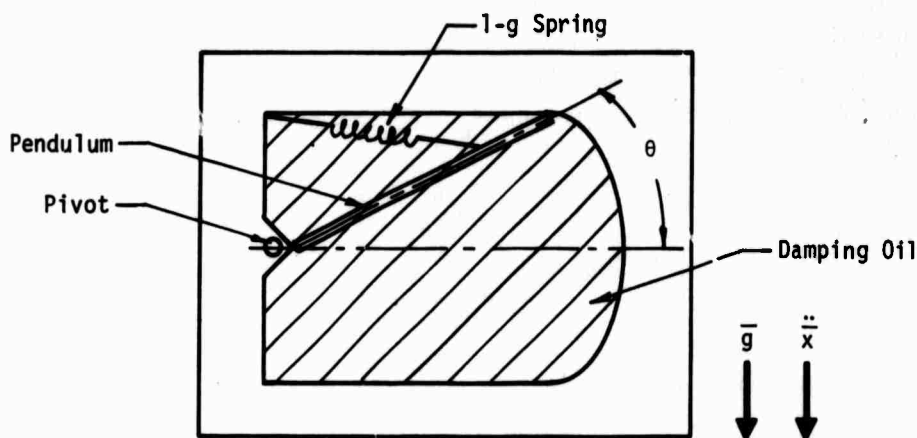


Figure 76. Vertical Pendulous Transducer Mechanics

when the transducer is at rest in its proper orientation. The governing equation is the same as that for the horizontal transducer except that the input displacement is in a vertical direction perpendicular to the pendulum pivot axis and parallel to \bar{g} , the gravity acceleration vector.

Having established that θ is the parameter of interest when a velocity transducer is operating within its passband, one must establish some means of sensing θ and telemetering a proportional electrical signal. Most pendulous velocity transducers have variable inductance ratio sensors (commonly called *E - cores*) for this purpose. When this E-core system (fig. 77) is placed in a bridge circuit (fig. 78) which is driven by a constant-amplitude, constant-frequency, sinusoidal voltage, E_i , the bridge output voltage, E_o , is a sinusoidal voltage with a magnitude proportional to

$$E_o = E_i \left[\frac{L_1}{L_1 + L_2} - 0.5 \right]$$

This sinusoidal voltage, E_o , may now be telemetered over lines to a phase-sensitive demodulator which provides a dc output voltage proportional to θ . Knowing the proper scale factor, one may now use this dc voltage as a velocity analog.

A balance is achieved in this bridge circuit when $L_1 = L_2$; with this condition, $E_o = 0$. This balance will be upset for all conditions where $L_1 \neq L_2$; with these conditions, $E_o \neq 0$. Considering, now, a balanced bridge ($L_1 = L_2$, $R_1 = R_2$), we now examine the effect of a shunting resistor, R_2 , at terminals B and C with a resistor of value R_C . E_o then becomes

$$E_o = \left[\frac{L_1}{L_1 + L_2} - \frac{\frac{R_C R_2}{R_C + R_2}}{R_1 + \frac{R_C R_2}{R_C + R_2}} \right] E_i$$

However, $L_1 = L_2$ and $R_1 = R_2$, so

$$E_o = E_i \left[0.5 - \frac{\frac{R_C R_1}{R_C + R_1}}{R_1 + \frac{R_C R_1}{R_C + R_1}} \right]$$

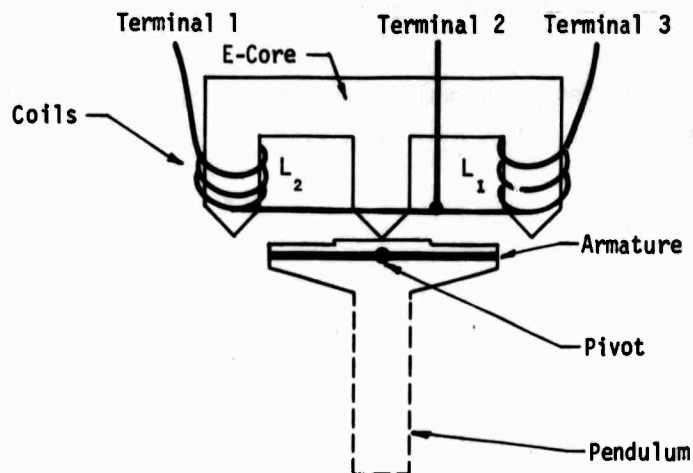


Figure 77. Pendulous Transducer E-Core and Armature Assembly

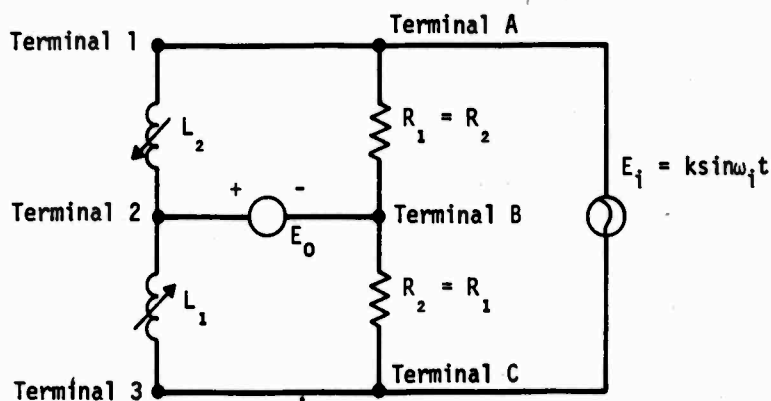


Figure 78. Pendulous Transducer Electrical Bridge Circuit

$$= E_i \left(0.5 - \frac{R_c}{R_1 + 2R_c} \right)$$

This output voltage corresponds uniquely to an output voltage without the R_c shunt at one and only one $L_1/(L_1 + L_2)$ ratio, γ , where

$$0.5 \leq \gamma \leq 1$$

$$E_i(\gamma - 0.5) = E_i \left(0.5 - \frac{R_c}{R_1 + 2R_c} \right)$$

$$\gamma = 1 - \frac{R_c}{R_1 + 2R_c}, \quad R_c = \frac{R(1 - \gamma)}{2\gamma - 1}$$

Since this unique ratio, γ , is associated with a unique pendulum/case angle, and case velocity, \dot{X}_Y , the output voltage developed when the shunt resistor, R_c , upsets the balanced bridge ($\dot{X}_Y = 0$) is the same as the output voltage in the unshunted bridge when $\dot{X} = \dot{X}_Y$. Thus, the shunt or calibration resistor, R_c , may be inserted in the bridge circuit to develop a bridge output equivalent to the output at $\dot{X} = \dot{X}_Y$. This is how velocity equivalent calibration outputs are created with pendulous velocity transducers. The method of selecting a shunt calibration resistor and relating bridge output upon its proper insertion to a velocity equivalent is discussed in detail later.

The Sparton Model 602 (FM) velocity transducer employs variable inductance ratio sensors which are part of a frequency modulation output scheme for electrically sensing θ . A device similar to the E-core assembly (fig. 77) is used to increase L_1 and decrease L_2 as θ increases. The two inductances, L_1 and L_2 , are used to vary the oscillation frequencies of two separate oscillators (fig. 79).

The inductors are designed such that the frequency of oscillator 1 increases linearly as θ increases and the frequency of oscillator 2 decreases linearly as θ increases (fig. 80a). The oscillator outputs are fed to a mixer. The mixer output contains components at frequencies which are the sum and the difference of the two oscillator frequencies. The mixed signal goes to a filter which passes only the difference-frequency signal component (fig. 80b). This signal goes to a discriminator which generates a dc signal which is proportional

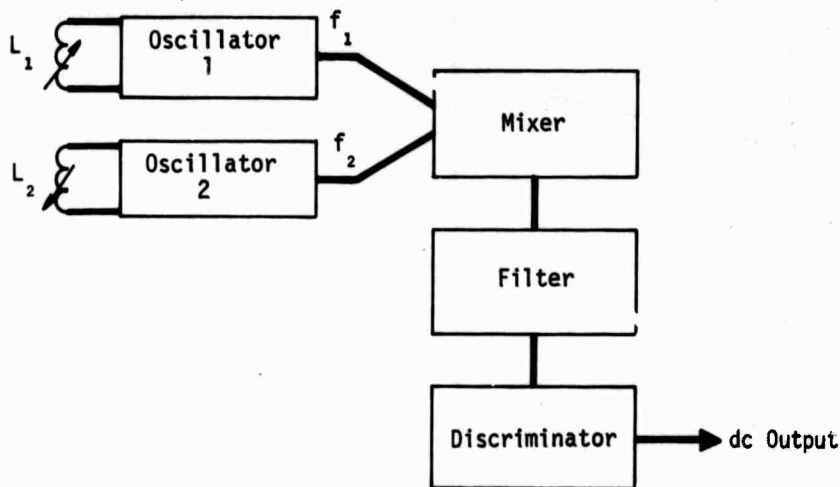


Figure 79. FM Velocity Transducer Signal Conditioning System

to the difference of the two oscillator frequencies, and thus linear and directly proportional to θ (fig. 80c).

2. LINEAR TRANSDUCERS

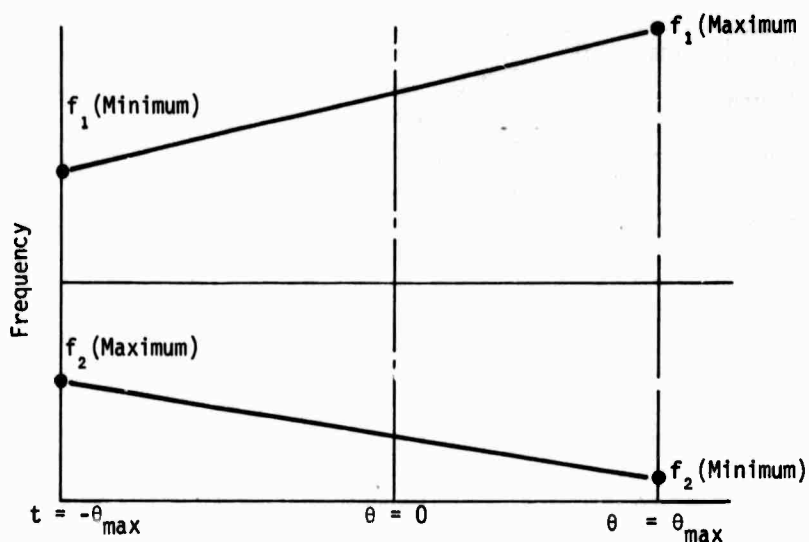
A linear velocity transducer consists of a seismic system with spring, mass, and damping (fig. 81). The transfer function for this type of device relating output, x , to input, \dot{X} , is

$$\frac{x(s)}{\dot{X}(s)} = \frac{-Ms}{Ms^2 + Cs + K} = \frac{-s}{s^2 + 2h\omega_n s + \omega_n^2}$$

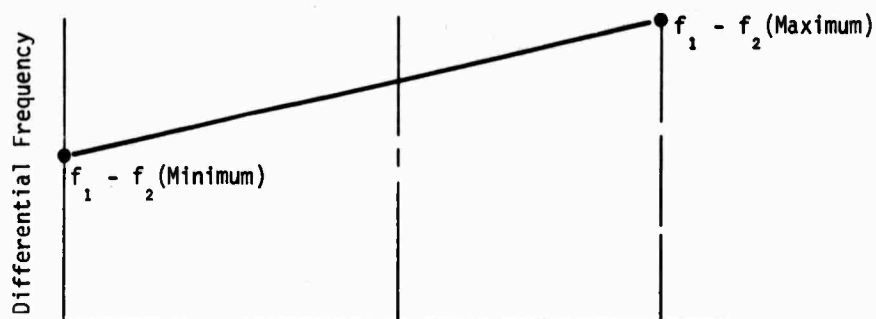
This transfer function is similar to the transfer function developed for the pendulous velocity transducer.

For the case of a highly damped system, passband cutoff frequencies, f_{CL} and f_{CH} , are the same as those for the pendulous velocity transducer. Midband gain is $1/2h\omega_n$. Most of the linear velocity transducers tested were highly damped seismic systems.

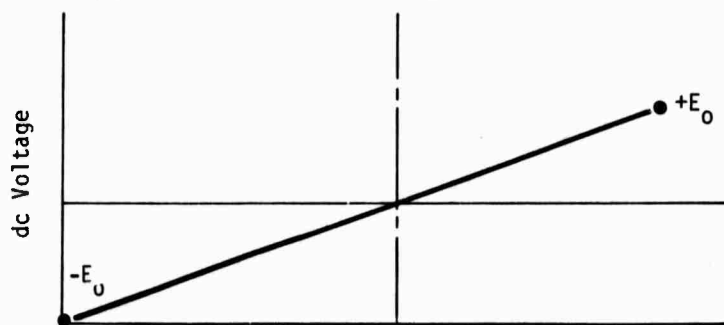
One system, the Endevco Model 2269-150, was an integrated accelerometer



(a) Oscillator 1 and 2 Output Frequencies versus θ

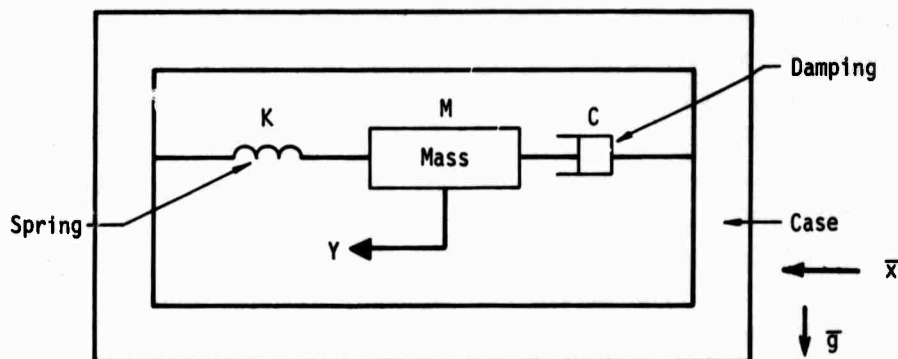


(b) Filtered Mixer Frequency Output versus θ



(c) Discriminator dc Voltage Output versus θ

Figure 80. FM Velocity Transducer Outputs



M = mass

C = damping constant

K = spring constant

X = case absolute displacement in sensitive axis

Y = mass absolute displacement in sensitive axis

x = mass/case relative displacement (X/Y)

$h = \text{damping ratio} = C/2MK$

$$\omega_n = \sqrt{K/M}$$

Figure 81. Horizontal Linear Transducer Mechanics

system. In this system, the primary element (transducer) senses case acceleration, and the signal conditioner integrates a voltage analog of case acceleration, thus yielding a voltage analog of case velocity. This system is underdamped. With this condition

$$x(s) = -s \dot{X}(s) / \omega_n^2$$

when

$$\omega_n^2 \gg |-\omega^2 + j2h\omega_n\omega|$$

With this condition satisfied

$$\frac{x(s)}{s} = \frac{-\dot{X}(s)}{\omega_n^2}$$

and

$$\omega_n^2 \int_0^t x(t) dt = -X(t) - X_0$$

It is obvious that f_{CL} for this system is zero. In this system, midband gain is $1/\omega_n^2$. The useable high-frequency limit of this type of transducer is subject to various system data requirements which are not specified here.

a. EG&G System

The EG&G velocity measurement system is a linear overdamped seismic system with damping provided by 230-centistoke viscous silicon oil at 100°F. Relative mass/case position is sensed by a differential variable reluctance sensor (as are the signal conditioner compatible pendulous velocity transducers) in conjunction with a separate signal conditioner system. Although the signal conditioner and seismic system are separate, they are mounted together and subjected to the same motion in field use. Included in the signal conditioning module is a heater which is capable of supplying up to 100 w to maintain both the signal conditioner and the seismic system at a temperature of 100°F*.

Specifications for this system are as follows:

EG&G MODEL 100 TRANSDUCER

Velocity Range

Vertical: ± 1.0 fps(min); ± 50 fps(max)

Horizontal: ± 0.6 fps(min); ± 30 fps(max)

Response Time: 0.5 msec (max)

Frequency Response: $\pm 2.0\%$ maximum deviation over the range of
0.1 Hz to 1.0 kHz

Linearity: $\pm 3.0\%$ (max)

Transverse Response: $\pm 1.0\%$ (max)

Stability, Output Deviation: 0.1% maximum of full scale for
28 \pm 2vdc input

Shock Resistance: 5,000 g (min), axial and lateral

Output: ± 2.5 v for full set range

Output Signal-to-Noise Ratio: 35 dB

SYSTEM (Including Transducers and Signal Conditioning)

Operating Temperature Range: 25° to 90°F

Hydrostatic Pressure Proofing (Test): 0 to 65 psig

* Ross, George, *Soil Velocity Transducer System*, AFSWC-TR-69-6, Air Force Special Weapons Center, Kirtland Air Force Base, New Mexico, November 1969.

Output Deviation versus Temperature: $\pm 1.3\%$ maximum over the range of
25° to 90°F with heaters in use
0.9% reduction in output per °F
reduction for heaters not in use

Electrical Isolation: 10 GΩ

Reliability: 100 tests minimum without failure

b. Setra System

The Setra transducer also falls in the category of linear overdamped seismic systems. Squeeze film gas damping which is accomplished through orifices in a seismic diaphragm is provided (fig. 82). This system has a variable pulse-width modulation scheme for signal conditioning. Within the mechanical transducer passband, the seismic mass relative displacement is proportional to the absolute case velocity, and in the pulse-width modulation scheme, transducer performance is such that

$$x \text{ is proportional to } \frac{C_1 - C_2}{C_1 + C_2}$$

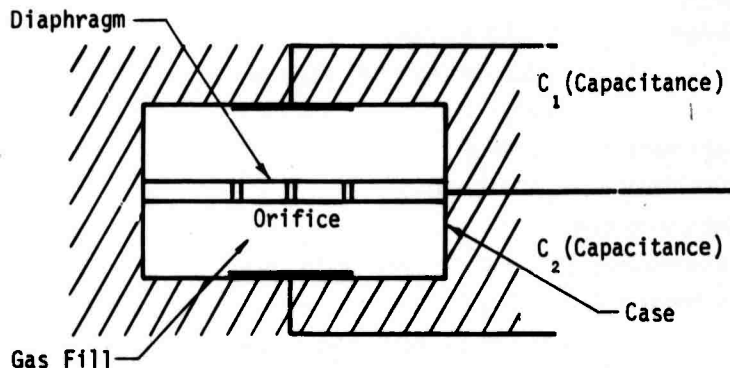


Figure 82. Setra Transducer Mechanics

and within the permissible range of x , $C_1 + C_2$ is constant.

In the pulse-width modulation scheme two algebraically summed voltages (E_1 and E_2) associated with C_1 and C_2 , are generated (fig. 83). At t_0 , C_2 is discharged and E_2 goes to zero while C_1 charges through a charging resistor until at $t_1 = KR_C$, a reference voltage level, V_R , is reached. During the interval $t_1 - t_0$, E_1 is generated at a level V . At t_1 , E_1 goes to zero and C_1 is immediately discharged while E_2 goes to level $-V$ and C_2 charges through another resistor of value R until reference voltage level, $-V_R$, is reached at t_2 . This completes one modulation cycle and the process starts again. The two voltages, $E_1 :: C_1$ and $-E_2 :: C_2$ are summed and passed through a low-pass filter whose output is proportional to the average of $E_1 - E_2$. Thus at zero input velocity, the system output is zero since $E_1 - E_2 = 0$. For positive input velocities, the system output is positive since $E_1 > E_2$ and for negative input velocities, the system output is negative since $E_1 < E_2$.

To extend the low-frequency capability of this system, a lag-lead network is used to restore and flatten a portion of the mechanical low-frequency gain rolloff characteristic, thus decreasing f_{CL} while still allowing a higher natural frequency to be used in the mechanical system (fig. 84).

The manufacturer's specifications for this system are as follows:

SETRA MODEL 151 TRANSDUCER

Maximum Velocity Range:	± 200 in./sec
Frequency Range:	0.1 to 2000 Hz, flat to $\pm 5\%$
Maximum Output:	± 2.5 vdc
Maximum Range (in all axes):	5000 g
Operating Temperature Range:	40° to 100°F
Sensitivity to Temperature Over	
Operating Temperature Range:	$< \pm 3\%$ of full scale
Static Acceleration Range:	± 20 g
Nonlinearity:	$< \pm 3\%$ of full scale static calibration
Excitation:	15 to 28 vdc
Output Impedance:	$< 10 \Omega$
Zero Output (in zero g	
direction):	$< \pm 100$ mv
Resolution:	Infinite
Calibration Signal:	50% of full scale on command

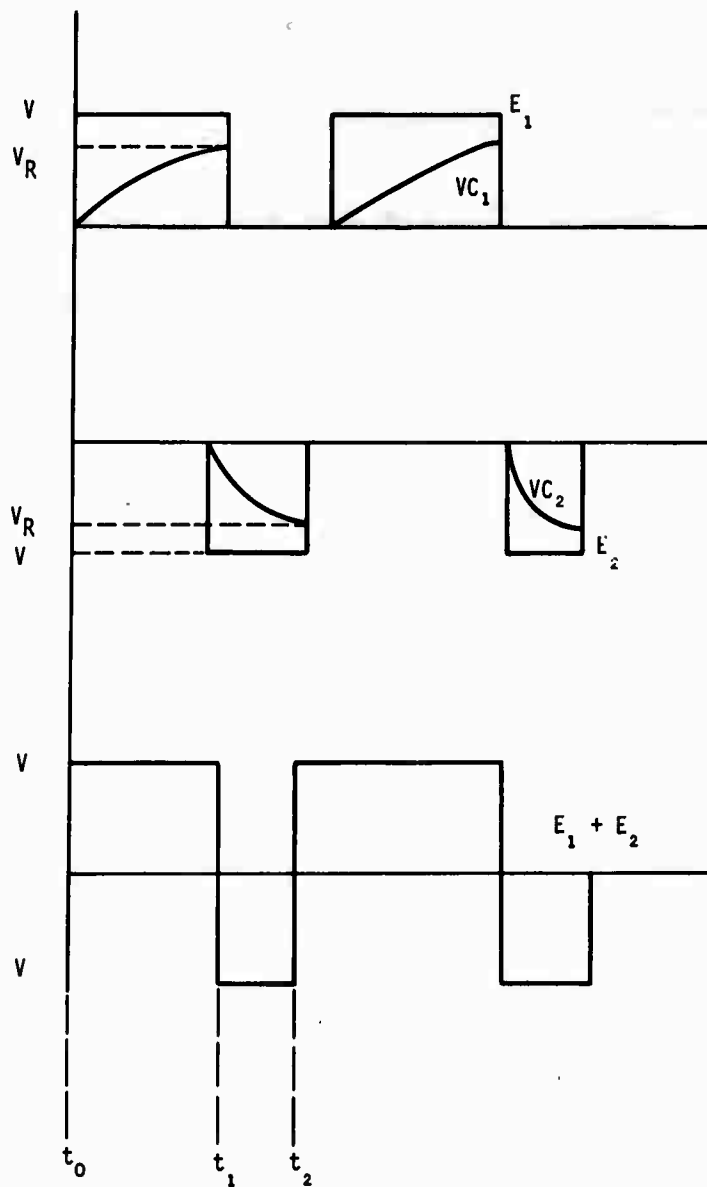


Figure 83. Setra Transducer Voltage Levels During Two Modulation Cycles

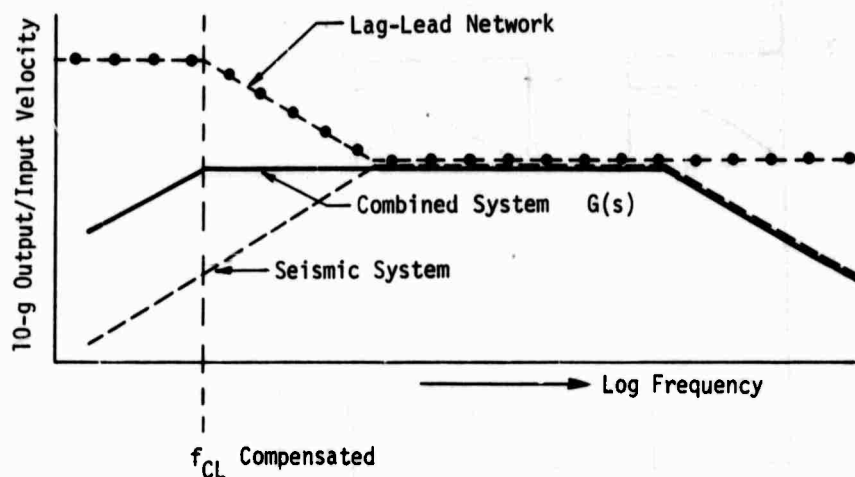


Figure 84. Gain versus Frequency for Setra Velocity System

Output Noise:	< 10 mv RMS
Weight:	5 oz (approx.)
Dimensions:	2 x 2-1/2 x 1-1/4 in.
Electrical Connections:	Bendix PT02H-8-4P or equivalent

c. Endevco System

The Endevco Model 28562 measurement system consists of a transducer containing three Endevco Model 2269 accelerometers triaxially mounted in a metal canister which also contains a ± 5 -v excitation regulator to eliminate effects of line voltage drops, and three integrated circuit voltage followers.

Outputs from the individual accelerometers are wired to a remote signal conditioning unit which contains three acceleration-conditioning amplifiers, three velocity integrators and associated power supply, zeroing controls, and calibration controls.

Acceleration voltage analogs are integrated by the signal conditioner to provide velocity outputs of the three mutually orthogonal case axes. A unique feature of the Endevco system is the automatic zeroing capability.

By initiating a zeroing command through a momentary contact closure on the signal conditioner unit, all three channel outputs are zeroed while logic circuits step through consecutive bucking voltage levels until zero input is found on all three channels. All three channels are automatically zeroed in about 1 sec.

The manufacturer's specifications for this system are as follows:

ENDEVCO MODEL 28562 SYSTEM

Acceleration

Three channels (X, Y, Z) per conditioner

Sensitivity: Continuously variable from 10 to 100 g/v

Velocity

Three channels (X, Y, Z) per conditioner

Sensitivity: Acceleration output sensitivity (in g/v) multiplied by the velocity range factor is equal to the velocity output sensitivity in fps/v

Velocity Range Factor: $\times 1$ or $\times 1/10$

Frequency Response

Absolute Maximum: $\pm 2\%$, 0 to 200 Hz; $\pm 4\%$, 200 to 400 Hz;
 $\pm 12\%$ at 800 Hz

Typical: $\pm 2\%$, 0 to 1 kHz

Calibration/Zeroing

Remote contact closure will initiate zeroing or calibration

MODEL 4830 SIGNAL CONDITIONER

Inputs (3 accelerations)

Single ended, one side tied to ground

Impedance: $> 10 \text{ M}\Omega$

Maximum Input Voltage: $\pm 15 \text{ v}$

$\pm 15 \text{ v}$ supplied for transducer excitation

Outputs (3 accelerations, 3 velocities)

Single ended

Output Impedance: 2.5Ω maximum

Maximum Linear Output Voltage

Acceleration: $1 \text{ v} \times \text{gain}$ for gains 2 to 10;
 10 v for gains 10 to 80

Velocity: 10 v

Minimum Resistive Load: 10 k Ω

Maximum Capacitive Load: 10,000 pF

Transfer Characteristics

Acceleration

Gain: Approximately 2 to 80, continuously variable

Frequency Response: $\pm 1\%$ dc to 1 kHz

Velocity

Integrator input is from acceleration output

Integration Time Constant: 3.16 msec or 31.6 msec switch selectable

Time Constant Accuracy: $\pm 2\%$

Zero Circuit

Accepts up to ± 75 mv or input offset

Accuracy (referred to acceleration input from velocity output):

> ± 50 μ v effective offset

Contact Closure: +5 v logic level, or front panel pushbutton
switch initiation

Zero Cycling Time: < 1 sec

All three integrators zeroed with single initiation

Temperature Stability: 10 μ v/ $^{\circ}$ C nominal

Calibration

Front panel switch activation of circuit which removes the zero
circuit from the signal path and reverses the transducer
excitation

Power

115v, 60 Hz

Environment

Temperature: 0 $^{\circ}$ to 50 $^{\circ}$ C

Humidity: 95%

Physical

Velocity Range Switches: Three

Zero Initiate Switch

MODEL 2269-150 ACCELEROMETER

Dynamic

Applies to each axis: X, Y, Z

Range: -150 to +150 g
Sensitivity (at rated excitation*): 2.5 mv/g minimum
Sensitivity Shift with Excitation Voltage: 0.2% \pm 10 to \pm 15 v
Linearity, End Point*: < \pm 3% of range
Frequency Response (reference 100 Hz): Within \pm 10%, at 800 Hz
at +75°F (24°C)
Mounted Resonant Frequency: 3.4 kHz, nominal
Transverse Sensitivity: 5% maximum
Thermal Sensitivity Shift: Maximum of \pm 10%, 0° to 150°F
reference + 75°F (24°C)
Thermal Zero Shift: \pm 50 mv over rated temperature range
Zero Balance: \pm 50 mv dc maximum at +75°F (24°C)
Warmup Time: 10 min

Electrical

Excitation: \pm 10 to \pm 15 vdc
Outputs
Single ended
Output Impedance: 2.5 Ω maximum
Minimum Resistive Load: 2.5 k Ω
Maximum Capacitive Load: 1 μ f

Physical

Configuration: 1.25-in. diameter x 2.88-in. length; mounting
flange 0.750 in. from base
Weight: 234 grams, nominal
Case Material: CRES

Environment

Acceleration Limit: \pm 1000 peak g, 1 msec half-sine pulse
or longer in any axis
Operating Temperature: -10° to +50°C
Humidity: Hermetically sealed

* Measured with steady-state acceleration.

APPENDIX II

SLED TRACK PROBLEMS

1. SLOW PRESSURE RELEASE OF FRONT CHAMBER - -

The first minor problem encountered was the method of firing the impact ram. Initially, the front-chamber pressure-release system consisted of a 5-ft-long hose with a mechanical push-button relief valve attached to one end. When the release valve was depressed, it took approximately 15 sec for the front chamber pressure to decrease sufficiently to fire the ram. For a large number of tests, this is considered inadequate because of the additional length of magnetic recording tape required for each test. To solve this problem, the hose and mechanical valve were replaced with a large exhaust port-type electric solenoid valve. The electric valve also simplified the test procedure since this valve could be activated by a toggle switch mounted on the control panel. With the solenoid valve, pressure in the front chamber decreased sufficiently to fire the impact ram in approximately 0.5 sec.

2. ACCELEROMETER RINGING

The initial reference accelerometers purchased for testing were of the miniature, piezoresistive type (Endevco Model 2264) rated at 4,500 g with a nominal resonant frequency of 40 kHz. These accelerometers were thought to be ideal transducers because of their g rating and small size. However, when first used, their outputs *rang* at approximately 37 kHz. Since all three reference accelerometers had the same type of output, the possibility of a defective transducer was eliminated. Extensive testing verified that a frequency of approximately 37 kHz was being generated within or transmitted to the canister and was exciting the three transducers into resonance. Two piezoelectric accelerometers with a resonant frequency of 80 kHz were mounted to the canister. Due to the high resonant frequency of these accelerometers, the 37 kHz was observed in the data but of a lesser magnitude. Therefore, a recognizable single output pulse was obtained. (Note: The new piezoelectric accelerometers were rated at 20,000 g with a nominal resonant frequency of 80 kHz. Because of these ratings and their high reliability, it was decided to use these transducers as the sled-track and drop-tower reference accelerometers.)

3. ACCELERATION PULSES WITH UNDESIRABLE HIGH FREQUENCIES

As mentioned above, the acceleration pulses were distinguishable as a single pulse, but they also included undesirable high-frequency components. By running a number of sled-track tests, it was concluded that the high-frequency components were characteristic of the canister and sled configurations. A new design which would attenuate these high frequencies was required. The present design (fig. 6) seemed to offer the best possibility for minimizing the problem. The elimination of the L-shaped sled and associated canister (fig. 85) would also eliminate any striker plate bending effects upon initial piston impact. The insert within the canister provides the least amount of machining when a velocity transducer with a new mechanical configuration is used. The reference accelerometers could be mounted directly on the insert instead of on the outer surface of the canister and, therefore, in closer proximity to the velocity transducer for a more accurate reading of acceleration. The most desirable feature of this new design was the isolation of the insert from the high frequencies within the canister. Several types of materials were used for high-frequency attenuation (isolation) during

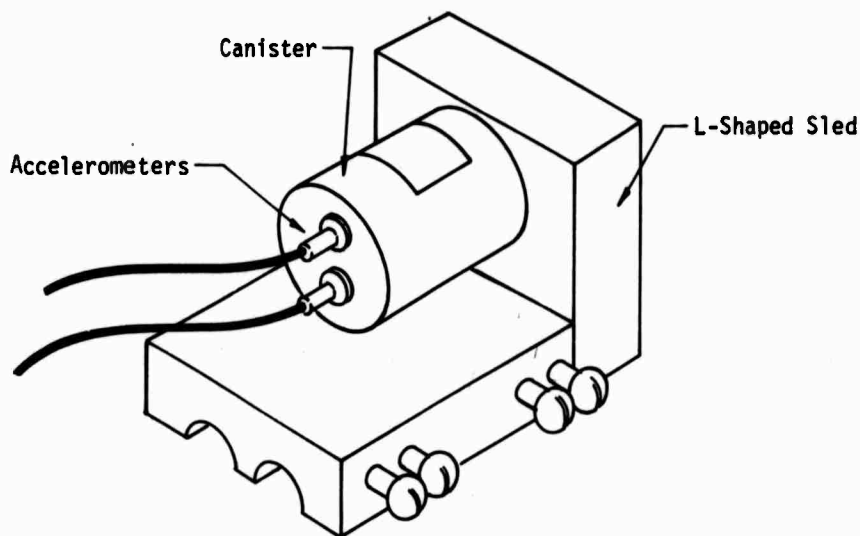


Figure 85. L-Shaped Sled and Canister

test runs of the sled track. The best results were obtained using several pieces of simple desk pad blotter material. By placing five pieces of this material on each of two sides of the insert, the high-frequency components were greatly attenuated. However, to keep the acceleration pulse width greater than 0.35 msec, it was necessary to add an additional five pieces of blotter material to the striking surface of the canister. This additional padding also helped to attenuate any unwanted high frequencies generated by the impact ram and transferred to the canister. After 8 to 12 test firings of the sled track, the isolation pads for the insert and canister had to be replaced.

APPENDIX III

JUSTIFICATION FOR 1- AND 2-g FALLTHROUGH PROCEDURE

1- and 2-g fallthroughs are used to determine the input/output scale factors for pendulous-type velocity transducers. The total velocity transducer system may be considered a single black box with input velocity and output voltage. The system transfer function, δ , is a real constant with units of ft/v-sec when the system is operating within the following constraints:

- (1) maximum rated case velocity not exceeded
- (2) both natural frequency and damping ratio of the system constant
- (3) velocity inputs such that

$$2h\omega_n \dot{\theta} \gg \left| \ddot{\theta} + \frac{\omega_n^2}{g} \theta \right|$$

If any of these constraints are violated, system output voltage may not be a real time-scaled analog of the velocity input, without employing data correction techniques. The scale factor, ζ , as defined above must be known in order to determine the ratio of input velocity to output voltage for inputs within the transducer passband.

From examination of a horizontal pendulous velocity transducer operating in its normal mode (fig. 86), a governing differential equation may be developed. When $\dot{\theta} = 0$ and $\ddot{Y} = \dot{y} = 0$, $\Sigma F_v \equiv 0$.

$$T \cos \theta = mg$$

$$T = \frac{mg}{\cos \theta}$$

Summing forces horizontally without restrictions on $\dot{\theta}$ and \dot{y} ($\ddot{Y} = 0$), one obtains

$$\Sigma F_H = M(\ddot{X} + \ddot{x})$$

$$- mCl\dot{\theta}\cos\theta - \left(\frac{mg}{\cos\theta} + m\dot{\theta}^2 l \right) \sin\theta = M(\ddot{X} + \ddot{x})$$

$$x = l \sin\theta$$

$$\dot{x} = l \cos\theta \dot{\theta}$$

$$\ddot{x} = l [\cos\theta \ddot{\theta} - \sin\theta (\dot{\theta})^2]$$

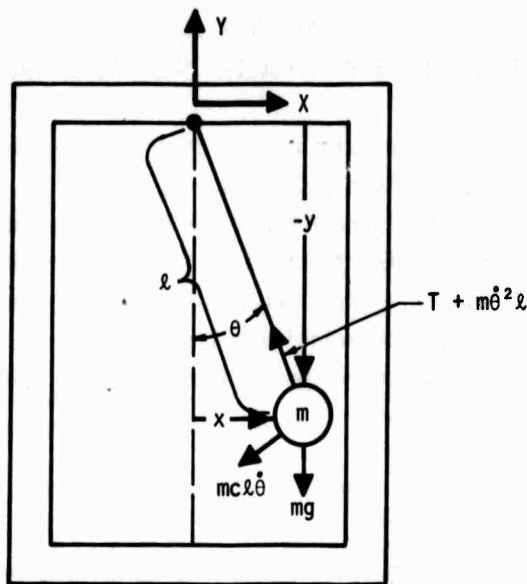


Figure 86. Normal Operating Mode of Horizontal Pendulous Transducer

$$-ml\cos\theta\ddot{\theta} - mCl\dot{\theta}\cos\theta - \frac{mg\sin\theta}{\cos\theta} = m\ddot{X}$$

with small angle approximations

$$\cos\theta \approx 1, \sin\theta \approx \theta$$

$$-ml\ddot{\theta} - mCl\dot{\theta} - mg\theta = m\ddot{X}$$

$$\ddot{\theta} + C\dot{\theta} + \frac{g}{l}\theta = \frac{-\ddot{X}}{l}$$

Within the passband of the transducer

$$|\ddot{\theta} + \frac{g}{l}\theta| \ll C\dot{\theta}$$

Ignoring these terms, one may reduce the differential equation to

$$C\dot{\theta} = \frac{-\ddot{X}}{l}$$

and for the case where

$$\ddot{X} = g$$

$$\dot{\theta} = \frac{-g}{c\ell}$$

$$\theta = \frac{-gt}{C\ell} + \theta_0$$

again with $\ddot{X} = \ddot{Y} = \dot{\theta} = 0$

$$T \equiv 0$$

In the 1-g fallthrough test, the horizontal transducer is positioned as shown in figure 87. The differential equation for this system is

$$-mg - mC\ell\dot{\theta}\cos\theta - m\ell(\dot{\theta})^2 \sin\theta = M(\ddot{X} + \ddot{x})$$

and again

$$\ddot{x} = \ell[\cos\theta\ddot{\theta} - \sin\theta(\dot{\theta})^2]$$

$$-m\ell\cos\theta\ddot{\theta} - mC\ell\dot{\theta}\cos\theta - mg = m(\ddot{x})$$

with small angle approximations

$$\ddot{\theta} + C\dot{\theta} = \frac{\ddot{X}}{\ell} - \frac{g}{\ell}$$

Since during the 1-g fallthrough test $\ddot{X} = 0$

$$\ddot{\theta} + C\dot{\theta} = \frac{g}{\ell}$$

Examining only the steady-state solution to this equation, one obtains

$$\theta = \frac{-gt}{\ell C}$$

Therefore, the steady-state response of a horizontal pendulous overdamped velocity transducer during 1-g fallthrough is exactly that of an ideal transducer (i.e., $|\ddot{\theta} + \frac{g\theta}{\ell}| \ll C\dot{\theta}$ subjected to 1-g horizontal acceleration).

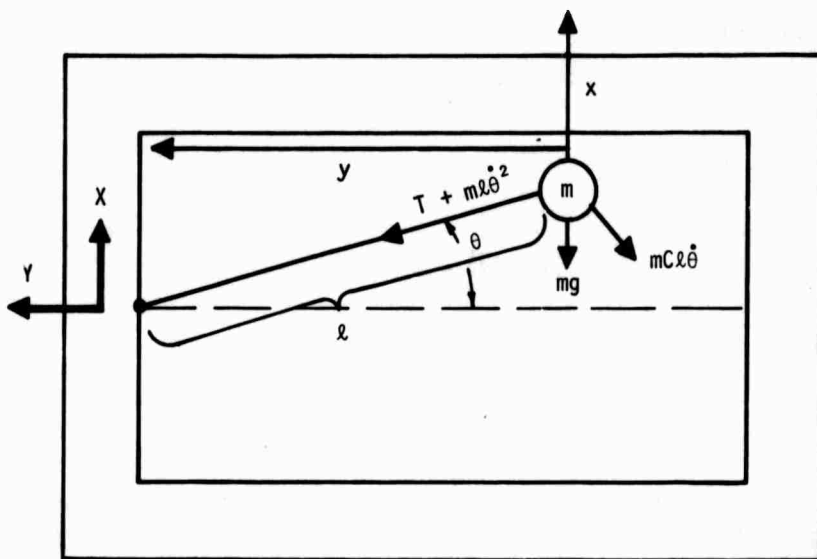


Figure 87. 1-g Fallthrough Mode of Horizontal Pendulous Transducer

Vertical pendulous velocity transducers are tested in the same manner; but, because of the 1-g spring in these transducers, the steady-state fallthrough response is equivalent to an ideal transducer experiencing a constant 2-g acceleration.

APPENDIX IV

JUSTIFICATION FOR EXPONENTIAL FALLTHROUGH PROCEDURE

The exponential fallthrough test may be used to provide a transducer output which is exactly the same as all but a finite portion of the transducer's response to a step input if the mathematical models presented in section I adequately describe the transducer system.

For the pendulous mechanical system

$$\ddot{\theta} + 2h\omega_n \dot{\theta} + \omega_n^2 \theta = \frac{\omega_n^2}{g} \ddot{x}$$

Letting

$$\alpha = \omega_n (h + \sqrt{h^2 - 1})$$

$$\beta = \omega_n (h - \sqrt{h^2 - 1})$$

one obtains

$$\ddot{\theta} + (\alpha + \beta) \dot{\theta} + \alpha\beta\theta = \frac{\alpha\beta}{g} \ddot{x} \quad (1)$$

1. STEP VELOCITY INPUT (CASE I)

$$\dot{x} = 0 \quad \text{for} \quad t < t_0$$

$$\dot{x} = 1 \quad \text{for} \quad t > t_0$$

Initial conditions are

$$\theta_{I_0} = \dot{\theta}_{I_0} = 0$$

The Laplace transform of eq. (1) with these conditions is

$$\theta_I(s) [S^2 + (\alpha + \beta) S + \alpha\beta] = \frac{\alpha\beta}{g}$$

$$\theta_I(s) = \frac{\alpha\beta}{g(s + \alpha)(s + \beta)}$$

$$\theta_I = \frac{\alpha\beta}{g(\beta - \alpha)} (e^{-\alpha t} - e^{-\beta t}) \quad (2)$$

Differentiating and equating to zero, one obtains

$$\frac{d\theta_I}{dt} = 0 = -\alpha e^{-\alpha t} + \beta e^{-\beta t}$$

$$\alpha e^{-\alpha t} = \beta e^{-\beta t}$$

$$\frac{\beta}{\alpha} = e^{(\beta - \alpha)t} = e^{(\beta - \alpha)t_p}$$

$$\ln\left(\frac{\beta}{\alpha}\right) = \ln e^{(\beta - \alpha)t_p} = (\beta - \alpha)t_p$$

Solving for t , one obtains

$$t = \frac{\ln(\beta/\alpha)}{\beta - \alpha} = t_p$$

At this value of t , θ is maximum. Substituting t_p in eq. (2), one finds θ_{Im} .

$$\begin{aligned}\theta_{Im} &= \frac{\alpha\beta}{g(\beta - \alpha)} \left[e^{-\alpha t_p} - \alpha/\beta e^{-\beta t_p} \right] = \frac{\alpha\beta}{g(\beta - \alpha)} e^{-\alpha t_p} (1 - \alpha/\beta) \\ &= \frac{\alpha}{g} e^{-\alpha t_p} = \frac{\alpha}{g} e^{-\alpha \ln(\beta/\alpha)/(\beta - \alpha)} = \frac{\alpha}{g} (\beta/\alpha)^{-\alpha/(\beta - \alpha)}\end{aligned}$$

Letting $T = t - t_p$, $t = T + t_p$, one obtains

$$\theta_{I(T)} = \frac{\alpha\beta}{g(\beta - \alpha)} \left[\left(\frac{\beta}{\alpha}\right)^{-\alpha/(\beta - \alpha)} e^{-\alpha T} - \left(\frac{\beta}{\alpha}\right)^{-\beta/(\beta - \alpha)} e^{-\beta T} \right] \quad (3)$$

2. EXPONENTIAL FALLTHROUGH (CASE II)

$$\theta_{II_0} = \theta_{Im}^*$$

$$\dot{\theta}_{II_0} = 0$$

$$\ddot{\theta}_{II_0} = \dot{\chi} = 0$$

$$\ddot{\theta}_{II} + (\alpha + \beta) \dot{\theta}_{II} + \alpha\beta\theta_{II} = 0$$

* We have purposely forced this in order that θ_{peak} for $\theta_{II_0} = \theta_{peak}$ for θ_{I_0} .

$$\begin{aligned}
\theta_{II}(T) &= \frac{\theta_{Im}}{(\beta - \alpha)} \begin{bmatrix} -\alpha T & -\beta T \\ \beta e & -\alpha e \end{bmatrix} \\
&= \frac{\alpha}{g(\beta - \alpha)} \begin{bmatrix} -\alpha/(\beta - \alpha) \\ \beta/\alpha \end{bmatrix} \begin{bmatrix} -\alpha T & -\beta T \\ \beta e & -\alpha e \end{bmatrix} \\
&= \frac{\alpha}{g(\beta - \alpha)} \begin{bmatrix} \beta \left(\frac{\beta}{\alpha}\right)^{-\alpha/(\beta - \alpha)} e^{-\alpha T} & -\alpha \left(\frac{\beta}{\alpha}\right)^{-\alpha/(\beta - \alpha)} e^{-\beta T} \end{bmatrix} \\
&= \frac{\alpha\beta}{g(\beta - \alpha)} \begin{bmatrix} \left(\frac{\beta}{\alpha}\right)^{-\alpha/(\beta - \alpha)} e^{-\alpha T} & -\left[\frac{\beta^{-\alpha/(\beta - \alpha)} + 1}{\alpha^{-\alpha/(\beta - \alpha)} + 1}\right] e^{-\beta T} \end{bmatrix} \\
&= \frac{\alpha\beta}{g(\beta - \alpha)} \begin{bmatrix} \left(\frac{\beta}{\alpha}\right)^{-\alpha/(\beta - \alpha)} e^{-\alpha T} & -\left(\frac{\beta}{\alpha}\right)^{-\beta/(\beta - \alpha)} e^{-\beta T} \end{bmatrix} \quad (4)
\end{aligned}$$

Equations (3) and (4) are identical and thus establish that transducer output after peak response to a step input is identical to transducer output during the exponential fallthrough test.

For the linear mechanical system

$$\ddot{X} + 2h\omega_n \dot{X} + \omega_n^2 X = \ddot{X} \quad (5)$$

This differential equation is almost exactly the same as eq. (1) except for the $\frac{\alpha\beta}{g}$ constant. Consider the special case for eq. (1) where $|\frac{\alpha\beta}{g}| = 1$. For this special case, eq. (1) becomes

$$\ddot{\theta} + (\alpha + \beta)\dot{\theta} + \alpha\beta\theta = \ddot{X}$$

$$\ddot{\theta} + 2h\omega_n \dot{\theta} + \omega_n^2 \theta = \ddot{X}$$

and thus has exactly the same form as eq. (5). Therefore, the justification for exponential fallthrough in a linear mechanical velocity transducer is established.

APPENDIX V DAMPING RATIO DETERMINATION FROM EXPONENTIAL FALLTHROUGH DATA

This appendix presents the determination of the damping ratio for overdamped seismic velocity transducers by exponential fallthrough testing.

With initial conditions

$$\theta_0 = \theta_m$$

$$\dot{\theta}_0 = 0$$

and forcing function

$$\ddot{X} = \dot{X} = 0$$

the equation for $\theta(t)$ is

$$\theta(t) = \frac{\theta_m}{\beta - \alpha} \left(\beta e^{-\alpha t} - \alpha e^{-\beta t} \right)$$

where

$$\alpha = \omega_n (h + \sqrt{h^2 - 1})$$

$$\beta = \omega_n (h - \sqrt{h^2 - 1})$$

(See appendix IV.) For $h \gg 1$

$$\theta(t) \approx \frac{\theta_m}{-\alpha} \left(-\alpha e^{-\beta t} \right) = \theta_m e^{-\beta t}$$

This approximation reduces $\theta(t)$ to a single mode exponential decay and is justified only for high damping ratios.

Now let t_1 = time required (sec) for

$$\theta_{t_1} = \frac{\theta_m}{2} \quad (\text{half life of } \theta)$$

then

$$\theta_{2t_1} = \frac{\theta_m}{4}$$

$$\theta_{t_1} = 2\theta_{2t_1}$$

$$\theta_{t_1} = \theta_m e^{-\beta t_1} = 2\theta_{2t_1} = 2\theta_m e^{-2\beta t_1}$$

$$e^{-\beta t_1} = 2e^{-2\beta t_1}$$

$$-\beta t_1 = \ln 2 - 2\beta t_1$$

$$\beta t_1 = \ln 2$$

$$\beta = \frac{\ln 2}{t_1} = \omega_n (h - \sqrt{h^2 - 1})$$

$$h - \sqrt{h^2 - 1} = \frac{\ln 2}{\omega_n t_1}$$

$$h = \frac{\ln 2}{\omega_n t_1} + \sqrt{h^2 - 1}$$

$$h^2 = \frac{(\ln 2)^2}{(\omega_n t_1)^2} + \frac{2\sqrt{h^2 - 1}}{\omega_n t_1} \ln 2 + h^2 - 1$$

$$\frac{2\sqrt{h^2 - 1}}{\omega_n t_1} \ln 2 = 1 - \frac{(\ln 2)^2}{(\omega_n t_1)^2}$$

$$\sqrt{h^2 - 1} = \frac{\omega_n t_1}{2\ln 2} - \frac{\ln 2}{2\omega_n t_1}$$

$$h^2 - 1 = \left(\frac{\omega_n t_1}{2\ln 2} - \frac{\ln 2}{2\omega_n t_1} \right)^2$$

$$h^2 = \left(\frac{\omega_n t_1}{2\ln 2} - \frac{\ln 2}{2\omega_n t_1} \right)^2 + 1$$

$$h = \sqrt{\left[\frac{\omega_n t_1}{2\ln 2} - \frac{\ln 2}{\omega_n t_1} \right]^2 + 1}$$

For most pendulous-type velocity transducers, ω_n is nominally 6π . For these transducers

$$h \approx \sqrt{\left(\frac{6\pi t_1}{1.388} - \frac{0.694}{6\pi t_1}\right)^2 + 1}$$

Since t_1 observed for these type transducers is about 2 to 25 sec

$$h \approx \frac{6\pi t_1}{1.388} = 13.6t_1$$

Therefore, the damping ratio may be closely approximated for most pendulous-type transducers at $13.6t_1$. If

$$\frac{\ell n 2}{\omega_n t_1} \ll \frac{\omega_n t_1}{2\ell n 2} \gg 1$$

$$h \approx \frac{\omega_n t_1}{2\ell n 2}$$

All overdamped transducers tested satisfied this condition. The lowest ω_n was 18.8 and the lowest t_1 was greater than 2 sec; the typical t_1 was 10 to 20 sec.

APPENDIX VI

JUSTIFICATION FOR HAVERSINE TERMINATION

This appendix presents justification for haversine termination to compute fast Fourier transforms for overdamped velocity transducers.

The governing equation for an overdamped pendulous velocity transducer may be written

$$\ddot{\theta} + (\alpha + \beta)\dot{\theta} + \alpha\beta\theta = \frac{\alpha\beta}{g} \dot{V}$$

where

$$\alpha = \omega_n (h + \sqrt{h^2 - 1})$$

$$\beta = \omega_n (h - \sqrt{h^2 - 1})$$

θ = pendulum angle with respect to case

\dot{V} = case input acceleration (on axis)

Since the equation for a linear overdamped velocity transducer is similar except for the case input acceleration scale factor, this development verifies haversine termination for both pendulous and linear overdamped transducers.

Typical overdamped seismic transducer response from data generated in this test program is shown in figure 88. The assumption validated in this appendix is as follows: If at $t = t_f$ the forcing function were

$$V_{\max} \left[\frac{1 + \cos \omega (t - t_f)}{2} \right]$$

for $0 \leq t - t_f \leq \pi/\omega$, and 0 for $t - t_f > \pi/\omega$ then for a properly selected value of ω , the output θ will be

$$\theta \approx \theta_m \frac{(1 + \cos \omega (t - t_f))}{2}$$

in the same interval. This yields the input/output record shown in figure 89. In applying the haversine termination, t_f is chosen such that

$$\left. \frac{dV}{dt} \right|_{t=t_f} \approx 0$$

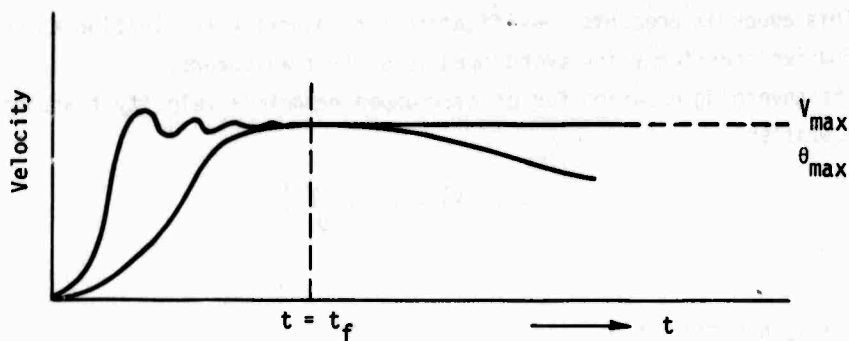


Figure 88. Typical Seismic Transducer Input/Output Record

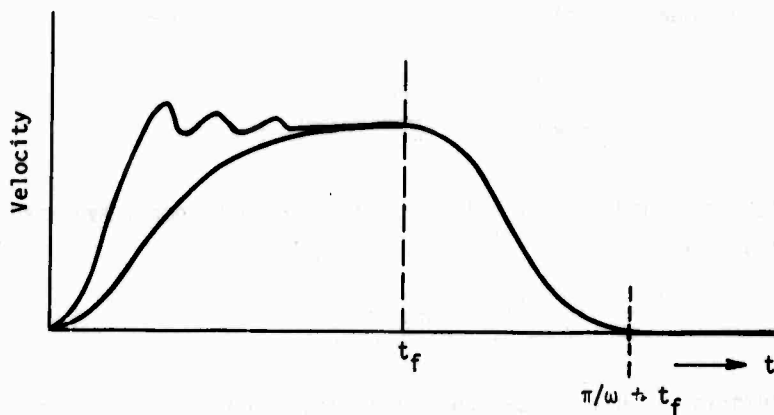


Figure 89. Seismic Transducer Input and Output with Haversine Termination

and

$$\left. \frac{d\theta}{dt} \right|_{t=t_f} \approx 0$$

With the following conditions, θ may be found from the governing differential equation:

$$t_f = 0$$

$$V = \frac{1 + \cos \omega t}{2}$$

$$\frac{dV}{dt} = \frac{-\omega \sin \omega t}{2}$$

$$\theta_0 = \frac{\alpha\beta}{g(\alpha + \beta)} \dot{\theta}_0 = 0$$

$$\theta + (\alpha + \beta)\dot{\theta} + \alpha\beta\ddot{\theta} = -\frac{\alpha\beta}{2g} \omega \sin \omega t$$

For the special case where

$$\omega = \omega_n = \alpha\beta$$

$$\theta = \frac{\alpha\beta}{2g(\alpha^2 - \beta^2)} (\alpha e^{-\beta t} - \beta e^{-\alpha t}) + \frac{\alpha\beta}{2g(\alpha + \beta)} \cos \omega_n t$$

For a DX-type pendulous transducer

$$\omega_n = 18.85$$

The lowest observed damping ratio occurring with slow inputs is 25.

$$h = 25$$

$$\alpha = \omega_n (h + \sqrt{h^2 - 1}) = 942$$

$$\beta = \omega_n (h - \sqrt{h^2 - 1}) = 0.377$$

At $t = \pi/\omega_n$, the input function is zero. The output is $\theta = -0.354 \times 10^{-3}$ rad.

Peak output, θ_0 , is 0.0117 rad. In terms of percent of peak output; the

natural frequency haversine termination has a maximum error of -3.02 percent of peak reading. Therefore, during haversine termination at natural frequency

$$\theta \approx \theta_m \frac{[1 + \cos(t - t_f)]}{2}$$

Since the 7-Hz haversine termination was used in preparing input/output fast Fourier transforms, the special case which applies to most pendulous-type velocity transducers is examined. Again, assume

$$h = 25$$

$$\omega_n = 18.85$$

$$\alpha = 942$$

$$\beta = 0.377$$

$$\dot{V} = -22 \sin 44t \text{ (at 7 Hz)}$$

In this case

$$\begin{aligned} \theta = & 8.059 \times 10^{-6} e^{-942t} + 5.862 \times 10^{-3} e^{-0.377t} \\ & + 2.228 \times 10^{-4} \sin 44t \\ & + 5.83 \times 10^{-3} \cos 44t \end{aligned}$$

At $t = \pi/44$

$$\theta = 0.1237 \times 10^{-3} \text{ rad}$$

and again

$$\theta_m = 0.0117 \text{ rad}$$

Percentage of peak error is $12.37/11.7 = -1.05$ percent. This indicates that the output of a pendulous velocity transducer with a 3-Hz natural frequency terminated with a 7-Hz haversine matches the input with approximately 1/3 the error that the same transducer would have terminated by a 3-Hz or natural-frequency haversine. This may be intuitively obvious when one realizes that since 7 Hz is so near midband (3 Hz), attenuation at 7 Hz is negligible; but,

during the 7-Hz haversine-termination interval, the droop or exponential decay due to the constant term in the forcing function $(1 + \cos 44t/2)$ is far less than the droop during the 3-Hz haversine-termination interval.

DISTRIBUTION

No. cys

1 Hq USAF, Wash, DC 20330
 1 (RDPQ, 1C370)
 1 (RDQPN, 1D424)
 1 Hq USAF, AFTAC (TAP), Patrick AFB, FL 32925
 1 AFISC, Norton AFB, CA 92409
 1 Dir Nuc Safety (SN), Kirtland AFB, NM 87117
 1 AFSC (DOB), Andrews AFB, Wash, DC 20334
 1 AUL (LDE), Maxwell AFB, AL 36112
 1 AFIT (CES), Wright-Patterson AFB, OH 45433
 1 USAFA (DFSLB), CO 80840
 1 ARL, Wright-Patterson AFB, OH 45433
 1 ESD (DEE), L. G. Hanscom Fld, Bedford, MA 01730
 1 RADC (Doc Lib), Griffiss AFB, NY 13441
 1 AFSWC (HO), Kirtland AFB, NM 87115
 1 AFWL, Kirtland AFB, NM 87117
 2 (SUH)
 5 (DEX)
 1 Comdg Off, BRL (AMXBR-TB, J. Meszaros), Aberdeen Pvg Gnd, MD 21005
 1 Dir, USA Eng WW Exp Sta (WESRL), PO Box 631, Vicksburg, MS 39181
 1 NCEL, Port Hueneme, CA 93041
 1 Dir, DNA (DDST), Wash, DC 20305
 2 DDC (TCA), Cameron Sta, Alexandria, VA 22314
 1 Sandia Lab, Kirtland AFB, NM 87115
 1 (Org 3141)
 1 (Mr. Joe Wister)
 1 (Mr. Ben Benjamin)
 1 Sandia Lab, PO Box 969, Livermore, CA 94550
 1 (Org 8000)
 1 (Mr. Larry Starrh, LLL)
 1 Dir Ofc, LLL (Tech Info Dept), PO Box 808, Livermore, CA 94550
 5 Univ of New Mexico, CERF, PO Box 188, University Sta, Albuquerque, NM 87131
 1 AFSCF/DOZ-A (Capt Newell), Sunnyvale AF Station, CA 94086
 1 Physics International (Mr. Fred Sauer), San Leandro, CA 94577
 1 TRW Systems (Mr. Charles Bucky/MS 524/407), San Bernardino, CA 92402
 1 Official Record Copy (Mr. Schneider/AFWL/DEX)